UNIVERSITÀ
DEGLI STUDI
DI MILANO

Facoltà di Scienze Matematiche, Fisiche e Naturali
Dipartimento di Chimica Inorganica, Metallorganica e Analitica

Corso di Dottorato di Ricerca in Scienze Chimiche
XXV Ciclo

Tesi di Dottorato di Ricerca

Design, characterization and application of heterogeneous silica supported catalysts, based on Pd nanoparticles and metal single sites (Rh, Cu)

Tutore: Dott. Vladimiro Dal Santo
Coordinatore: Dott. Alessandro Caselli

Dottoranda: Dott.ssa Yvonne Carina Hönemann
Matr. No. R08881

Anno Accademico 2011/2012

NANO-HOST

Homogeneous Supported Catalyst Technologies:
The sustainable approach to highly-selective, fine chemicals production

“Chemistry without catalysis would be a sword without a handle,
a light without brilliance, a bell without sound.”

Alwin Mittasch

List of abbreviations

Ac	Acetyl
Ar	Aryl
BET	Brunauer-Emmett-Teller
BMIM	1-butyl-3-methyl-imidazolium
Bu	Butyl
c	Concentration
c (in terms of monolith)	Calcined
cod	Cyclooctadiene
cp	Cyclopentadienyl
CVD	Chemical Vapour Deposition
d	Day
DMSO	Dimethylsulfoxide
dppe	1,2-bis(diphenylphosphino)ethane
DRIFTS	Diffuse Reflectance Infrared Fourier Transform Spectroscopy
EBL	Electron Beam Lithography
EDA	Ethyl diazoacetate
ee	Enantiomeric Excess
EO	Ethylene oxide
Et	Ethyl
EWG	Electron-Withdrawing Group
EXAFS	Extended X-ray Absorption Fine Structure
GC	Gas Chromatography
GC-MS	Gas Chromatography – Mass Spectrometry
h	Hour
HMDA	Hexamethylenediamine
HMF	5-hydroxymethylfurfural
HPLC	High Performance Liquid Chromatography
HR-TEM	High-Resolution Transmission Electron Microscopy
ICP-OES	Inductively Coupled Plasma Optical Emission Spectrometry
ILs	Ionic Liquids
IR	Infrared

K	Kelvin
L	Ligand
LG	Leaving group
M	Metal
Me	Methyl
min	Minute
MIRC	Michael-Initiated Ring Closure
NBD	Norbornadiene
nm	Nanometer
NMR	Nuclear Magnetic Resonance
NO_x	Nitrogen oxides
NPs	Nanoparticles
Nuc	Nucleophile
p	para
PAMAM	Poly(amidoamine)
PC	Pyridine-containing
PEO	Polyethylene oxide
Ph	Phenyl
PO	Propylene oxide
ppm	Parts per million
PVC	Polyvinylchloride
PVP	Poly(*N*-vinyl-2-pyrrolidone)
R	Rest
RT	Room temperature
s	Second
SAXS	Small Angle X-ray Scattering
sc	Supercritical
SEM	Scanning Electron Microscopy
SFC	Supercritical Fluid Chromatography
SSHC	Single-Site Heterogeneous Catalysts
t	Time
T	Temperature
TEM	Transmission Electron Microscopy

TEOS	Tetraethoxysilane
Tf	Triflate
THF	Tetrahydrofuran
TMPD	N,N,N',N'-tetramethyl-*p*-phenylenediamine
TMS	Tetramethylsilane
TOF	Turnover frequency
TON	Turnover number
TOP	Trioctylphosphine
TPS	Tetra-*n*-propoxysilane
Ts	Tosylate
v	Velocity
wt	Weight

Table of contents

Introduction 12

CHAPTER 1: Design, characterization and application of heterogeneized Rh^{I}-Pd^{0}/SiO_2 "hybrid catalysts" 28

General part 29

1. Metal nanoparticles and their impact on catalysis 30

1.1 The historical development of metal NPs – an overview 30
1.2 Supported PdNPs 31
1.2.1 Silica supported PdNPs 32
1.2.1.1 Preparation of the silica support materials 32
1.2.1.2 Immobilization of PdNPs onto silica 32
1.3 Catalytic application of PdNPs 33
1.4 Innovations in the field of NPs 34
1.4.1 Stabilizers 34
1.4.1.1 Polymers 34
1.4.1.2 Dendrimers 35
1.4.1.3 Ligands 37
1.4.1.4 Micelles, microemulsions and surfactants 37
1.4.2 Ionic liquids as media 39
1.4.3 Solid support materials 40
1.4.3.1 Carbon supports 40
1.4.3.2 Oxide supports 41

2. Silica supports 42

2.1 MCM-41 42
2.2 SBA-15 46

3. Rh^{I}-Pd^{0}/SiO_2 "hybrid catalysts" 50

4. Rh^{I} single sites 56

4.1 Grafting of isolated species on mesoporous silica support materials 57
4.2 Grafting of asymmetric organometallic complexes on mesoporous support materials 60
4.3 "Ship-in-bottle" catalysts 61

4.4 Open-structured SSHC 63
Results and discussion 65
1. Immobilization of PdNPs onto silica 66
2. Impregnation of Pd^0/SiO_2 with Rh^I 72
Concluding remarks 76
References 78
CHAPTER 2: Synthesis, characterization and application of heterogeneized chiral $[Cu^I(PC\text{-}L^*)]CF_3SO_3$ complexes on silica support materials 87
General part 88
1. Cu^I in cyclopropanation reactions 89
2. Cyclopropanation reactions 92
2.1 Halomethyl-metal-mediated cyclopropanation 93
2.2 Transition metal-catalyzed decomposition of diazo compounds 93
2.2.1 Intermolecular Cyclopropanation 93
2.2.1.1 Diazomethane 93
2.2.1.2 Diazoalkanes with one EWG 94
2.2.1.3 Diazoalkanes with two EWGs 95
2.2.2 Intramolecular Cyclopropanation 95
2.3 Nucleophilic addition – ring closure sequence 96
Results and discussion 98
1. Synthesis of $[Cu^I(PC\text{-}L^*)]CF_3SO_3/SiO_2$ 99
2. Application of $[Cu^I(PC\text{-}L^*)]CF_3SO_3/SiO_2$: Asymmetric cyclopropanation 101
3. Analytical characterization of $[Cu^I(PC\text{-}L^*)]CF_3SO_3/SiO_2$ 102
Concluding remarks 108
References 110

CHAPTER 3: Preparation of grafted silica monoliths and their catalytic application in the dehydration of D-fructose to 5-hydroxymethylfurfural (HMF) 113

General part 114

1. D-Fructose – a promising renewable resource 115

2. The dehydration of fructose to 5-hydroxymethylfurfural (HMF) 117

3. Silica monoliths as microreactors for continuous flow reactions 125

Results and discussion 132

Concluding remarks 145

References 147

Conclusion 149

Experimental part 152

Experimental part – General information 153

Experimental part I – CHAPTER 1 155

Experimental part II – CHAPTER 2 160

Experimental part III – CHAPTER 3 165

List of figures 170

List of tables 178

Acknowledgements 180

Introduction

Heterogeneous catalysis

The today's role of catalysts

Catalysts play an important and essential role in the modern world. Nowadays, it is impossible to imagine industrial chemical processes without the use of catalysts. A multitude of significant products are synthesized catalytically, e.g. economic transportation fuels, lubricants which are stable even at high temperatures, polymers with a high strength, drugs against cancer, and many more.[1] In addition, catalysts are required in the environmental chemistry, in order to reduce the pollution of air and water.[1] Hence, it is obvious that the today's world without the application of catalysts would be unimaginable.

Nanotechnology – a new and promising field of catalysis

Excellent catalysts combine both high selectivity and high activity.[2] Highly-selective reactions proceed without the formation of any waste products. Accordingly, no separation and purification steps are necessary; therefore, the process is energy-saving and cost-efficient.

The concept of selectivity – a comparison to the enzymatic world

In order to exemplify the definition of selectivity, it is helpful to draw a comparison between chemical heterogeneous catalysts and enzymes as biological catalysts.[2]

Enzymatic reactions proceed with very high selectivities and occur at the active site of the enzyme.[2] The difference between enzymes and other catalysts is the environment of this active site. Regarding the enzyme, the active site is placed in a kind of cavity, which contains binding sites, i.e. functional groups, on its inner walls. These functionalities enable the chemical interaction between the enzyme and the

substrate. It was observed that the cavity, and thereby the active site and the binding sites as well, shift during the enzymatic process.[3] It this way, the docking of the substrate and the detachment of the product are facilitated.
On these grounds, it is aspired to control all important parameters about the active site when a new heterogeneous catalyst is developed: The formation of the active site, its environment, its binding sites and how to reach them.[2]

Active sites and atomic control

Considering a metal crystallite, it is evident that the atoms show different properties at different locations.[2] Atoms at the corners and edges of the crystallite differ from those atoms, which can be found at the interface between metal and support material. In order to create active sites, it is indispensable to examine the atomic properties at the different locations thoroughly, i.e. to gain atomic control.

Several studies report about the possibility to obtain supported metal clusters with atomic control.[2,4] A very common method is the use of organometallic complexes, which act as precursor and have well-defined properties. Another technique is the *Electron Beam Lithography (EBL)*, studied by *Somorjai et al.*[5] This method enables the control of the particle size as well as the distance between the individual particles.

The environment of the active sites

As already mentioned, the environmental nature of the active sites has a great impact on the catalyst and thereby on the activity and selectivity of the reaction.

A multitude of methods enables the control of the environment, e.g. its synthesis by a so-called “unit-by-unit” method.[2] Atoms or rather units, which serve as a kind of “spacer”, are combined stepwise with the active site. The addition of more and more

"spacer" units leads to an increase of the distance to the active site. As recently as the desired distance is attained, the second active site is constructed. In this way, the distance between the individual active sites can be controlled.
A further method is the molecular templating technique, shown in Figure 1.[2,6,7]

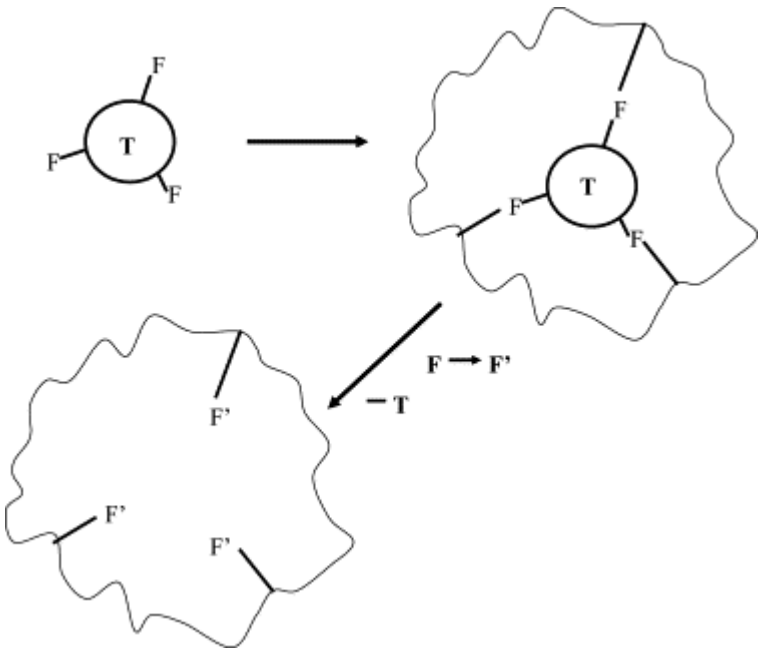

Figure 1: Molecular templating technique for the control of the active sites' environment.[2]

A template T with functional groups F is enclosed by a silica matrix, whereat the functional groups act as linkers and bridge the template with the walls of the matrix. After the removal of the templating molecule, the functional groups F become active sites F'. Their location is determined by the template.

Concluding, it is obvious that the control of the active site itself as well as its environmental nature is indispensable for the design of highly-selective heterogeneous catalysts.

Dispersed nanoparticles

Numerous catalysts, which are applied in industrial processes, are solids with a high surface area.[1] Very small particles – so-called nanoparticles (NPs) – having dimensions between 1 and 20 nm are dispersed on the surface.[1]

Dispersed NPs are of great industrial interest; a very famous example for their application is the automotive catalytic converter, which is part of every new built car since the beginning of the 1970s (Figure 2).[1]

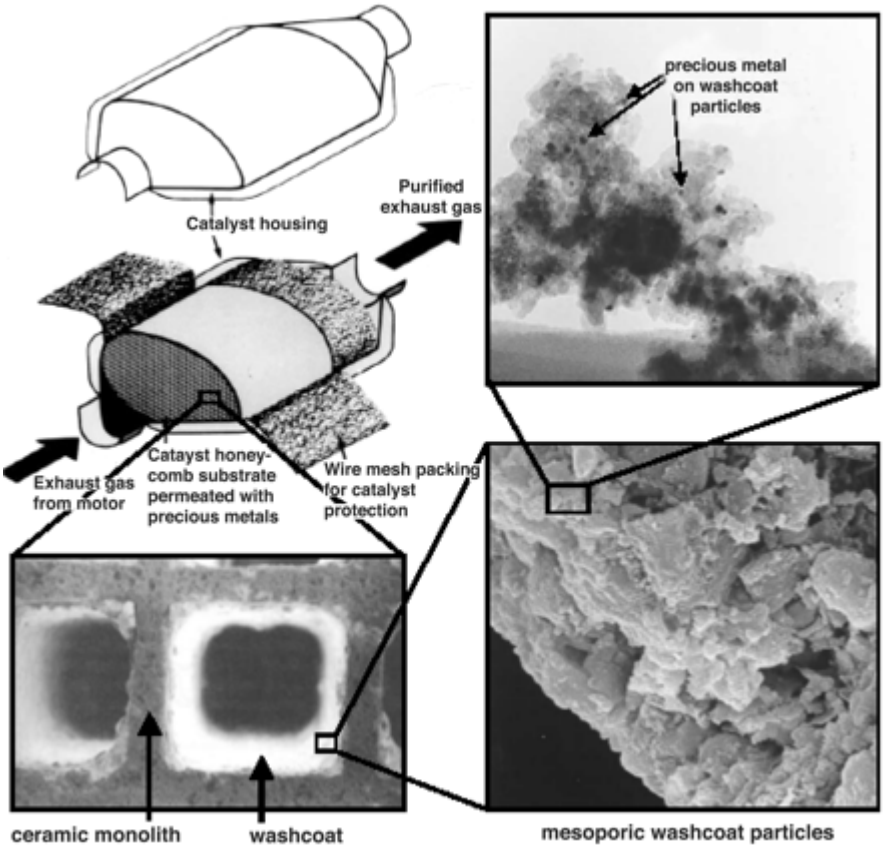

Figure 2: Application of NPs in the automotive catalytic converter.[1]

The automotive catalytic converter consists of a so-called honeycomb.[1] NPs of platinum, rhodium, cerium, zirconia and lanthana are applied. They are immobilized

by impregnation on the inner side of the honeycomb on a thin layer of porous aluminum oxide. Every single metal has its particular task: The platinum NPs oxidize hydrocarbons and carbon monoxide, the rhodium NPs, however, catalyze the reduction of nitrogen oxides NO_x. The cerium and zirconia NPs are applied in order to storage the oxygen, whereas the lanthana NPs are helpful to stabilize the aluminum oxide surface.

Dispersed supported NPs have multifarious applications. For instance, gold NPs, supported on titanium dioxide, are used in paintings, in order to oxidize carbon monoxide to carbon dioxide and, hence, to reduce the carbon monoxide concentration and pollution of the inner walls of buildings.[1,8] Parameters like the size and the local composition of NPs have a great impact on the catalysts activity and selectivity.[1] Thus, the activity of the gold NPs depends highly on their size as shown in Figure 3.

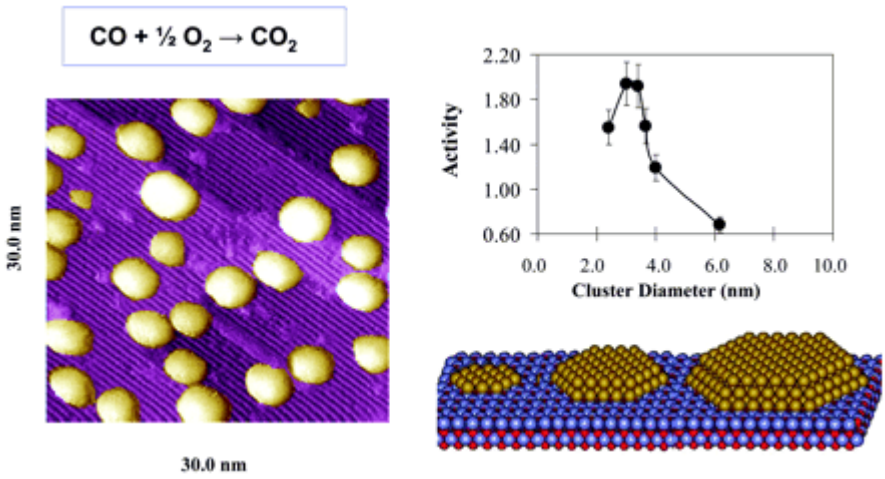

Figure 3: The impact of the size of AuNPs on their catalytic activity.[1,8]

As it can be seen from the plot, only NPs having a size between 2 and 3 nm are catalytically active in the oxidation of carbon monoxide to carbon dioxide.[9]

As already mentioned above, the activity and the selectivity are not only dependent on the particle size, but also from the local composition of the NPs.[1] A concrete example for this circumstance is the MoS_2/Al_2O_3 catalyst, which is used for the desulfurization of petroleum and its products.[1] It was found that the addition of a small amount of cobalt to MoS_2 leads to a considerable increase of the catalysts activity.[1,10]

In order to investigate the size and the shape of the MoS_2 particles as well as to localize the cobalt atoms, two important analytical techniques are applied: *High-Resolution Transmission Electron Microscopy (HR-TEM)* and *Extended X-ray Absorption Fine Structure (EXAFS)*, respectively.[1] HR-TEM is one of the most used techniques for the characterization of NPs because it gives a multitude of information: Of course, the size and the shape of the NPs are determined; but also the structure of the lattice and furthermore, the composition of single NPs can be identified.[1]

Heterogeneous catalysis in the production of fine chemicals

In general, heterogeneous catalysis is applied in the field of petro- and bulk chemicals.[11] However, also fine chemicals, like agro-chemicals and pharmaceuticals, can be produced by heterogeneous catalysis. A variety of chemical reactions and transformations provides application for heterogeneous catalysts: Starting with hydrogenations of aromatics, to metathesis of unfunctionalized olefins and selective hydrogenations of C≡C to *cis*-olefins.

Limits of heterogeneous catalysts

Though, heterogeneous catalysts implicate several problems when they are applied in the production of fine chemicals.

Not uncommonly, the transfer from research to the industrial large-scale production generates the problem of poor catalyst performance:[11] The developed catalysts do not cope with the high industrial demands; their efforts in selectivity (chemo-, regio-, stereo- and enantioselectivity), activity, productivity and stability are insufficient. In general, a catalyst should give selectivities > 95 % because of costly substrates (starting materials as well as intermediates) and separation steps.
An industrially applied catalyst can be characterized by the two factors TON and TOF: The TON is defined as the "Turnover number" and it describes the productivity of the catalyst; it can be also defined as the ratio of substrate to catalyst. The TOF ("Turnover frequency") specifies the catalyst's activity; it determines the capacity of the process.

Another important aspect, concerning the application of heterogeneous catalysis in the production of fine chemicals, is the required high purity of the starting materials, especially for the production of pharmaceuticals.[11] The commonly used amount of a catalyst in a reaction batch is very small; moreover, the active centers of the catalytic species react readily with any molecules. Therefore, even little impurities can lead to a decrease of the catalyst's selectivity. Accordingly, the purity of the starting materials has to be ensured before the reaction.
A great advantage of heterogeneous catalysts in comparison to the homogeneous ones is the catalyst's separation from the reaction mixture at the end of the process.[11] Depending on the particular used metal, catalysts are costly and therefore need to be recycled. The separation from the reaction mixture is much more facile in the case of a heterogeneous and thus solid catalyst; in this case, the catalyst can be easily recycled via filtration. Nevertheless, also the heterogeneous catalysts show the

problem of leaching, which causes impurities of the applied metal in the reaction products. In particular, this problem is relevant in the production of pharmaceuticals.

Finally, a general problem in the heterogeneously catalyzed synthesis of fine chemicals is the deficiency of time and money, what makes it difficult to find a convenient catalyst, which fulfills are the requirements of the reaction.[11]

How to find the "right" heterogeneous catalyst?

A multiplicity of different parameters can be chosen to find the "right" catalyst.[11]
First of all, the choice of the metal plays an important role. Commonly used metals are e.g. palladium, platinum, nickel, copper, rhodium and ruthenium. Furthermore, also complexes consisting of two different metals are applied.
Then, the type of the catalyst has to be specified: Besides powdery catalysts, supported and skeletal compounds are suitable. If a supported catalyst is used, the loading of the metal has to be specified; moreover, different types of supports are possible, e.g. silica, alumina or active carbon.
With regard to the active metal, different aspects have to be considered: Besides the surface area, the dispersion is an important parameter. Moreover, the size of the metallic crystallites has to be determined and it has to be investigated, if the metal is placed inside or outside of the pores of the support material. Finally, it is necessary to know the oxidation state of the metal, if the metal exists in its reduced or its unreduced form.
Concerning the support material, parameters like the particle size, the surface area, the structure of the pores (volume and size distribution) and the acid-base properties have to be considered.[11]
The choice of the reaction conditions has a considerable influence on the performance of the catalyst.[11] Parameters that can be diversified individually are – besides the solvent – the temperature, the gas pressure (e.g. the hydrogen pressure in hydrogenation reactions), the concentration of substrate and catalyst and, if applicable, additional modifiers. In general, the choice of the solvent is the most

significant parameter; by its variation it is possible to enhance the performance of the catalyst.

The preparation of heterogeneous catalysts

In general, heterogeneous catalysts can be divided into two groups, corresponding to their preparation method: (a) bulk catalysts and (b) supported catalysts.[12]

The preparation of bulk catalysts

In terms of the bulk catalysts, the preparation starts from a liquid solution, which generates a solid by precipitation, whereupon the solid can have either the form of a precipitate or of a gel.[12] The precipitation occurs in three steps, the first one is the supersaturation. In this first step, the precipitation is observed due to any physical transformation (e.g. temperature variation, evaporation of the solvent) or chemical process (e.g. addition of complexing substances, acids or bases). The second step is the nucleation: Here, small stable particles are formed. These particles can become larger or can even aggregate to clusters, what occurs in the third final step, the growth of the particles.
Figure 4 shows the multitude of different parameters, which influence the properties of the precipitated catalyst. The modification of these parameters enables to obtain the desired catalysts.

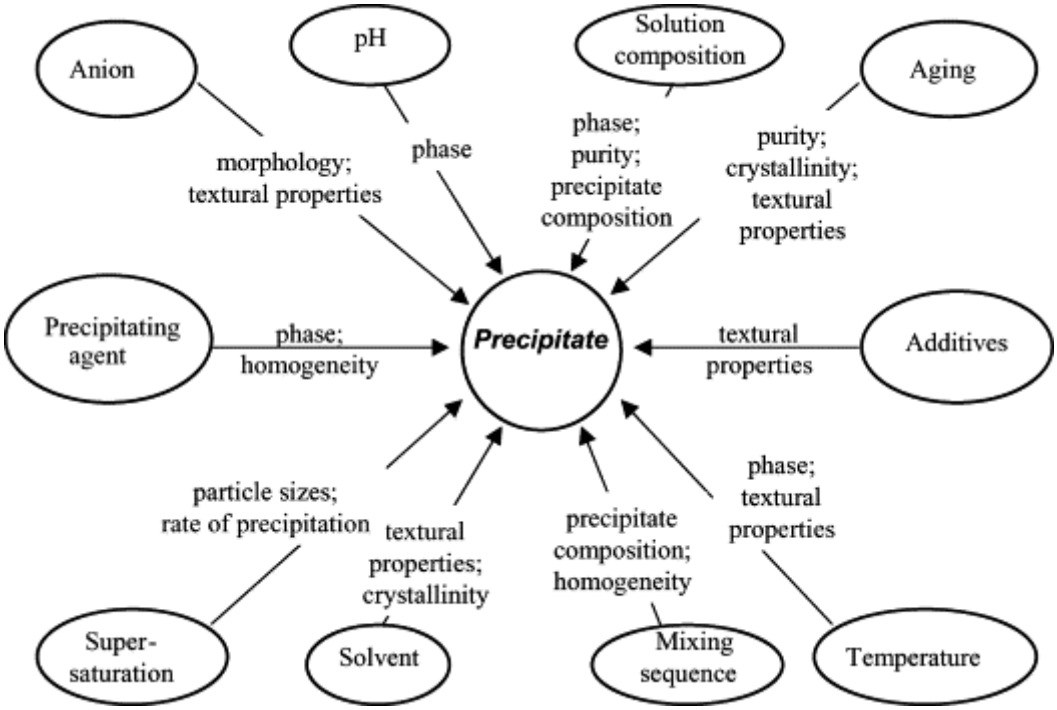

Figure 4: The preparation of precipitated catalysts by variation of different parameters.[12]

For instance, by tuning parameters like the temperature and the solvent it is possible to determine the structural properties of the precipitated catalyst. The supersaturation step has influence on the size of the formed particles as well as on the rate of the precipitation. Moreover, many parameters affect the phase of the precipitated catalyst, like e.g. the pH, the temperature and the composition of the solution.

The preparation of supported catalysts

Supported heterogeneous catalysts are composed of an active phase, which is well dispersed on a carrier material.[12] There are different methods for the preparation, amongst others impregnation, ionic exchange, adsorption and deposition-precipitation.

The impregnation method includes the reaction of the active phase with a solid support material and subsequent drying in order to remove the solvent. There are

two different types of impregnation: The wet impregnation and the incipient wetness impregnation, a scheme of both shown in Figure 5a and 5b.

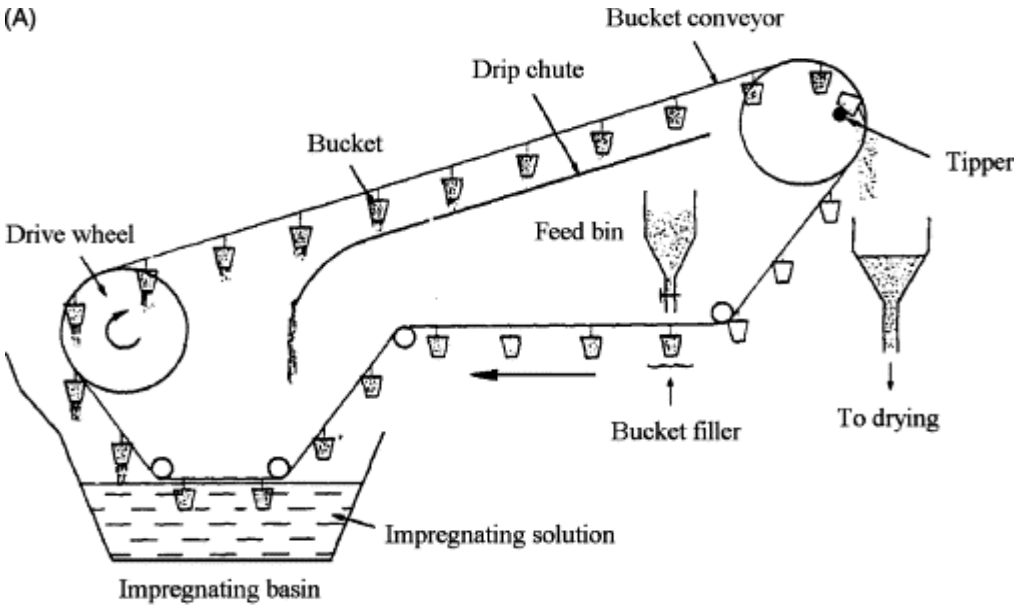

Figure 5a: Wet impregnation.[12]

The two methods differ from each other in terms of the used amount of solution.[12] The wet impregnation – shown in Figure 5a – works with an excess of impregnating solution. After separation of the solid from the solution, the solid is dried in order to remove excess solvent.

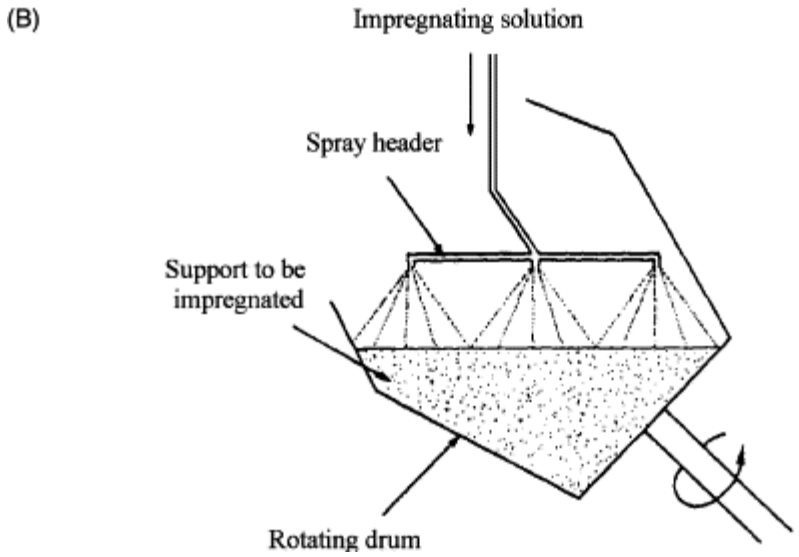

Figure 5b: Incipient wetness impregnation.[12]

The incipient wetness impregnation (Figure 5b), however, requires the same amount of impregnating solution and support material.
The common aspect of both procedures is the influence of the temperature: By tuning the temperature, the solubility of the precursor as well as the viscosity of the impregnating solution can be affected.

Besides the impregnation, the ionic exchange is a further method in order to synthesize supported catalysts.[12] This method considers the exchange of two ion species during the electrostatic interaction between the ionic active species and the surface of a support material.

Adsorption, as a further method for the synthesis of supported catalysts, enables the grafting of an aqueous precursor solution on a support material.[12] The grafting occurs via electrostatic attraction between the ionic precursor and the surface of the support.

The last method in this context is the deposition-precipitation method.[12] Here, the precipitation is achieved by adding alkali solution to the corresponding salt, whereat the latter is applied in the form of powder or particles. An interaction between the hydroxyl groups of the support (e.g. silanol groups of a silica support) and the ionic species of the solution leads to a formation of an active phase, which is ideally homogeneous. The homogeneity can be controlled by substitution of the alkali; as substitute urea is used. The hydrolysis of urea provides the required hydroxyl groups.

Motivation and aim of the work

The target of this work is the design of highly-selective heterogeneized catalysts for the production of fine chemicals.

The first part of the studies deals with the development of heterogeneized “hybrid catalysts” for hydrogenation reactions of prochiral substrates. These “hybrid catalysts” consist of PdNPs and Rh “single sites”, both immobilized on various silica support materials. Regarding the support material, powdery silicas (e.g. MCM-41, SBA-15, Davisil) as well as silica monoliths are tested. Using different immobilization methods (impregnation, Ionic Exchange, Chemical Vapour Deposition), high metal loadings are aspired.

Within the second part of the work, chiral silica-supported Cu catalysts are designed for cyclopropanation reactions. The latter are industrially of great interest due to their large field of application, e.g. as insecticides, drugs and terpenes.

The third part of this work deals solely with silica monoliths. Within the scope of a three-month stay at the *Institute Charles Gerhardt* in Montpellier (France), silica monoliths have been grafted and tested as catalysts in the dehydration reaction of fructose to 5-hydroxymethylfurfural (HMF). This reaction is of great importance, as HMF represents an attractive precursor for a multitude of chemical products and intermediates, e.g. for the polymer and pharmaceutical industry. Starting from simple renewable raw materials (fructose, glucose, sucrose, cellulose), HMF is a potential alternative for many petrochemistry-based compounds and thus future-oriented.

References

[1] A. T. Bell, *Science* **2003**, *Vol. 299*, 1688-1691.

[2] H. H. Kung, M. C. Kung, *Catalysis Today* **2004**, *97*, 219-224.

[3] E. Z. Eisenmeser, D. A. Bosco, M. Akke, D. Kern, *Science* **2002**, *295*, 1520-1523.

[4] B. C. Gates, *Journal of Molecular Catalysis A: Chemical* **2000**, *163,* 55-65.

[5] A. S. Eppler, G. Rupprechter, L. Guczi, G. A. Somorjai, *J. Phys. Chem. B* **1997**, *101*, 9973-9977.

[6] A. Katz, M. E. Davis, *Nature* **2000**, *403*, 286-289.

[7] V. Dufaud, M. E. Davis, *J. Am. Chem. Soc.* **2003**, *125*, 9403-9413.

[8] G. C. Bond, D. T. Thompson, *Catal. Rev. Sci. Eng.* **1999**, *41*, 319-388.

[9] M. Valden, X. Lai, D. W. Goodman, *Science* **1998**, *281*, 1647-1650.

[10] H. Topsoe, B. S. Clausen, F. Massoth, in *Catalysis: Science and Technology*, Vol. 11, J. R. Anderson, M. Boudart, Eds. (Springer, New York, **1996**).

[11] H.-U. Blaser, *Catalysis Today* **2000**, *60*, 161-165.

[12] M. Campanati, G. Fornasari, A. Vaccari, *Catalysis Today* **2003**, *77*, 299-314.

CHAPTER 1:

Design, characterization and application of heterogeneized Rh^{I}-Pd^{0}/SiO_2 “hybrid catalysts”

General part

1. Metal nanoparticles and their impact on catalysis

In recent years, metal nanoparticles (NPs) became more and more important, as they represent a bridge between homogeneous and heterogeneous catalysis; thus, the field of catalysis using NPs is often named as "semi-heterogeneous catalysis".[1] NPs have a broad catalytic scope of application in various fields of organic synthesis, e.g. hydrogenation reactions, coupling reactions of C–C bonds (Heck C–C coupling) and the heterogeneously catalyzed oxidation of carbon monoxide by AuNPs.[1]
Starting from a metal salt, NPs are generally prepared by immobilization on diverse support materials, like silica, oxides, charcoal or zeolites. Recent studies report about numerous renewals in the design of NPs.[1] A large quantity of new stabilizers (e.g. polymers, dendrimers, micelles), reaction media (e.g. ionic liquids) and support materials (e.g. carbon nanotubes) has been found.

1.1 The historical development of metal NPs – an overview

For the first time, the application of NPs in catalysis was reported in the 19th century: AgNPs and PtNPs have been foremost used in photography and in the decomposition of hydrogen peroxide, respectively.[1] Further innovative applications of NPs were the reduction of nitrobenzene in 1940 by *Nord* [2a-c] and the hydrogen-atom transfer between benzene and cyclohexane as well as the oxygen-atom transfer between carbon monoxide and carbon dioxide, both catalyzed by AuNPs and discovered by *Parravano* in 1970.[3] Finally, *Haruta* succeeded with his application of AuNPs in the oxidation of carbon monoxide under mild and ecologically beneficial conditions (low temperatures; oxygen as oxidizing agent).[4a-d] Moreover, AuNPs have been used in the hydrogenation of olefins.[5a-c] In the 1980s, NPs entered more and more into various fields of catalysis, like redox- and photocatalysis,[6a-g] hydrogenation of unsaturated substrates and oxidation.[7a-b] One decade later, in the mid-1990s, *Reetz* discovered the first innovative catalytic application of PdNPs: The Heck-coupling of C–C bonds.[8a-f]

1.2 Supported PdNPs

Supported highly-dispersed PdNPs are suitable for a large number of applications like catalysts and sensors as well as in the field of non-linear optics.[9,10-16] They show catalytically and technically interesting properties, which can be individually adjusted by the variation of different parameters, e.g. the choice of the support material, the immobilization method of the PdNPs onto the support and finally also the NP size.[9]

Related to the support material, two important requirements have to be fulfilled, that is on the one hand the thermal and chemical stability during the reaction and on the other hand the "right" structure.[9] The latter means that for an optimal application in catalysis an all-over dispersion of the active sites on the support's surface is obligatory; moreover, the active sites must be easily accessible for the substrate.[9]
Mesoporous support materials with a high surface area are greatly suitable. Their surface area is larger than 100 $m^2 g^{-1}$; furthermore, their pore size amounts to more than 2 nm.[9] In various studies, mesoporous silica supports have proved to be one of the most convenient support materials for the immobilization of PdNPs; they afford high surface areas larger than 600 $m^2 g^{-1}$ and pore sizes between 1 and 20 nm; moreover, they are exceedingly thermally and chemically stable.[17-21]

Further issues that play an important role are the incorporation of the PdNPs in the silica support material and also the metal loading.[12,22,23]

Palladium is a very attractive metal in catalysis, particularly in C–C coupling reactions, e.g. the Heck-Mizoroki coupling, which can be catalyzed by supported PdNPs.[24,25] It could be proved that the use of other transition metals instead of palladium do not achieve such good results pertaining to the catalytic activity.[24]
However, the recycling of supported PdNPs is still a problem. The TON of such catalysts is low; they can be reused only few times, which is caused by aggregation

of the PdNPs on the one hand and, on the other hand, by leaching of the NPs from the support material.[16,24,26]

1.2.1 Silica supported PdNPs

1.2.1.1 Preparation of the silica support materials

The silica support materials are prepared by the dropwise addition of tetraethoxysilane (TEOS) to a system of dodecylamine, acetonitrile and water.[9,18] After stirring at RT for 20 h, the silica is obtained in the form of a white solid. Filtering, drying (24 h, 100 °C) and extraction with ethanol give the silica in its final form.

1.2.1.2 Immobilization of PdNPs onto silica

Silica supported PdNPs can be prepared by various methods. Some of them include the addition of a reducing agent, in order to obtain Pd^0 from Pd^{II}.[9] Other methods work without reductive.[9]

V. L. Nguyen et al. report about the synthesis of PdNPs, using Na_2PdCl_4 as palladium source and precursor, as well as ethylene glycol as reducing agent.[27] Moreover, the NPs are stabilized by a polymer, poly(*N*-vinyl-2-pyrrolidone) (PVP).[27] *V. L. Nguyen et al.* found that the size as well as the shape of the PdNPs can be controlled and regulated by the choice of the reaction parameters (t, T) and, moreover, by the use of an additional agent, like $AgNO_3$, $FeCl_3$ or NaI.[27] It was observed that the addition of a small amount of $AgNO_3$ enables the control of size and shape of the PdNPs.[27]

Further immobilization methods are the “co-gelation” and the “post-synthesis wetness impregnation” that both have been tested by *Barau et al.*[9] The “co-gelation” method is a sol-gel method, which allows the simultaneous hydrolysis and condensation of a

complex that includes Pd^{2+} and methoxy groups (-OCH_2), whereat the latter can be hydrolyzed.[28] Tetraethoxysilane (TEOS) is used as silica source.[9,28] The "post-synthesis wetness impregnation" method describes the treatment of the silica support material with a Pd^{2+}/ethanol solution whereat ethanol acts as the reducing agent for Pd^{2+}.[9]

Another very common immobilization method is the ionic exchange, amongst others reported by *Yuranov et al.*[19,29] Tetraammine platinum(II) chloride ($Pd(NH_3)_4Cl_2$) or palladium acetate ($Pd(CH_3COO)_2$), available as aqueous solution, are used as palladium source.[19,29] The procedure includes the deposition of palladium on the mesoporous silica surface as well as the oxidative calcination (in air, at 550 °C) and reduction (in H_2, at 300 °C), in order to obtain the dispersed PdNPs.[19,29]
Kim et al. report about the synthesis of monodispersed PdNPs.[30] The addition of trioctylphosphine (TOP) as surfactant to $Pd(acac)_2$ gives a metal-surfactant complex which decomposes at higher temperatures and yields monodispersed PdNPs with various particle sizes (3.5 – 7 nm).[30]

1.3 Catalytic application of PdNPs

PdNPs have broad application in organic synthesis, especially in reactions with C–C and C–N bond formations.[1] The use of PdNPs affords the easy functionalization of olefins, alkynes and aromatics and hence a facile access to the production of pharmaceuticals. The important aspect in this regard is the complete recycling of the palladium catalyst, otherwise traces of the metal would contaminate the drug as the final product. The advantage of the use of supported PdNPs is that one of the heterogeneous catalysis: The catalyst can be easily separated from the reaction products via filtration and recycled several times.
One very important and common catalytic application of PdNPs are hydrogenation reactions of unsaturated substrates.[31a-b] It has been shown that only PdNPs have

the ability to catalyze hydrogenation reactions of alkenes, in contrast single crystals of palladium turned out to be inefficient.[31a-b]

A very significant reaction that is catalyzed by PdNPs is the Heck reaction.[1,32a-b] The Heck reaction has a broad range of industrial application, e.g. in the field of herbicides,[33] anti-inflamatorys[34] and anti-asthma agents like singulair.[35] *Zhang et al.* found a new microemulsion system for the Heck reaction of butyl acrylate with iodobenzene.[36] The system consists of water as reaction medium, TX-100 as surfactant and 1-butyl-3-methylimidazolium hexafluorophosphate ([BMIM]PF_6) as ionic liquid.[36] The TX-100 has the task to reduce the Pd^{II} to Pd^0 and to stabilize the PdNPs.[36] The results showed that the microemulsion system is optimally suitable for the ligand-free Heck reaction; the PdNPs could be recycled up to four times without loss of activity.[36]

1.4 Innovations in the field of NPs

1.4.1 Stabilizers

1.4.1.1 Polymers

One possible stabilizer for NPs are polymers.[1] They stabilize the NPs in two different ways: On the one hand the stabilization occurs by the bulkiness of the polymeric structure, on the other hand a weak binding between the NPs and the polymer can be observed.
The most known and most used stabilizing polymer is poly(*N*-vinyl-2-pyrrolidone) (PVP) (Figure 1).[1,37]

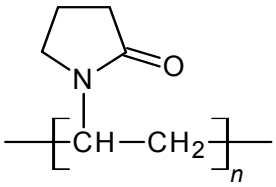

Figure 1: PVP.[1]

Common NPs that can be stabilized by PVP are Pt-, Pd- and RhNPs. All mentioned PVP-stabilized NPs show high activity in hydrogenation reactions of olefins and benzene.[38] The reactions can be carried out at mild conditions (T = 40 °C), moreover the PVP-stabilized NPs can be recycled without difficulty.
Different reaction parameters, e.g. the size of the PVP-stabilized NPs, can be investigated.[1] With respect to the Suzuki-reaction, it was found that a small size of 3 nm leads to an improvement of the catalysts activity.[39a-b]

In the 1970s, an innovative idea of NPs has been developed: the concept of the core-shell-NPs.[1,40a-c] This concept includes the idea of two different metals, e.g. Au and Pd, that are part of the same NP. In this context, *Toshima et al.* reported about the PVP-stabilized Au-PdNPs; these bimetallic NPs show a core of Au and a shell of Pd.[41a-c] The advantage of such bimetallic PVP-stabilized core-shell-NPs is the improved catalytic activity compared to the one-metal-NPs.[1] In addition to the mentioned core-shell-concept (Au core, Pd shell), it is also possible to create bimetallic structures that show a Pd core and a Au shell.[41a-c]

1.4.1.2 Dendrimers

In 1998, it was found by *Crooks*, *Tomalia* and *Esumi* that dendrimers can serve as stabilizers for NPs as they are able to incorporate them, either in the interior or in the exterior dendritic part.[1,42a-o,43a-e] *Crooks et al.* synthesized dendrimer-stabilized PdNPs, using poly(amidoamine) (PAMAM) as dendrimer (Figure 2).[42a-o]

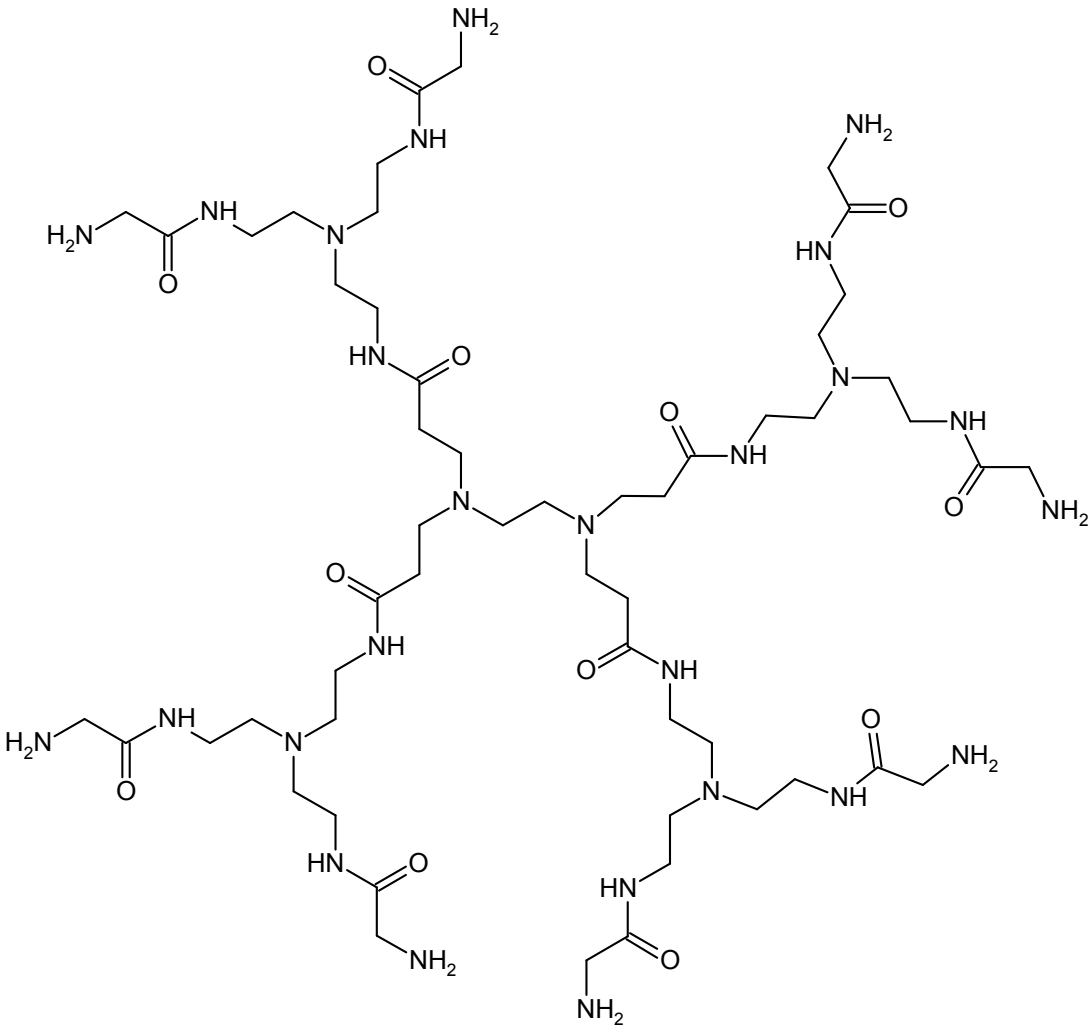

Figure 2: PAMAM dendrimer.[1]

For this purpose Pd^{2+} is coordinated to the PAMAM dendrimer; the complexation takes place at the inner nitrogen atoms of the tertiary amines of PAMAM.[42a-o] Subsequently, the Pd^{2+} ions are reduced to Pd^0 using $NaBH_4$ as reduction agent. Finally, the palladium atoms form a cluster of NPs in the inner part of the PAMAM dendrimer.

Such PAMAM-dendrimer stabilized PdNPs are able to catalyze hydrogenation reactions with high selectivity, e.g. of allylic alcohol and *N*-isopropyl acrylamide.[1]

1.4.1.3 Ligands

PdNPs in combination with stabilizing ligands like polyoxometallates[44a-h] and cyclodextrins[45a-c] show high catalytic activity in the hydrogenation of unsaturated substrates and in the Suzuki-, Heck- and Stille-reaction.[1] Using dodecathiolates as ligands, the stabilized PdNPs are able to catalyze the Suzuki-reaction even at room temperature, moreover the dodecathiolate-PdNPs can be recycled and still show high activity after several cycles.[46]

1.4.1.4 Micelles, microemulsions and surfactants

A further stabilizer for NPs are surfactants, as it could be shown by *Crooks et al.*[47a-e] and *Gladysz et al.*[48a-b] The stabilizing fluoro surfactants for PdNPs are dissolved in a microemulsion system consisting of water and supercritical CO_2 ($scCO_2$).[1] It has been demonstrated that such stabilized PdNPs catalyze e.g. hydrogenation reactions of olefins[49a-c] and citral[50] whereat the hydrogen assumes the role of the reducing agent for Pd^{II} to Pd^0 as well as for the olefin.[1] The following scheme shows the PdNP-catalyzed hydrogenation of 10-(3-propenyl) anthracene which is carried out in a microemulsion system (Figure 3).[51]

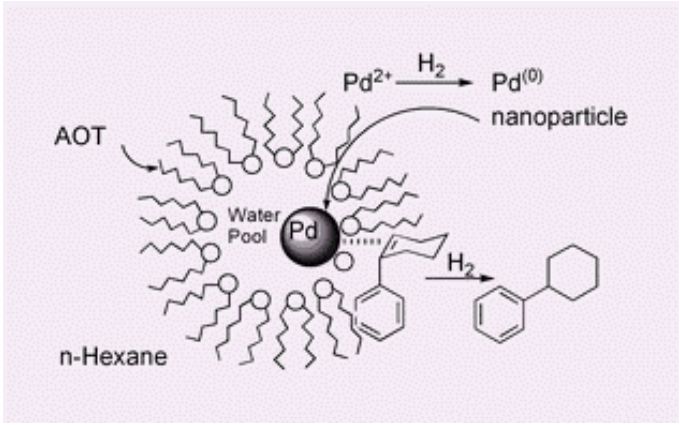

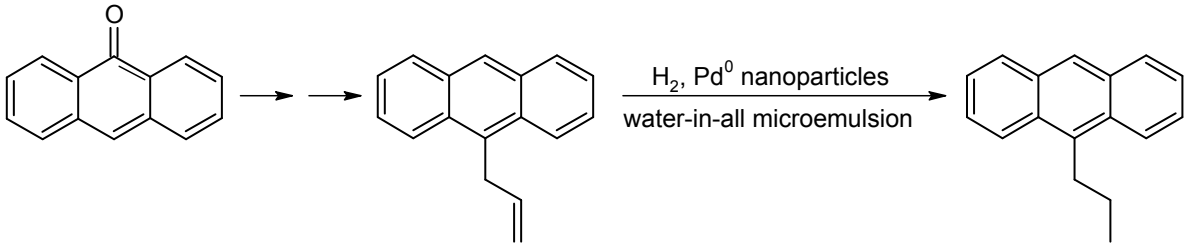

Figure 3: Hydrogenation of 10-(3-propenyl) anthracene, catalyzed by PdNPs in a microemulsion system.[51]

Yoon et al. could demonstrate that the above-mentioned system is able to catalyze the hydrogenation of 10-(3-propenyl) anthracene much faster in comparison to Pd/C.[1,51]

Other applications of surfactant-stabilized PdNPs are e.g. the oxidation of *N*,*N*,*N'*,*N'*-tetramethyl-*p*-phenylenediamine (TMPD)[52] and the selective hydrogenation of functional olefins in a microemulsion containing water and $scCO_2$[53].

1.4.2 Ionic liquids as media

Ionic liquids (ILs) are anhydrous organic salts with relatively low melting points, below or around 100 °C.[54,55] They show comparable properties like common inorganic salts at by far higher temperatures of 300-600 °C.[54,55] ILs have a very broad industrial application in many various fields, e.g. in electrochemistry, in the biological field (e.g. development of drugs, conversion of biomass), in analytics, in engineering (e.g. application as coatings and lubricants) and of course as solvent as well as in the field of catalysis.[54]

Also in the field of PdNP-catalyzed reactions, ILs have turned out to be advantageous concerning the choice of the reaction media.[1] The sterically demanding cations (e.g. imidazolium cation (Figure 4)) of the ILs stabilize the NPs.[1]

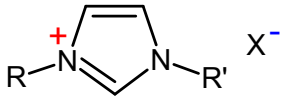

R = *n*Bu, R' = Me or *n*Bu

Figure 4: Imidazolium salt.[1]

By modification of the cation's substituents, different parameters of the PdNPs can be individually varied, like the size, the stabilization or the solubility.[1] The reaction between the imidazolium salt and the Pd^{II} species (e.g. palladium acetate) gives a palladium-*N*-heterocyclic carbene complex which subsequently decomposes to PdNPs at high temperatures, as shown in Figure 5.[1]

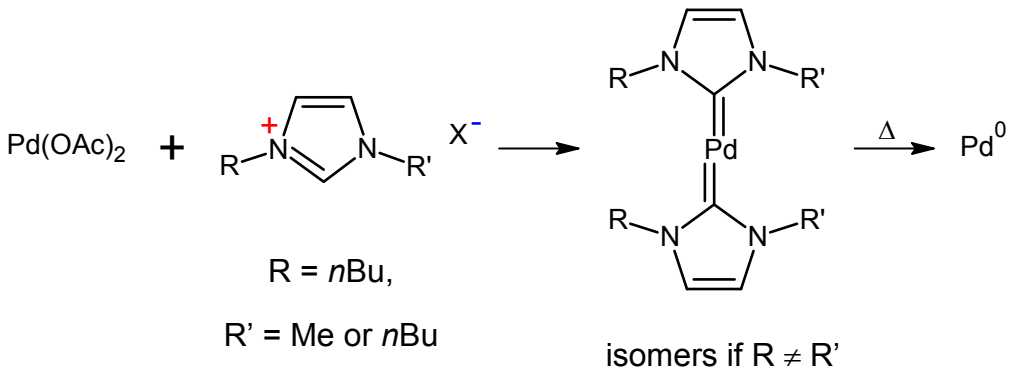

Figure 5: Formation of palladium carbene complex and subsequent thermal decomposition to PdNPs.[1]

1.4.3 Solid support materials

1.4.3.1 Carbon supports

As a very common support material, charcoal is often used e.g. for the immobilization of PdNPs (Pd/C).[1] The very simple impregnation procedure is performed by stirring the charcoal in the corresponding NP suspension; the latter is generally prepared by reduction of quaternary ammonium salts of Pd^{2+} in THF.[1]

Pd/C is catalytically applied in many different reactions, in particular in hydrogenation reactions[47a-e] and C–C coupling reactions (e.g. Suzuki reaction)[48a-b].

Various parameters influence the activity of Pd/C, like the dispersion of palladium, the impregnation method or the pretreatment of the charcoal.[1] Concerning the mechanism, it was observed that the Pd/C-catalyzed reactions occur quasi-homogeneously.[49a-c] When starting the reaction, the palladium is well dissolved in solution (in the form of small palladium species) which results in a high concentration of Pd.[49a-c] Then, due to the leaching and subsequent redeposition of the Pd species, the concentration decreases to a minimum (< 1 ppm).[49a-c] Because of the redeposition the palladium can be easily recycled, however the resultant decrease of activity makes a reutilization difficult.[49a-c]

1.4.3.2 Oxide supports

Another very common support material for NPs are the metal oxide supports of a variety of elements, e.g. Si, Al, Ti, Zr, Ca, Mg and Zn.[1] These metal oxides are available in many different forms, e.g. SiO_2 aerogels, sol-gels, high-surface silica, MCM-41 mesoporous silicates, zeolites (SiO_2, Al_2O_3) or molecular sieves.[1] Such oxide-supported NPs are catalytically applied in hydrogenation reactions of unsaturated substrates, C–C coupling reactions (e.g. Heck reaction) and oxidations of carbon monoxide and alcohols with molecular oxygen as oxidizing agent.[1]

The use of oxide-supported NPs has several advantages that are typical for heterogeneous catalysis: The catalysts are stable even at high temperatures; moreover, they can be easily separated and recycled after catalysis.[1] Another advantage of such heterogeneized catalysts is the so-called “bottom-up approach” of the synthesis of NPs.[1,50] The latter expression is used in the nanotechnology and describes the behaviour of atoms or molecules to form macromolecular structures.[50]

2. Silica supports

Silica support materials are likely and often used in heterogeneous catalysis, as they feature a multitude of advantages, for instance their high robustness and their easy way of preparation.[56] Further merits are their high surface area as well as their property not to swell in the presence of organic solvents. Their thermal stability and their structural flexibility can be emphasized. One of the most important issues is the ability of silica to bind to a multitude of metals. The latter enables the access to numerous heterogeneous catalysts.
In the following, two popular and often applied mesoporous silica support materials are described in detail, MCM-41 and SBA-15.

2.1 MCM-41

MCM-41 is known as mesoporous support material since 1992.[57,58] Due to its outstanding properties, it is very attractive for catalysis. MCM-41 offers a remarkable regular pore structure with a pore diameter of 2-10 nm.[58,59] This attribute is beneficial particularly with regard to the adsorption of gases or vapours.[60,61] Moreover, MCM-41 has a highly specific surface (up to 1500 m^2 g^{-1}) as well as a specific pore volume (up to 1.3 mL g^{-1}).[59] Finally, it is exceedingly stable, even at high temperatures.[59] Because of all these excellent properties, MCM-41 is often and gladly used as support material in catalysis. The incorporation of metals, e.g. Ti or Al, enables the variation and the desired adjustment of the properties.[62-64]

In general, it is advantageous and desirable to prepare huge amounts of MCM-41 in a short time.[59] For this purpose, *Grün et al.* developed two innovative methods, one homogeneous and one heterogeneous, which allow the precise control of the silica's porosity and morphology.[59]

Both methods include the use of tetra-*n*-alkoxysilanes as silica source, i.e. tetraethoxysilane (TEOS) or rather tetra-*n*-propoxysilane (TPS), which are added to an aqueous solution of a cationic surfactant. The latter serves as a template that is thermally removed via calcination subsequent to the formation of the silica hydrogel.
In terms of the heterogeneous version, the synthesis is performed in water. The tetra-*n*-alkoxysilane is indissoluble in the reaction medium; thus, the formed particles of MCM-41 show an irregular structure. However, the homogeneous type, using a low-boiling alcohol as co-solvent (e.g. ethanol or isopropanol), gives the MCM-41 particles in a spherical regular form. The co-solvent has the task to solve the tetra-*n*-alkoxysilane.
The size, the morphology and the distribution of the MCM-41 particles are analyzed via *Scanning Electron Microscopy (SEM)*. *Grün et al.* could prove that, using the homogeneous preparation method, spherical, regularly formed particles are obtained (Figure 6).

(a)

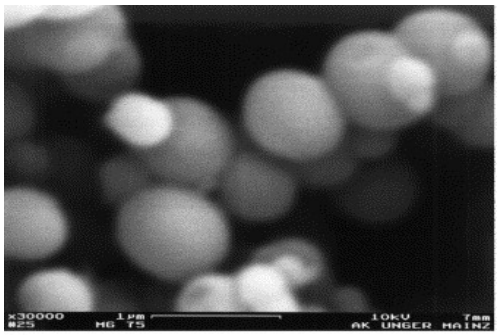

(b)

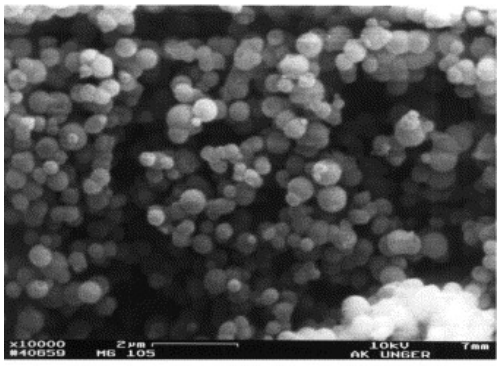

Figure 6: SEM of spherical MCM-41; (a) prepared with *n*-hexadecyltrimethylammonium bromide, (b) prepared with *n*-hexadecylpyridinium chloride.[59]

The heterogeneous as well as the homogeneous method offer a multitude of advantages; besides the short reaction times, the two methods facilitate both the reproducibility and the large-scale preparation.[59] The latter is significant for the industrial application of MCM-41.

Due to their regular spherical nature, the MCM-41 particles are interesting species in the field of analytical separation, e.g. *High-Pressure Liquid Chromatography (HPLC)* or *Supercritical Fluid Chromatography (SFC)*. Moreover, MCM-41 is suitable as adsorbent for the adsorption of gases; further applications can be found in the delivery of drugs, in the preparation of nanostructured materials as well as in the field of catalysis.[65-67]

Regarding the analysis of the MCM-41 materials via *X-ray diffraction*, characteristic patterns for MCM-41 are obtained, showing typical Bragg peaks from 2.5 to 7.0° 2θ (Figure 7 (a) and (b)).[59] These peaks prove the ordered structure and the regular arrangement of the mesopores in MCM-41.

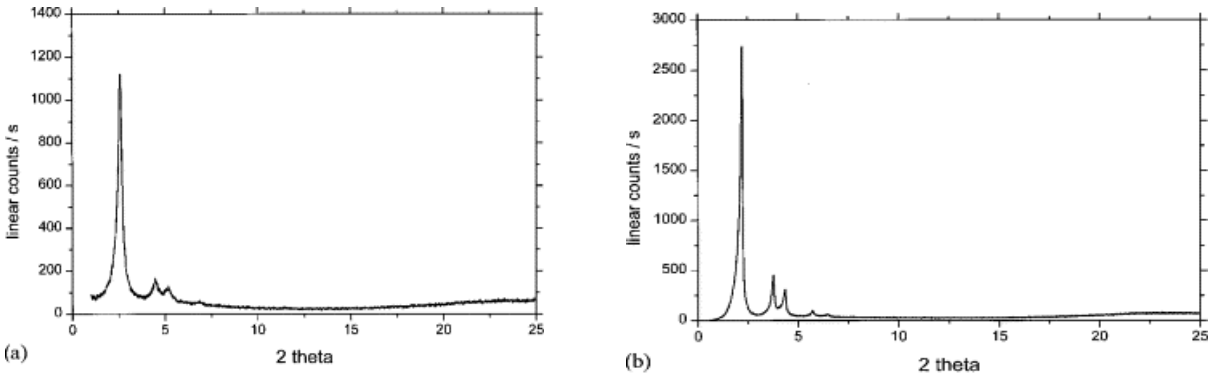

Figure 7: X-ray diffraction patterns of MCM-41,
(a) prepared with *n*-hexadecyltrimethylammonium bromide as template,
(b) prepared with *n*-hexadecylpyridinium chloride as template.[59]

A further analytical method for the investigation of MCM-41 materials is the nitrogen adsorption-desorption. The corresponding isotherms show a rather linear course at the beginning, before featuring an abrupt increase at higher nitrogen pressures

(Figure 8 (a) and (b)).[59] The latter is induced by the capillary condensation, which occurs inside the mesopores. At relative pressures P/P_0 from 0.4, the isotherms do not show an increase anymore, owing to the filling of the pores, which takes place in a confined P/P_0 region.

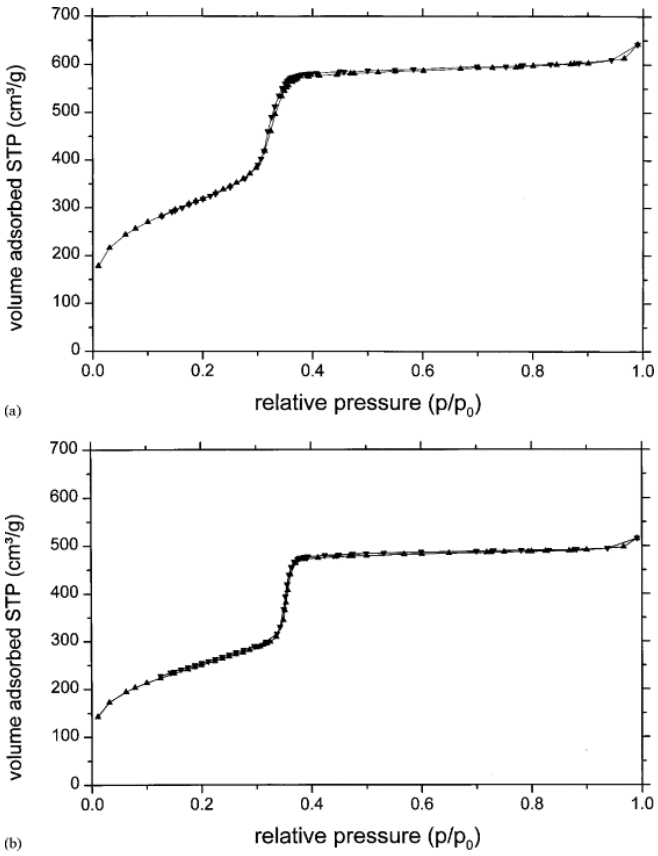

Figure 8: Nitrogen adsorption (▲) and desorption(▼) isotherms of MCM-41,
(a) prepared with *n*-hexadecyltrimethylammonium bromide as template,
(b) prepared with *n*-hexadecylpyridinium chloride as template.[59]

The regular uniform pore structure of MCM-41 allows a versatile field of application, as already mentioned above.[65-67,80] MCM-41 shows hexagonal cylindrical pores, which are not connected. Therefore, MCM-41 serves as a reference system when nanoporous materials are investigated with regard to the adsorption of gas.[81]

2.2 SBA-15

The ordered hexagonal mesoporous silica SBA-15 was discovered in 1998 by *Stucky et al.*[68,69,70] Starting from the triblock copolymers polyethylene oxide – polypropylene oxide – polyethylene oxide, i.e. EO_n–PO_m–EO_n, as templating agent, a silica with outstanding properties was built up. For instance, SBA-15 features a distinguished hydrothermal stability; its structure remains stable up to 48 h in boiling water.[69] Using the copolymer EO_{20}–PO_{70}–EO_{20}, the resulting SBA-15 shows the following properties: The Brunauer-Emmett-Teller (BET) surface areas range between 690 and 920 m^2/g, the pore volumes amount to 0.80-1.23 mL/g and the pore sizes add up to 47-89 Å. Moreover, the pore walls show an extraordinary thickness ranging between 31 and 53 Å. An increase of the temperature from 35 to 100 °C leads to an augmentation of the pore size on the one hand and, on the other hand, to a decrease of the thickness of the pore walls. Besides the outstanding hydrothermal stability, SBA-15 shows a multitude of further remarkable properties, e.g. its simple preparation as well as its large pore size, which enables an easy transport of the molecules. Due to all these particular characteristics, SBA-15 is gladly used for a great number of applications, for instance in catalysis, as support material in order to graft catalysts, as template in the field of metal nanowires or as sorbent for heavy metals or rather proteins.

SBA-15 is synthesized in three steps, as shown in Figure 9.[71]

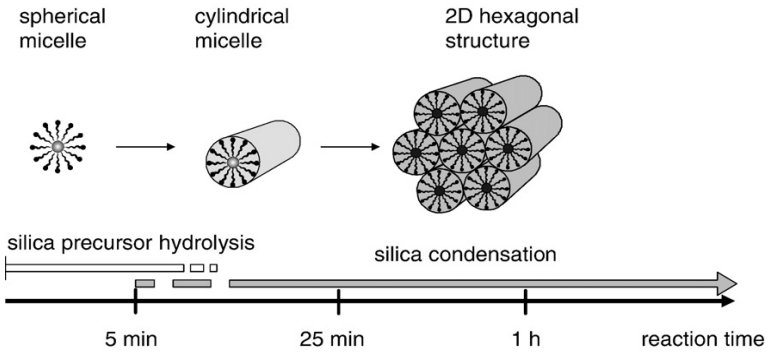

Figure 9: Three-step synthesis of SBA-15.[71]

The three steps are the formation of (a) the spherical micelle, (b) the cylindrical micelle and (c) the two-dimensional hexagonal structure. It could be shown via *small angle X-ray scattering (SAXS)* that the two-dimensional hexagonal structure is formed after 20-30 min.[71] The formation of SBA-15 was monitored over a period of 20 h. As apparent from Figure 9, within the first 15 min, no formation of any ordered phase was observed. The addition of tetraethylorthosilicate (TEOS) entails the precipitation of a white solid after ca. 20 min, which is reflected in the corresponding SAXS pattern by the significant intense peak 10 (Figure 10 (a)) as well as the two smaller peaks 20 and 21 with a lower intensity (Figure 10 (b)).

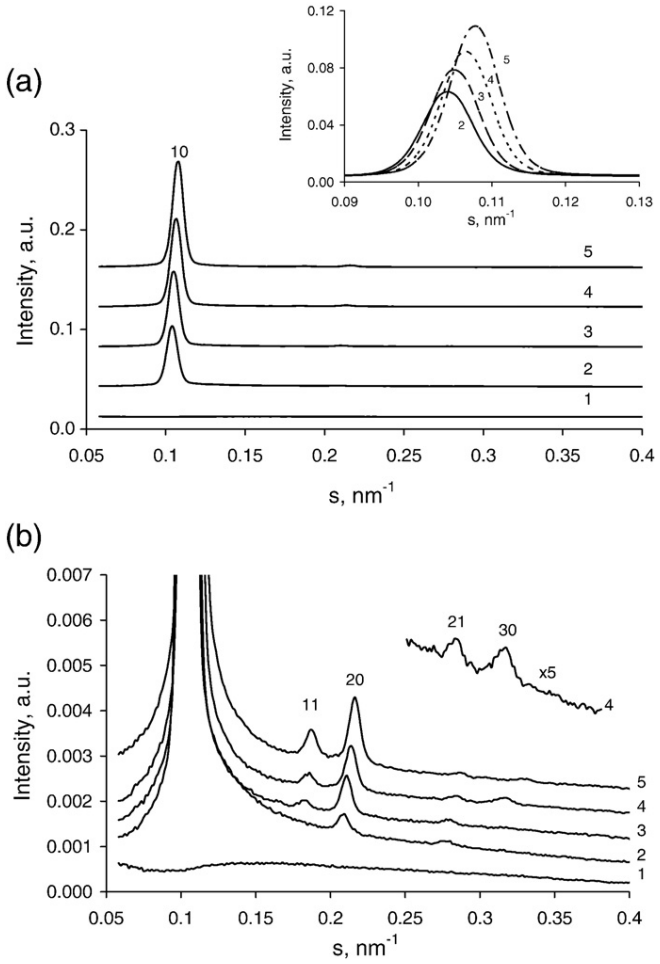

Figure 10: (a) SAXS patterns of SBA-15.
1: after 0.3 h, 2: after 1.2 h, 3: after 3.5 h, 4: after 15.6 h, 5: after 22.7 h.
(b) The same expanded SAXS patterns of SBA-15.[71]

It was noticed that the intensity of the peaks 11, 20, 21 and 30 changes with an extension of the reaction time (Figure 10 (b)). This observation can be associated with the condensation reactions, which occur in the walls of the pores. Hence, the ordered structure of SBA-15 is formed, offering a high density and hexagonal pores.

Analyzing the SBA-15 materials by *Scanning Electron Microscopy (SEM)* and *Transmission Electron Microscopy (TEM)*, the hexagonal structure is emphasized (Figure 11 (b)).[72] Furthermore, particularly the TEM image shows the hexagonal direction of the channels (Figure 11 (c)).

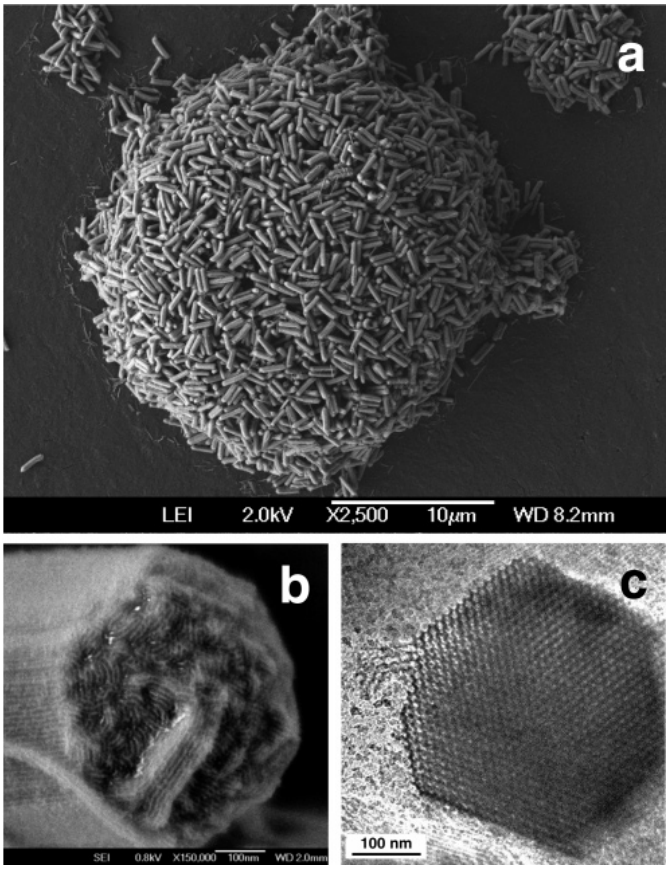

Figure 11: (a) Low-magnification SEM image of calcined SBA-15 (prepared at 100 °C), (b) high-magnification SEM image, (c) TEM.[72]

The two-dimensional hexagonal structure of the SBA-15 materials is evidenced by *X-ray diffraction analysis* as well, showing the characteristic peaks in the corresponding patterns (Figure 12 (A)).[72]

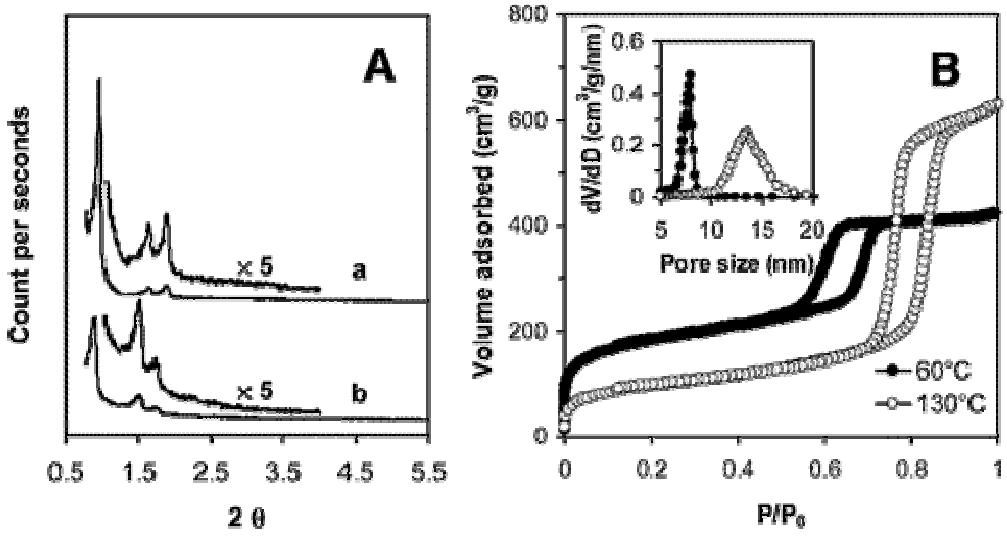

Figure 12: (A) XRD patterns of SBA-15 at (a) 60 °C and (b) 130 °C.
(B) Nitrogen adsorption-desorption isotherms and pore size distributions.[72]

The investigation via *nitrogen adsorption-desorption* demonstrates the characteristic isotherms of ordered mesoporous materials (Figure 12 (B)).[72] Comparing the isotherms at 60 °C and 130 °C, it is evident that a higher temperature entails an increasing relative filling pressure of the pores with nitrogen.[72,73]

Contrary to MCM-41, SBA-15 shows a connected pore system; therefore, it serves as a model system, in order to investigate the impact of the pore connectivity.[81] In particular, SBA-15 features nanopores, which are connected via transversal channels.[81]

3. Rh^{I}-Pd^{0}/SiO_2 "hybrid catalysts"

Recent studies report about the application of "silica-supported catalysts that combine a grafted rhodium complex and palladium nanoparticles" (cit.).[75] These kind of catalysts are named "hybrid catalysts", due to their double nature. They consist of NPs and single sites, both immobilized on silica support materials. An exemplary scheme of a "hybrid catalyst" is given below (Figure 13).

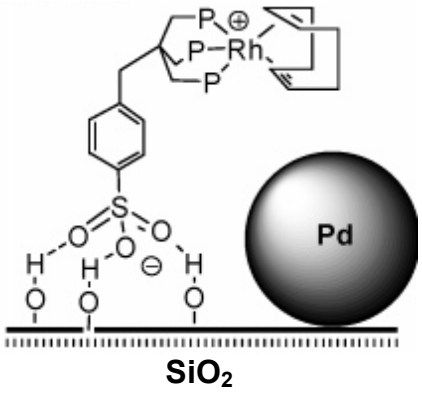

Figure 13: Rh^{I}-Pd^{0}/SiO_2.[75]

As shown in Figure 13, the Rh^{I} species has a sulfonate group, which enables the formation of hydrogen bonds to the terminal silanol groups of the silica support. These hydrogen bonds have proved to be stable and robust.[75] Via this bonding method it is possible to immobilize a variety of transition metal complexes onto silica support materials.[76-78] Recent studies deal with the grafting of rhodium(I) complexes, e.g. Rh(cod)(sulfos), shown in Figure 14.[75,76d]

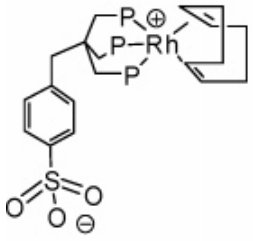

Figure 14: Rh(cod)(sulfos).[75]

The Rh(cod)(sulfos) complex can be immobilized onto silica either alone or in combination with metal NPs, as shown below (Figure 15).

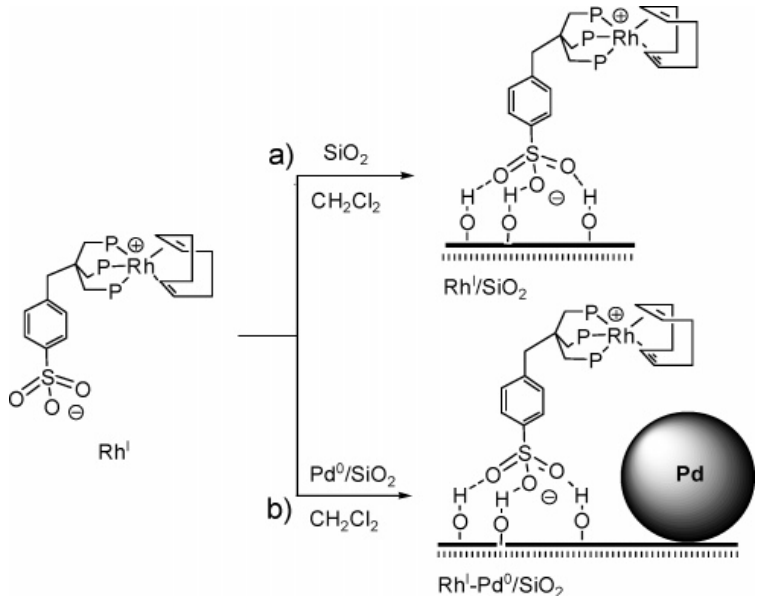

Figure 15: Rh(cod)(sulfos), (a) grafting of Rh(cod)(sulfos) onto silica, (b) grafting of Rh(cod)(sulfos) onto silica in combination with PdNPs.[75]

All three catalysts – Pd^0/SiO_2, Rh^I/SiO_2, and Rh^I-Pd^0/SiO_2 – have been applied in hydrogenation reactions. As a test reaction, the hydrogenation of benzene or toluene, respectively was considered. The results showed that the "hybrid catalysts" are 4 times more active than Pd^0/SiO_2.[75] Rh^I/SiO_2 was completely inactive and therefore inefficient for the reaction.

Regarding the Rh^{I}-Pd^{0}/SiO_2 catalyzed hydrogenation reaction of benzene to cyclohexane, the subsequent mechanism was proposed.[75]

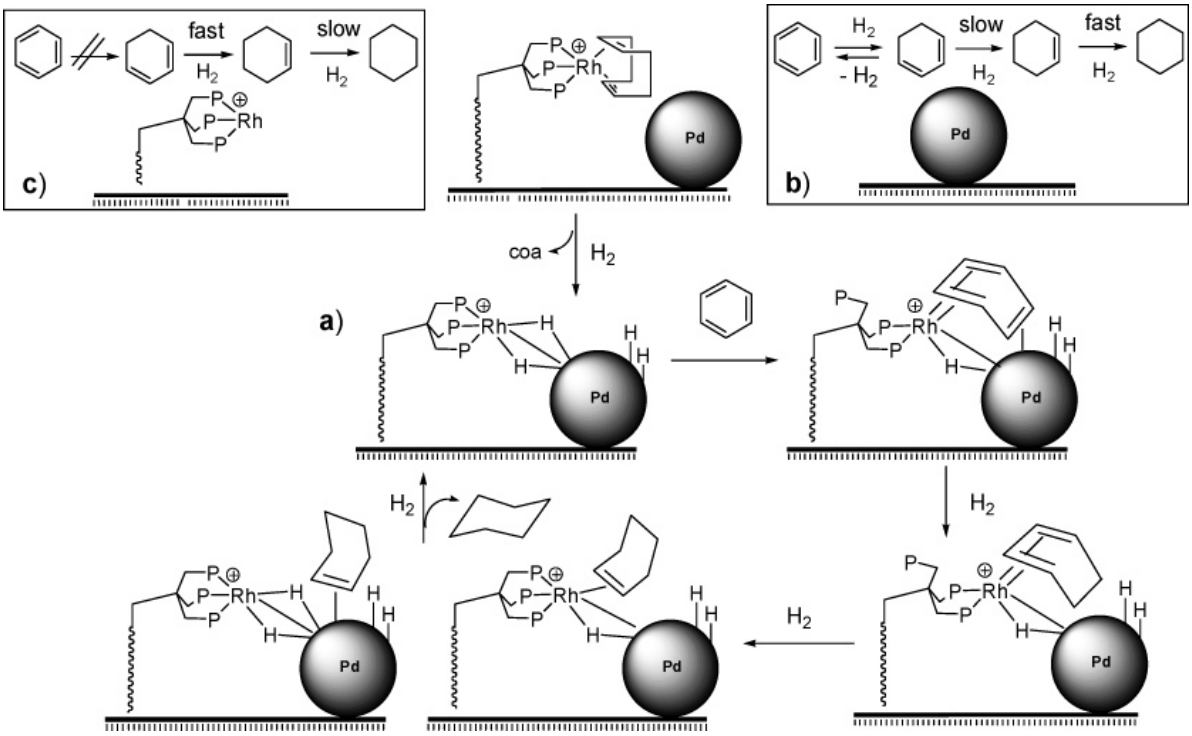

Figure 16: Proposed mechanism for the Rh^{I}-Pd^{0}/SiO_2 catalyzed hydrogenation of benzene to cyclohexane.[75]

In general, the mechanism consists of three parts, demonstrated in Figure 16: a) describes the reaction steps, which are catalyzed by the mixed Rh^{I}-Pd^{0}/SiO_2 "hybrid catalysts", whereas b) considers only the PdNPs and c) solely the Rh^{I} single sites. The reduction of benzene to cyclohexane occurs via a disproportionation of the cyclohexa-1,3-diene, followed by a fast hydrogenation of the cyclohexene to cyclohexane. As shown in Scheme c), the Rh^{I} single sites are not able to catalyze the first hydrogenation step of benzene to cyclohexa-1,3-diene. However, the subsequent step, the hydrogenation to cyclohexene, occurs fast. On the other hand, the pure PdNPs have the ability to catalyze the first hydrogenation step in order to

yield the cyclohexa-1,3-diene; though, the second hydrogenation step occurs slowly. Therefore, it was proposed that the PdNPs and the Rh^I single sites interact with each other in the form of the mixed Rh^I-Pd^0/SiO_2 "hybrid catalyst". Thus, the PdNPs and the Rh^I single sites can emphasize their particular strengths regarding every single step in the hydrogenation of benzene to cyclohexane.
Hence, it is proposed that the first step, the adsorption and the activation of the benzene, is accomplished by the PdNPs. Thereby, the coordination of benzene to the Rh^I single sites is enabled. Subsequently, the reduction of benzene to cyclohexa-1,3-diene occurs. The following hydrogenation of cyclohexa-1,3-diene to cyclohexene is mainly catalyzed by the Rh^I single sites, due to the fast rate of this single step (see also Scheme c)). However, the final step, the hydrogenation to cyclohexane, is predominantly effected by the PdNPs.

Combined Pd-Rh catalysts in a silica sol-gel matrix

The same synergetic effect was observed regarding a combined Pd-Rh catalyst, which is generated in a silica sol-gel matrix.[82] This catalyst is prepared by entrapment of both the Pd and the Rh species in the matrix. After dispersion of the PdNPs, the matrix is treated with $[Rh(cod)(\mu\text{-}Cl)]_2$. In general, catalysts being synthesized in a sol-gel matrix show a multitude of advantages, as they have a broad application field.[83] Moreover, they shaped up as "efficient and user friendly" species (cit.).[83] It could be shown that the combined Pd-Rh catalysts are highly active in hydrogenation reactions, e.g. of toluene and other benzene derivatives.[82]
In terms of the catalysts' preparation, various methods were applied. For instance, the generation of the PdNPs was performed starting from Na_2PdCl_4 as palladium source.[82,84] Reduction with $NaBH_4$ gave the PdNPs. Another preparation method, starting from Na_2PdCl_4 as well, uses $HSi(OEt)_3$ as reducing agent.[85] Subsequent to the dispersion of the PdNPs and the addition of $[Rh(cod)(\mu\text{-}Cl)]_2$, a poly-condensation of $Si(OEt)_4$ occurs. A further method considers the generation of the PdNPs in the presence of a thiol.[86] $Pd(OAc)_2$ or rather Na_2PdCl_4 are applied as palladium source,

being reduced by $NaBH_4$. $(MeO)_3Si(CH_2)_2SH$ is added as thiol source, in order to stabilize the PdNPs.

Testing the combined Pd-Rh catalysts in the hydrogenation reaction of arenes, e.g. toluene, it was observed that the catalysts being prepared by the third method explained above are totally inactive.[82] However, the other two methods gave highly active hydrogenation catalysts. It was demonstrated that the combined Pd-Rh catalysts can be reused; their manifold application (up to 5 times) did not show any impact on the high activity.

The combined Pd-Rh catalysts turned out to be suitable for hydrogenation reactions of higher substituted benzene derivatives as well. For instance, it was possible to hydrogenate even polycyclic aromatics, as shown below (Figure 17).

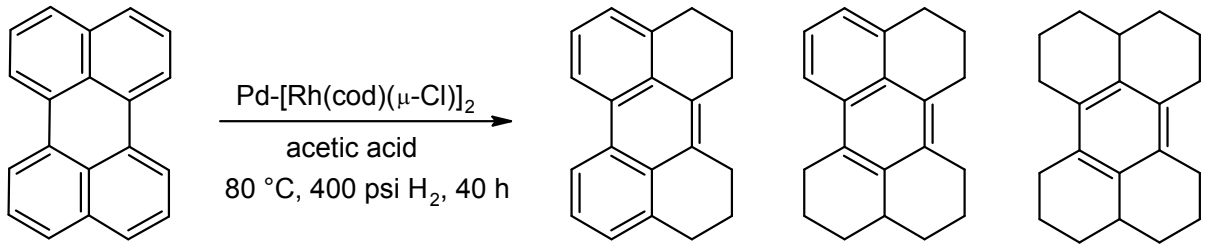

Figure 17: Hydrogenation of polycyclic aromatic hydrocarbons, catalyzed by Pd-[Rh(cod)(μ-Cl)]$_2$.[82]

It is remarkable that the hydrogenation conditions are rather mild.

The observed synergetic effect is explained by the higher activity, which is obtained when both metals Pd and Rh as applied. One single metal, either Pd or Rh, gives a remarkably lower activity.

Regarding the combined Pd-Rh catalysts, it was proposed that the two metal species have to be in a close contact with each other.[87] Otherwise no interaction in terms of the synergetic effect can occur. Based on this assumption, the mechanism shown above was proposed (Figure 16).

Hydrogen pretreatment prior to hydrogenation reactions

A thermal pretreatment with hydrogen before the actual hydrogenation reaction of toluene shows a strong impact on the catalysts' activity, distinguishing between Rh^{I}/SiO_2, Pd^{0}/SiO_2 and combined Rh^{I}-Pd^{0}/SiO_2 catalysts.[88] No pretreatment at all results in a higher selectivity regarding the mixed bimetallic species, in contrast to the single-metal Rh^{I}/SiO_2 catalysts. The latter, in general, require higher pretreatment temperatures, in order to give increased catalytic activities. It was observed that a pretreatment temperature of 200 °C gave optimal activities.[88] However, in terms of the single-metal Pd^{0}/SiO_2 species, lower pretreatment temperatures are more beneficial pertaining to the activities.

4. Rh^{I} single sites

Single-site catalysts feature a multitude of advantages. For instance, due to their heterogenization on support materials, they represent a combination of homogeneous and heterogeneous catalysis.[56] In this way, the catalyst can be easily separated and recycled. The latter is an essential aspect in particular for expensive (transition) metals like rhodium. A further great advantage of the single-site catalysts is their outstanding ability to give highly regioselective, shape-selective and enantioselective products. Moreover, they enable the easy determination of both the kinetics and mechanism of a reaction, which allows the access to the synthesis of new catalysts as well as the improvement of already existing catalysts.

In general, the single-site heterogeneous catalysts (SSHC) can be divided into four classes, which will be introduced in detail below.[56]

The first class describes the grafting of various isolated species – e.g. ions, atoms, complexes and bimetallic clusters – on a multitude of several support materials. The latter are usually silica materials, featuring a high surface area.
The second group of the SSHC includes the immobilization of asymmetric organometallic compounds on mesoporous support materials, which offer pore diameters between 15 and 500 Å.
A further SSHC-class describes the so-called “ship-in-bottle” structures. These species consist of zeolites incorporating organometallic complexes. The zeolites have the property to let pass only selected molecules and compounds, reactants as well as products. In this way, they act like filters, allowing a high selectivity.
The last group of the SSHC contains molecular sieves with a microporous and open structure, featuring pore diameters between 3.5 and 10 Å.

4.1 Grafting of isolated species on mesoporous silica support materials

The first SSHC-class can be classified into four sub-categories, i.e. the grafting of (a) ions, (b) atoms, (c) complexes and (d) bimetallic clusters on different support materials. These four sub-categories are described in detail below.

Grafting of isolated single-site transition-metal ions on mesoporous silica support materials

Isolated single-site transition-metal ions are often immobilized onto silica as support material, due to the numerous advantages of silica (see Chapter 1, subchapter 2). Preferably, mesoporous silica supports are applied, having pore diameters between 20 and 100 Å. However, silicas with larger pore diameters turned out to be even more convenient; silicas with pore diameters up to 500 Å offer very high surface areas between 600 and 1000 $m^2\ g^{-1}$. It was demonstrated that silicas with large pore diameters are perfectly suitable for the immobilization of single-sites, not only due to their high surface area but also to the multitude of isolated silanol groups on the silica surface: A very important and noteworthy example was done by *Maschmeyer et al.* by grafting Ti^{IV} single sites on the inner walls of MCM-41 as mesoporous silica support.[89] Further transition-metal ions, which can be grafted in the same way on mesoporous silica supports, are e.g. Mo^{VI}, Cr^{VI} and VO^{IV}.[90,91]

Grafting of isolated metal atoms on mesoporous silica support materials

Studies have shown the immobilization of isolated metal atoms like e.g. palladium on MgO as silica support material.[92,93] These supported single metal atoms are able to catalyze e.g. the cyclotrimerization of acetylene[92] or rather the oxidation of carbon monoxide to carbon dioxide, using oxygen as oxidizing agent[93]. Figure 18 shows a single palladium atom grafted on MgO.[92]

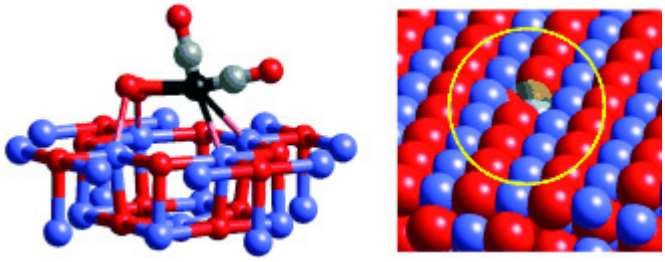

Figure 18: Isolated palladium atom grafted on MgO,
formation of the complex $Pd(CO)_2O_2$ (blue: Mg, red: O, grey: C, black: Pd).[92]

The isolated palladium atom is grafted on the magnesia surface via charge-transfer and it is bound to a so-called F-center. The latter describes the state of “an electron trapped at an oxygen anion vacancy”.[56] The binding of the isolated palladium atom onto the MgO surface results in the formation of a $Pd(CO)_2O_2$ complex, shown in Figure 18. This complex features a high stability.

Grafting of organometallic complexes on mesoporous silica support materials

Immobilized organometallic complexes can be applied as heterogeneous catalysts e.g. in metathesis reactions; three examples, using molybdenum, tungsten and rhenium as metals, are shown in Figure 19.

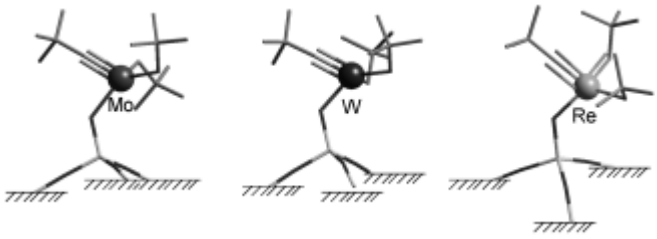

Figure 19: Immobilized organometallic complexes for metathesis reactions.[94]

Besides the metathesis, immobilized organometallic complexes are readily applied for instance in polymerization reactions of olefins.

The organometallic complexes can be anchored on the silica surface by either covalent or non-covalent bondings.[56] In this context, *Bianchini et al.* demonstrated that hydrogen bondings are notably strong.[76d] The hydrogen bonds are formed between the triflate counter ion of the metal complex and the isolated silanol groups of the silica support material, as shown in Figure 20.

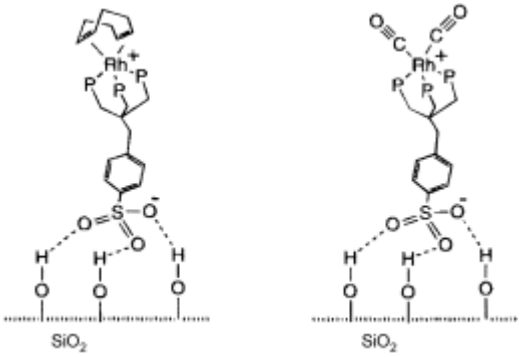

Figure 20: Organometallic complexes, immobilized on silica via hydrogen bonds.[76d]

The immobilized Rh^{I} complex on the left is the active species, which can be applied e.g. in hydroformylation reactions. By contrast, the complex on the right is the one after its catalytic application; as evident from the structure, the carbon monoxide, as one component of the syngas, coordinates to the Rh^{I} center, which results in a deactivation of the complex.

Grafting of bimetallic clusters on mesoporous silica support materials

Bimetallic clusters can be formed in the interior of mesoporous silica supports. Regarding the preparation of such clusters, two aspects have to be considered: On the one hand, the clusters must be identical pertaining to their stoichiometry and their size. On the other hand, particular attention has to be paid to the uniform distribution of the clusters on the inner walls of the silica support material. Due to the small size of the clusters, the metal atoms are mainly placed on the silica surface. Figure 21 gives an example of a bimetallic cluster, consisting of ruthenium and platinum, immobilized on mesoporous silica.

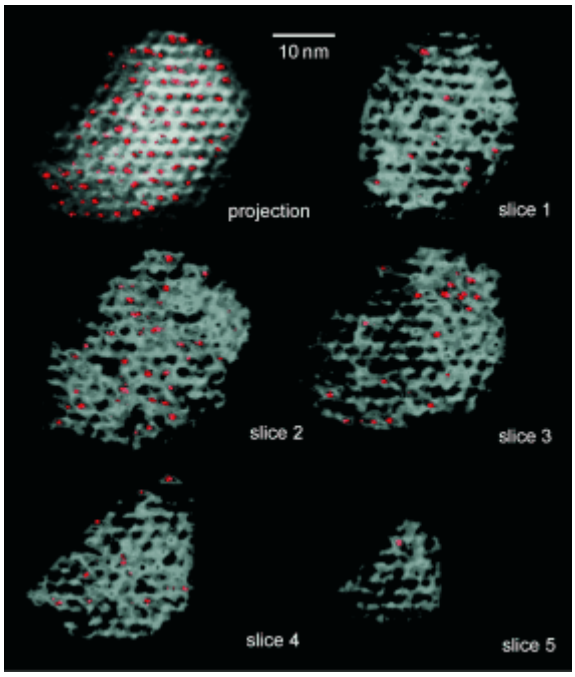

Figure 21: Bimetallic $Ru_{10}Pt_2C_2$ cluster immobilized on mesoporous silica (NPs are marked in red).[95]

It could be demonstrated that a synergetic effect between the two metals leads to high activities and selectivities in hydrogenation reactions.[56]

4.2 Grafting of asymmetric organometallic complexes on mesoporous support materials

The second class of SSHC includes the immobilization of chiral organometallic complexes solely on the inner walls of mesoporous support materials (e.g. MCM-41 or SBA-15), featuring pore diameters between 15 and 500 Å.[56] Figure 22 shows the procedure, which leads to the inactiveness of the exterior walls of the silica support. The free terminal silanol groups are hydrophobically functionalized by the reaction with dichlorodiphenyl silane. The reaction conditions are chosen in that way that the dichlorodiphenyl silane is not able to diffuse to the interior walls of the silica. Thus, the interior silanol groups are not functionalized in the same way as the exterior ones. By contrast, the silanol groups of the interior walls of the silica react with

trichlorosilane propyl bromide, which enables the immobilization of chiral organometallic species solely on the inner walls of the silica.

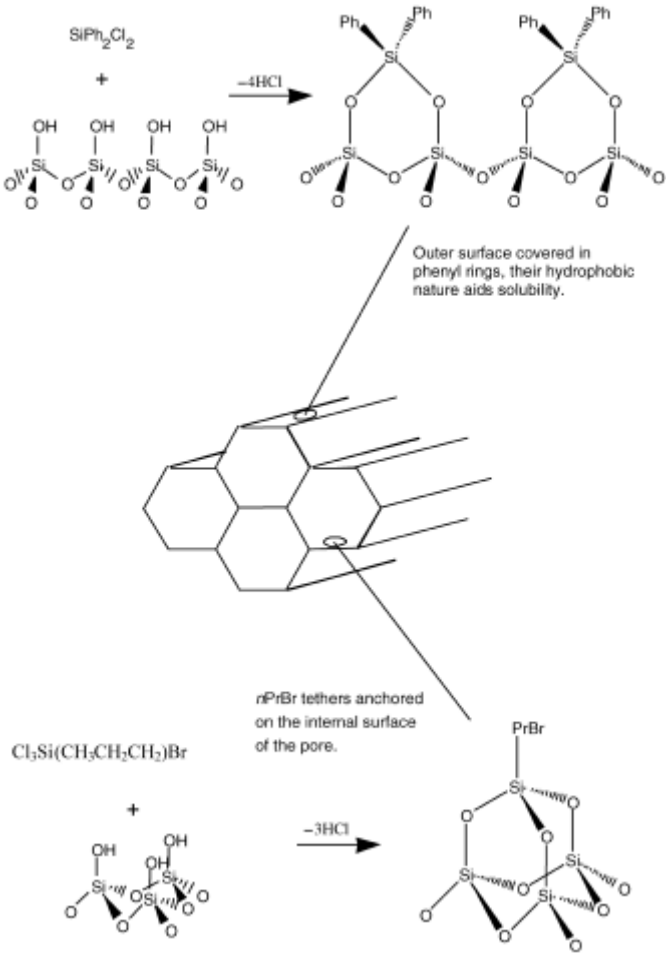

Figure 22: Blocking of the exterior walls of mesoporous silica support materials by the reaction with $SiPh_2Cl_2$.[56,96]

4.3 "Ship-in-bottle" catalysts

The so-called "ship-in-bottle" catalysts describe heterogeneous species consisting of zeolites, which incorporate organometallic complexes.[56] Some examples are given below (Figure 23).

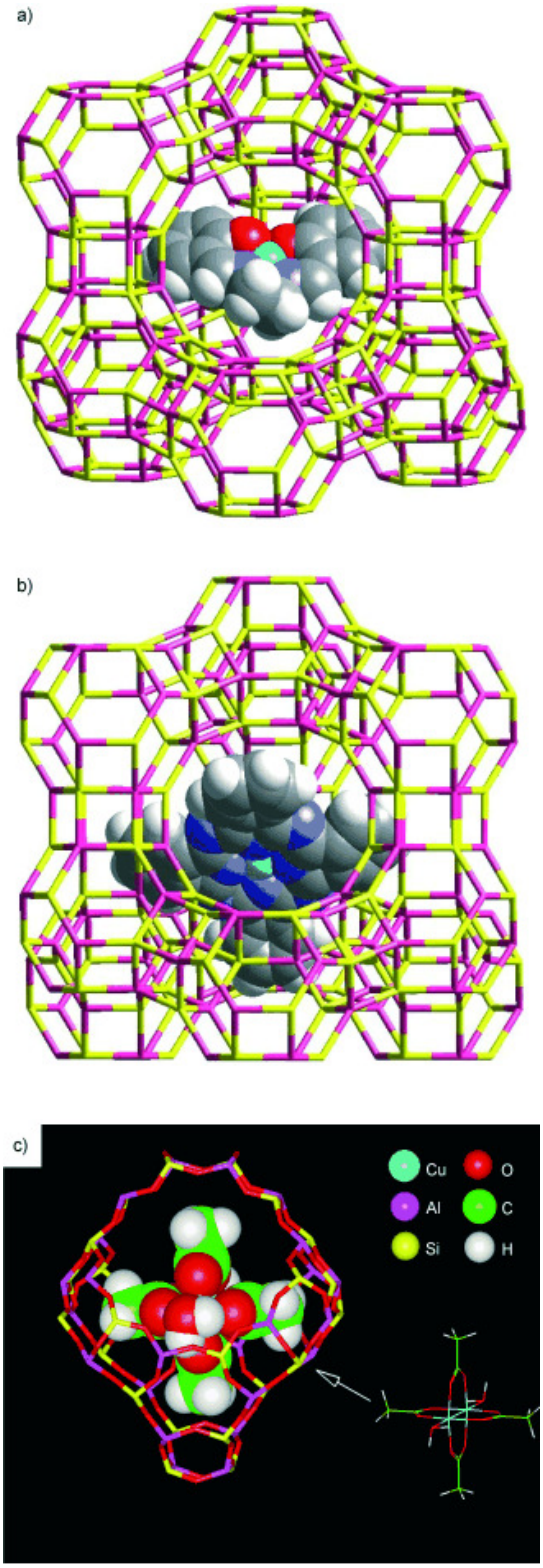

Figure 23: Examples for “ship-in-bottle” catalysts.[56]

The first example a) shows zeolite Y incorporating a cobalt complex with a salen ligand. This complex tends to the binding of oxygen as ligand, due to its pyridinic nature.
The second example b) demonstrates a cobalt complex entrapped in zeolite Y as well, featuring phthalocyanine as ligand. As shown above, the cobalt complex suffers from steric hindrance in the supercage of zeolite Y. Therefore, its structure is twisted, which is advantageous for its reactivity.
The third structure c) shows a copper dimer incorporated in zeolite Y.
All these types of “ship-in-bottle” SSHC are useful when active sites would like to be inhibited, in order to avoid side-reactions like dimerization. The advantage of zeolitic supercages is the access of selected reactants. In this way, they act like a kind of filter. Only molecules having a certain size are able to pass the zeolite. Because of their similarity to enzymes, the “ship-in-bottle” catalysts are also called “zeozymes” or rather “enzyme mimics”.[56] They can be applied for instance in the oxidation of methane to methanol or propane to isopropanol with oxygen as oxidizing agent.
The “ship-in-bottle” catalysts feature a range of outstanding advantages: First of all, simple filtration allows the separation of the SSHC from the reaction products as well as their reuse. Moreover, such “ship-in-bottle” catalysts show a very high specific rate, much higher than the single metal complex without the zeolite. Finally, the zeolite undertakes the task of absorbing water. Due to all these advantages, the “ship-in-bottle” SSHC are attractive and promising catalysts in the field of heterogeneous catalysis.

4.4 Open-structured SSHC

The fourth and last class of the SSHC describes the open-structured solid catalysts, e.g. molecular sieves, having pore diameters between 3.5 and 10 Å. Examples for open-structured species are, for instance, aluminosilicates (i.e. zeolites, natural as well as synthetic ones) and aluminophosphates. Below, the structure of an aluminophosphate is shown (Figure 24).

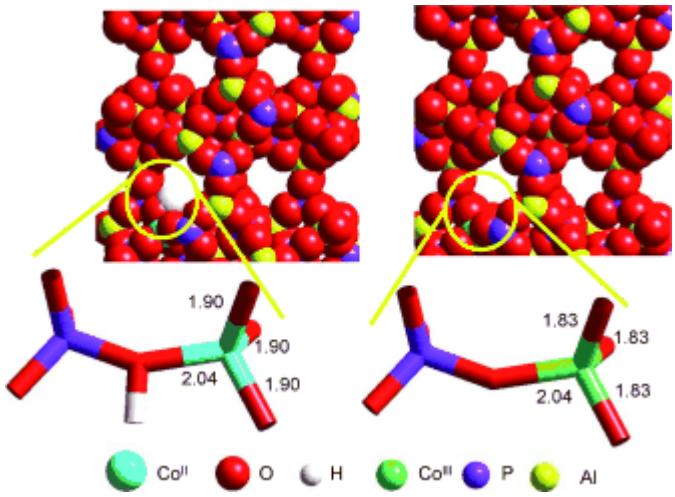

Figure 24: Open-structured aluminophosphate SSHC.[56]

As it can be seen from the structure on the left, some Al^{III} ions in the open-structured aluminophosphate AlPO-18 are exchanged by Co^{II}. This leads to the formation of the SSHC Co^{II}AlPO-18, which features Brønsted activity and can be applied e.g. in the dehydration of methanol in order to generate light olefins.[97] The structure on the right shows the oxidized SSHC Co^{III}AlPO-18. In general, only ca. 4 mol % of the Al^{III} ions are substituted by metal ions of the oxidation state II. Beside Co^{II}, also Mg^{II}, Zn^{II}, Mn^{II} and other M^{II} ions can be applied for the SSHC MAlPO-18. Due to the very small amount of substituted Al^{III} ions by M^{II}, only few Brønsted active sites are generated within the MAlPO-18 catalysts. They are far away from each other and thereby "isolated" within the framework of the MAlPO-18. Thus, these type of SSHC show a similar catalytic behavior like the first SSHC-class.

Results and discussion

The present part of this work can be considered in two topics: (1) the immobilization of Pd^0 on silica and (2) the grafting of Pd^0/SiO_2 with Rh^I.
Regarding the immobilization of the PdNPs, different methods have been tested (impregnation, Ionic Exchange, Chemical Vapour Deposition), which are described in detail below.

1. Immobilization of PdNPs onto silica

(a) Impregnation

In previous studies, PdNPs have been immobilized on silica via impregnation using $PdCl_2$ as palladium source. Contents of Pd between 1.66 and 2.08 wt % have been obtained, with an expectant content of 2 wt %.[73] Despite the high loadings, this method shows a significant disadvantage. Due to the chlorine, the silica structure can be easily damaged. Therefore, other immobilization methods have been tested.

(b) Ionic Exchange

In contrast to the impregnation, the ionic exchange is a much milder method for the immobilization of the PdNPs onto silica. Here, no chlorine incurs; hence, the silica structure does not run the risk of being destroyed.
In the following, the procedure of the Ionic Exchange is illustrated (Figure 25). A solution of $Pd(NH_3)_4Cl_2 \cdot H_2O$ in H_2O mQ is prepared, whereat the control of the pH is of great importance. A pH > 9 leads to a dissolving of the silica; therefore, the pH has to be adjusted to ca. 9. If the pH is too low, i.e. ~ 7-8, one drop of ammoniac solution can be added carefully in order to reach pH 9. Subsequently, the Pd solution is poured over the silica and the resulting mixture is stirred at RT for 24 h. During the course of the reaction, the Pd^{2+} ions displace 2 H^+ towards the solution. Accordingly, the solution becomes acidic and the pH decreases to 7. Pd^{II}/SiO_2 is obtained; the subsequent calcination and reduction of the samples yield Pd^0/SiO_2.

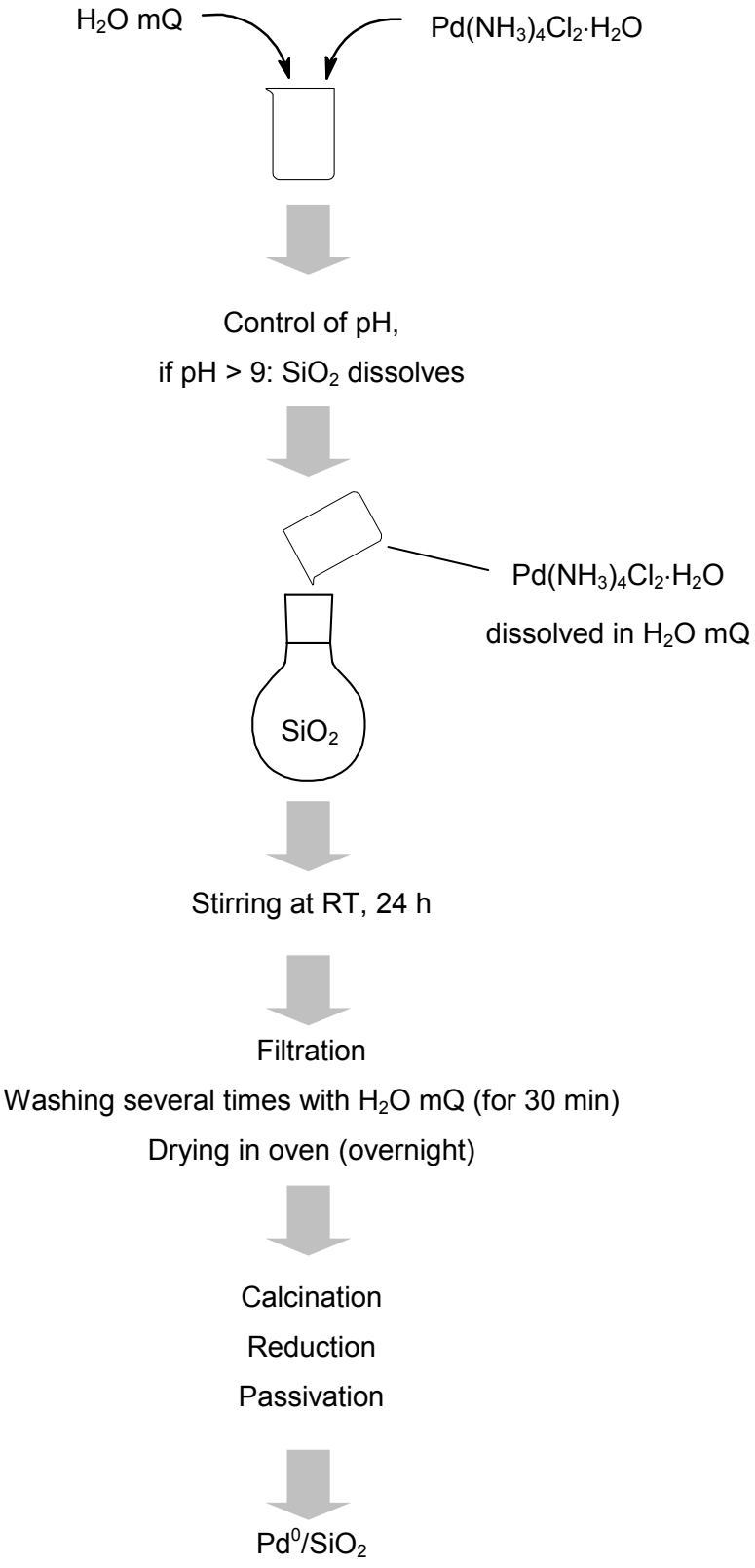

Figure 25: Procedure of Ionic Exchange.

The calcination is carried out in oxygen flow; the Pd^{II}/SiO_2 samples are heated up to 550 °C with a velocity of 5 °C / min (Figure 26).

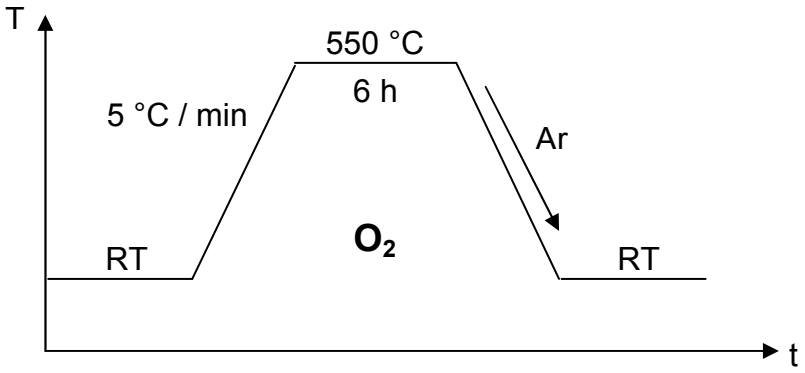

Figure 26: Ionic Exchange – Calcination.

The subsequent reduction is performed in hydrogen flow, at 300 °C (v = 50 °C / 5 min) for 1 h (Figure 27).

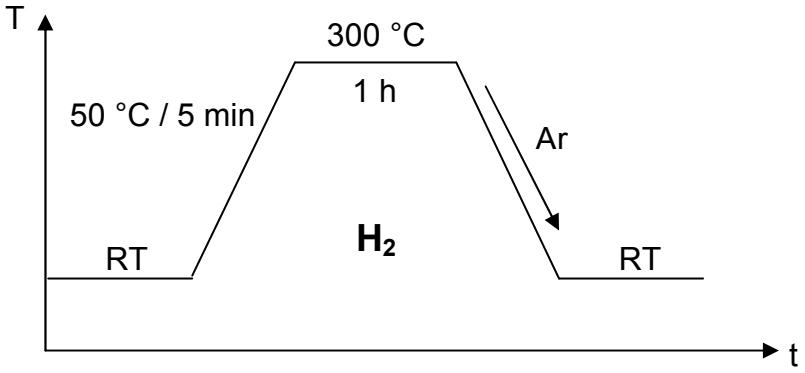

Figure 27: Ionic Exchange – Reduction.

Thereafter, the samples are passivated in oxygen flow for protection reasons. The surface of the PdNPs is sensitive towards chlorine. As the subsequent impregnation of the Pd^0/SiO_2 samples with Rh^I is carried out in dichloromethane as solvent, the chlorine is able to react with the surface of the PdNPs. Studies have shown that dichloromethane decomposes on immobilized PdNPs at temperatures above 77 °C to give ethylene, methane, HCl and H_2O, which was analytically proved by IR.[78] Via passivation a thin oxide layer is deposited onto the surface of the NPs; thus, the NPs

are protected against any attack of chlorine. However, experiments have shown that also this thin oxide layer is not completely inert; it can be rapidly removed under hydrogenation conditions.[74]

Despite the milder reactions conditions compared to the impregnation, the Ionic Exchange has not proved to be a proper immobilization method, as only low Pd loadings could be obtained (Table 1). They range between 0.47 and 1.00 wt %, depending on the silica support, the reaction time and temperature; thereby, they reach at most only 50 % of the expected loading. Thus, another immobilization method has been tested, in order to enhance the loading of Pd.

Table 1: Ionic Exchange – loadings of Pd.

Entry	Type of SiO_2	t	T [°C]	Loading of Pd [wt %]
1	Davisil B	24 h	RT	0.70 (exp. 2.00)
2	MCM-41	24 h	RT	0.90 (exp. 2.00)
3	Davisil B	48 h	RT	0.75 (exp. 2.00)
4	MCM-41	48 h	RT	0.87 (exp. 2.00)
5	Davisil B	24 h	45 (reflux)	0.77 (exp. 2.00)
6	MCM-41	24 h	45 (reflux)	1.00 (exp. 2.00)
7	Davisil B	24 h	RT	0.83 (exp. 4.00)
8	Davisil A	3 d	RT	0.47 (exp. 1.00)

(c) Chemical Vapour Deposition (CVD)

The principle of the CVD is the sublimation of the precursor in vacuum and its subsequent decomposition on the support. Due to its low sublimation and decomposition temperature, Pd(allyl)Cp has been chosen as palladium source and precursor (Figure 28).

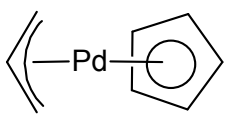

Figure 28: Pd(allyl)Cp.

The CVD was performed using a special glass reactor, which is shown in Figure 29.

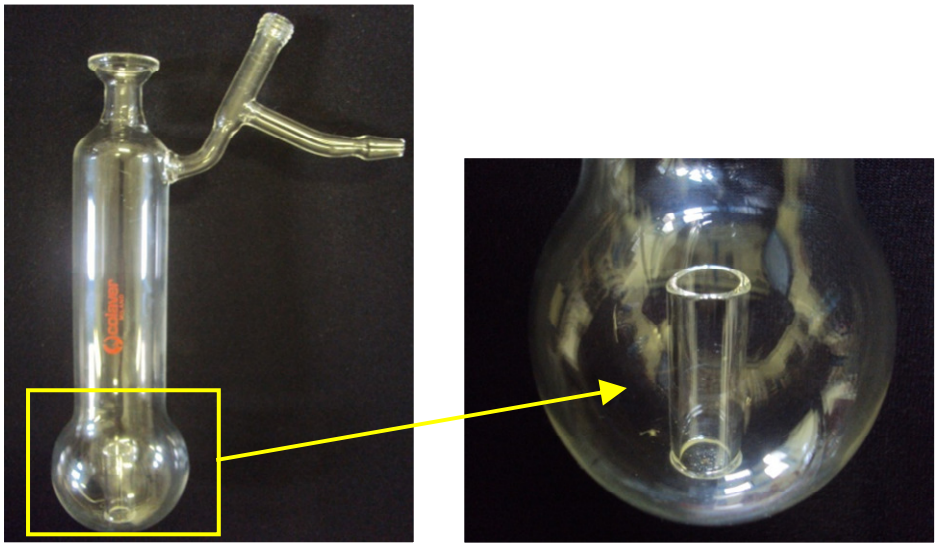

Figure 29: Glass reactor for CVD.

The flask possesses a small tube in the interior, where the Pd precursor is filled in. Around the tube, the silica support is placed. The flask is closed and evacuated to 4 mbar. While slow rotation, it is heated (35 °C via oil bath or rather 40 °C via heat gun), until the Pd precursor is completely sublimated. Generally, the latter is achieved after ca. 24 h, which is indicated by the dark coloration of the silica (Figure 30).

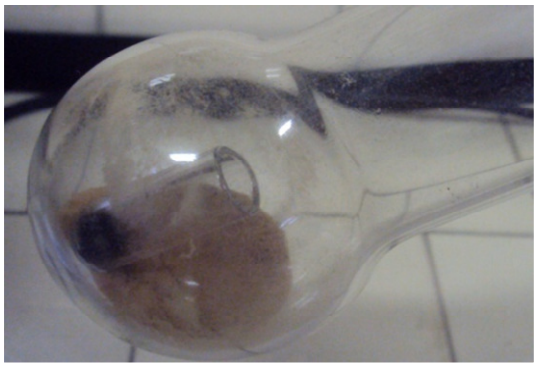

Figure 30: Coloration of the silica after CVD.

Subsequently, reduction and passivation are performed in order to obtain the immobilized PdNPs onto silica. The conditions of the reduction (H_2, T = 250 °C, v = 10 °C / 15 min, t = 1 h) are given below (Figure 31).

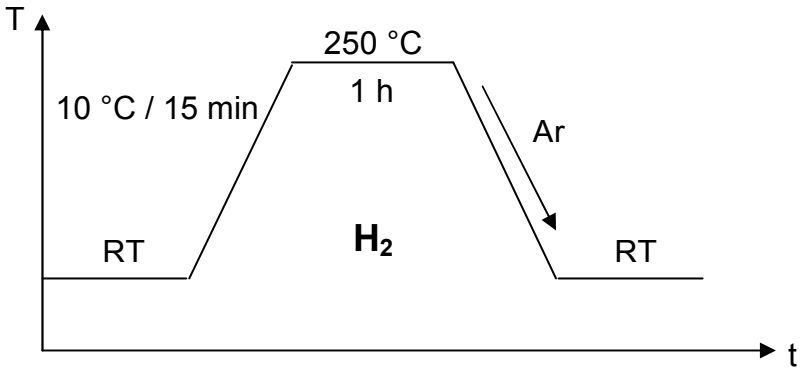

Figure 31: CVD – Reduction.

As apparent from Table 2, the obtained Pd loadings using CVD as immobilization method are much higher in comparison to those of the Ionic Exchange. Excellent loadings up to 1.95 wt % (exp. 2 wt %) were achieved (entry 5). It could be shown that both powdery silica supports and silica monoliths are compatible for the CVD. Thus, CVD has proved to be the most effective immobilization method for PdNPs in this context.

Table 2: CVD – loadings of Pd.

Entry	Type of SiO_2	Loading of Pd [wt %]
1	Silica Aldrich 403601	0.71 (exp. 1.00)
2	Davisil B	1.35 (exp. 2.00)
3	SBA-15	1.36 (exp. 2.00)
4	Monolith 6197c	1.51 (exp. 2.00)
5	Monolith 6197c	1.95 (exp. 2.00)

2. Impregnation of Pd^0/SiO_2 with Rh^I

Subsequent to the immobilization of the PdNPs, the grafting with chiral Rh^I phosphine complexes was performed. The procedure is graphically shown in Figure 32. Due to their high sensitivity towards air and water, the Rh^I complexes must be handled in inert atmosphere (Dry Box or rather in Ar flow). The Rh^I complexes are dissolved in anhydrous dichloromethane and the resulting solution is poured over the corresponding Pd^0/SiO_2 sample in Ar flow. After stirring at RT for 4 h and the subsequent work-up, the Rh^I single sites are anchored on the silica surface.

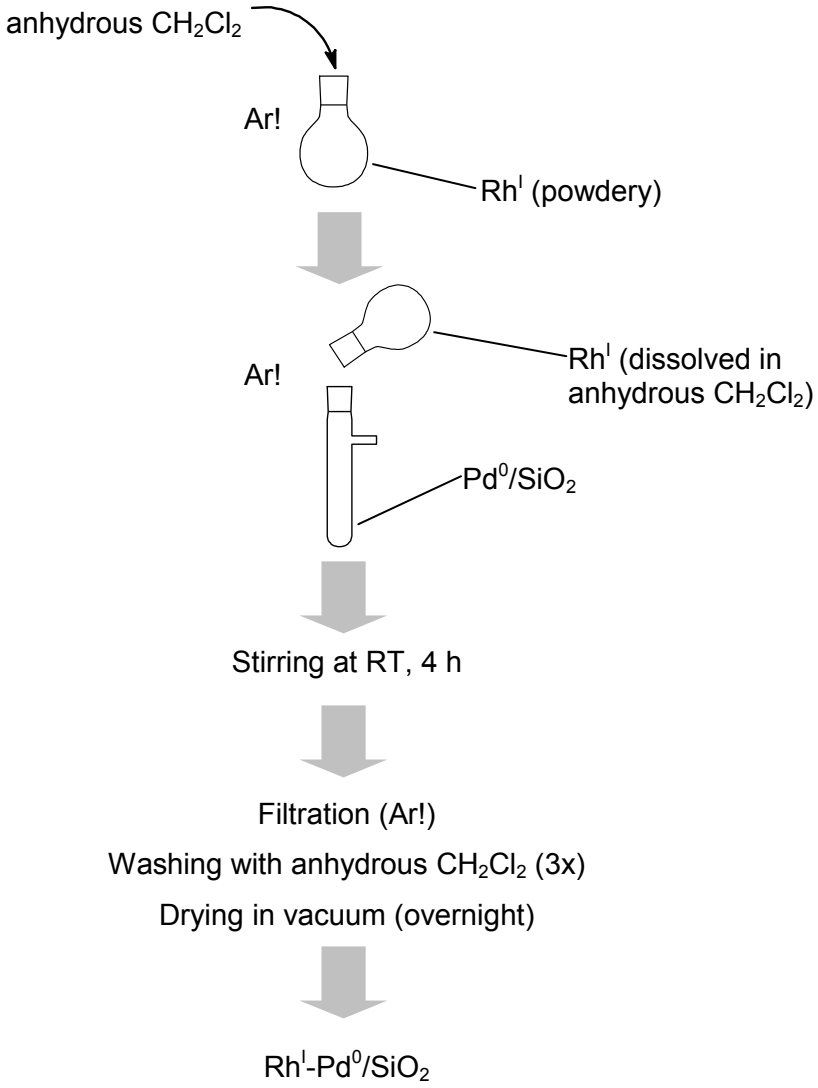

Figure 32: Procedure of impregnation of Pd^0/SiO_2 with Rh^I.

Table 3 (page 75) gives an overview about the obtained Rh loadings, beside other important parameters (type of the silica support, the Pd precursor as well as the immobilization method for Pd^0, the obtained Pd loadings and the applied Rh^I precursor). Both chiral and achiral Rh^I complexes were used for the grafting (Figure 33). They were prepared in the research group of *Dr. Pierluigi Barbaro* at the *ICCOM-CNR* in Sesto Fiorentino, Firenze.

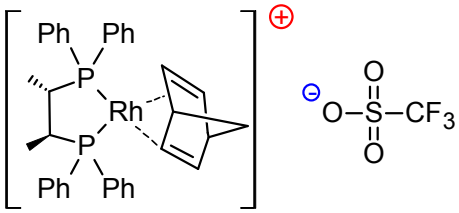

[(-)CHIRAPHOS(Rh)(NBD)]OTf

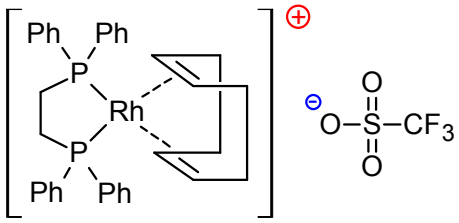

Rh(dppe)(COD)OTf

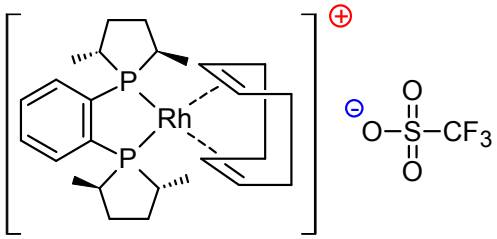

Rh-MeDuPhos

Figure 33: Chiral and achiral Rh^I complexes for grafting.

As apparent from Table 3 (page 75), Rh loadings between 0.26 and 0.83 wt % have been obtained, depending on several parameters, e.g. the type of the silica support or the Rh catalyst. Moreover, the impregnation procedure has a great influence on the Rh loading: Using the silica “Aldrich 403601” (entry 4), the work-up was performed without filtration. Hence, a higher Rh loading was obtained.

Table 3: Impregnation of Pd^0/SiO_2 with Rh^I – loadings of Pd and Rh.

Entry	Type of SiO_2	Pd precursor	Immobilization method for PdNPs	Loading of Pd [wt %]	Rh catalyst	Loading of Rh [wt %]
1	Davison 62	$PdCl_2$	Impregnation	1.17 (exp. 2.00)	[(-)CHIRAPHOS(Rh)(NBD)]OTf	0.37 (exp. 0.50)
2	Monolith 6197c	Pd(allyl)Cp	CVD	1.51 (exp. 2.00)	Rh(dppe)(COD)OTf	0.37 (exp. 0.50)
3	Monolith 6197c	Pd(allyl)Cp	CVD	1.95 (exp. 2.00)	[(-)CHIRAPHOS(Rh)(NBD)]OTf	0.26 (exp. 0.50)
4	Silica Aldrich 403601	Pd(allyl)Cp	CVD	0.71 (exp. 1.00)	Rh-MeDuPhos	0.43 (exp. 0.50)
5	Davisil A	$Pd(NH_3)_4Cl_2{\cdot}H_2O$	Ionic Exchange	0.47 (exp. 1.00)	Rh(dppe)(COD)OTf	0.48 (exp. 0.50)
6	Davisil B	Pd(allyl)Cp	CVD	1.35 (exp. 2.00)	Rh(dppe)(COD)OTf	0.83 (exp. 1.00)
7	SBA-15	Pd(allyl)Cp	CVD	1.36 (exp. 2.00)	Rh(dppe)(COD)OTf	0.77 (exp. 1.00)

Concluding remarks

Recently, Rh^{I}-Pd^{0}/SiO_2 “hybrid catalysts”, consisting of PdNPs and Rh^{I} single sites, both immobilized on various silica support materials, proved to be highly-effective for hydrogenation reactions, e.g. of benzene to cyclohexane. They showed a 4 times higher activity than Pd^{0}/SiO_2; Rh^{I}/SiO_2 turned out to be completely inactive.

Within the scope of this work, Rh^{I}-Pd^{0}/SiO_2 “hybrid catalysts” were prepared using chiral Rh^{I} species. Both, powdery silica (MCM-41, SBA-15, Davisil A, Davisil B, Davison 62, Silica Aldrich 403601) and silica monoliths were applied as support material. Regarding the immobilization of the PdNPs onto the silica, several methods have been tested (impregnation, Ionic Exchange, Chemical Vapour Deposition (CVD)), whereat CVD has proved to be the most effective method, yielding the highest metal loadings, up to 1.95 wt % (exp. loading 2.00 wt %). Moreover, CVD turned out to be compatible for both powdery silica and silica monoliths. In terms of the impregnation of the Pd^{0}/SiO_2 samples with Rh^{I}, metal loadings from 0.26 to 0.83 wt % were obtained, depending on different parameters, e.g. the type of the silica, the Rh catalyst and the impregnation procedure (with or without filtration in the work-up).

In further studies, the Rh^{I}-Pd^{0}/SiO_2 “hybrid catalysts” can be tested in selective hydrogenation reactions of prochiral substrates.

References

[1] D. Astruc, F. Lu, J. R. Aranzaes, *Angew. Chem. Int. Ed.* **2005**, *44*, 7852-7872.

[2] (a) L. D. Rapino, F. F. Nord, *J. Am. Chem. Soc.* **1941**, *63*, 2745.

(b) L. D. Rapino, F. F. Nord, *J. Am. Chem. Soc.* **1941**, *63*, 3268.

(c) K. E. Kavanagh, F. F. Nord, *J. Am. Chem. Soc.* **1943**, *65*, 2121.

[3] D. Y. Cha, G. Parravano, *J. Catal.* **1970**, *18*, 320.

[4] (a) M. Haruta, T. Kobayashi, H. Sano, N. Yamada, *Chem. Lett.* **1987**, 405.

(b) M. Haruta, N. Yamada, T. Kobayashi, S. Lijima, *J. Catal.* **1989**, *115*, 301.

(c) M. Haruta, S. Tsuboda, T. Kobayashi, H. Kagehiama, M. J. Genet, B. Demon, *J. Catal.* **1993**, *144*, 175.

(d) M. Haruta, *CATTECH* **2002**, *6*, 102.

[5] (a) G. C. Bond, P. A. Sermon, *Gold Bull.* **1973**, *6*, 102.

(b) H. Hirai, Y. Nakao, N. J. Toshima, *Macromol. Sci. Chem. A* **1978**, *12*, 1117.

(c) H. Hirai, Y. Nakao, N. J. Toshima, *Macromol. Sci. Chem. A* **1979**, *13*, 727.

[6] (a) A. Moradpour, E. Amouyal, P. Keller, H. Kagan, *Nouv. J. Chim.* **1978**, *2*, 547.

(b) A. Henglein, *J. Phys. Chem.* **1979**, *83*, 2858.

(c) A. Henglein, J. Lillie, *J. Am. Chem. Soc.* **1981**, *103*, 1059.

(d) K. Kurihara, J. H. Fendler, I. J. Ravet, *J. Mol. Catal.* **1986**, *34*, 325.

(e) M. Boutonnet, J. Kizling, R. Touroude, G. Maire, P. Stenius, *Appl. Catal.* **1986**, *20*, 163.

(f) Y. Degani, I. J. Willner, *J. Chem. Soc. Perkin Trans. 2* **1986**, 37.

(g) I. Willner, R. Maidan, D. Mandler, H. Dürr, G. Dörr, K. Zengerle, *J. Am. Chem. Soc.* **1987**, *109*, 6080.

[7] (a) J. S. Bradley, E. W. Hill, M. E. Leonowitz, H. Witzke, *J. Mol. Catal.* **1987**, *41*, 59.

(b) C. Larpent, H. Patin, *J. Mol. Catal.* **1988**, *44*, 191.

[8] (a) M. T. Reetz, W. Helbig, *J. Am. Chem. Soc.* **1994**, *116*, 7401.

(b) M. T. Reetz, S. A. Quaiser, *Angew. Chem.* **1995**, *107*, 2461.

(c) M. T. Reetz, S. A. Quaiser, *Angew. Chem. Int. Ed. Engl.* **1995**, *34*, 2240.

(d) M. T. Reetz, W. Helbig, S. A. Quaiser in *Active Metals: Preparation, Characterization, Applications* (Ed.: A. Fürstner), VCH, Weinheim, **1996**, p. 279.

(e) M. T. Reetz, R. Breinbauer, K. Wanninger, *Tetrahedron Lett.* **1996**, *37*, 4499.

(f) M. T. Reetz, G. Lohmer, *Chem. Commun.* **1996**, 1921.

[9] A. Barau, V. Budarin, A. Caragheorgheopol, R. Luque, D. J. Macquarrie, A. Prelle, V. S. Teodorescu, M. Zaharescu, *Catal. Lett.* **2008**, 124, 204.

[10] C. S. Chen, H. W. Chen, *Appl. Catal. A* **2004**, *260*, 207.

[11] P. A. Robles-Dutenhefner, M. G. Speziali, E. M. B. Sousa, E. N. dos Santos, E. V. Gusevskaya, *Appl. Catal. A* **2005**, *295*, 52.

[12] Y. F. Han, D. Kumar, C. Sivadinarayana, D. W. Goodman, *J. Catal.* **2004**, *224*, 60.

[13] T. Sasahara, A. Kido, H. Ishihara, T. Sunayama, M. Egashira, *Sensor Actuators B* **2005**, *108*, 478.

[14] T. Ichinde, S. Masaki, K. Uchida, S. Nozaki, H. Morisaki, *Thin Solid Films* **2004**, *466*, 27.

[15] V. Polshettiwar, A. Molnar, *Tetrahedron* **2007**, *63*, 6949.

[16] L.Yin, J. Liebscher, *Chem. Rev.* **2007**, *107*, 133.

[17] A. Taguchi, F. Schüth, *Micropor. Mesopor. Mater.* **2005**, *77*, 1.

[18] D. J. Macquarrie, B. C. Gilbert, L. J. Gilbey, A. Caragheorgheopol, F. Savonea, D. B. Jackson, B. Onida, E. Garrone, R. Luque, *J. Mater. Chem.* **2005**, *15*, 3946.

[19] I. Yuranov, L. Kiwi-Minsker, P. Buffat, A. Renken, *Chem. Mater.* **2004**, *16*, 760.

[20] A. Corma, *Chem. Rev.* **1997**, *97*, 2373.

[21] L. Huang, Z. Wang, T. P. Ang, J. Tan, P. K. Wong, *Catal. Lett.* **2006**, *112*, 219.

[22] J. Panpranot, K. Phandinhong, P. Proserthdam, M. Hasegawa, S. Fujita, M. Arai, *J. Mol. Catal. A* **2006**, *253*, 20.

[23] L. M. Yang, Y. J. Wang, Y. W. Sung, G. S. Luo, Y. Y. Dai, *J. Colloid Interface Sci.* **2006**, *299*, 823.

[24] J. Tsuji, *Palladium reagents and catalysts*, Wiley-VCH, **2004**.

[25] R. F. Heck, J. P. Nolly, *J. Org. Chem.* **1972**, *37*, 2320.

[26] A. Biffis, M. Zecca, M. Basato, *J. Mol. Catal. A* **2001**, *173*, 249.

[27] V. L. Nguyen, D. C. Nguyen, H. Hirata, M. Ohtaki, T. Hayakawa, M. Nogami, *Adv. Nat. Sci.: Nanosci. Nanotechnol.* **2010**, *1*, 35012.

[28] B. Heinrichsa, S. Lambert, C. Allé, J.-P. Pirard, G. Beketov, V. Nehasil, N. Kruseb, *Studies in Surface Science and Catalysis* **2000**, *143*, 25.

[29] I. Yuranov, P. Moeckli, E. Suvorova, P. Buffat, L. Kiwi-Minsker, A. Renken, *J. Mol. Catal. A: Chemical* **2003**, *192*, 239.

[30] S.-W. Kim, J. Park, Y. Jang, Y. Chung, S. Hwang, T. Hyeon, *Nano Lett.* **2003**, *3 (No. 9)*, 1289.

[31] (a) A. M. Doyle, S. K. Shaikhutdinov, S. D. Jackson, H.-J. Freund, *Angew. Chem.* **2003**, *115*, 5398.

(b) A. M. Doyle, S. K. Shaikhutdinov, S. D. Jackson, H.-J. Freund, *Angew. Chem. Int. Ed.* **2003**, *42*, 5240.

[32] (a) C. E. Tucker, J. G. de Vries, *Top. Catal.* **2002**, *19*, 111.

(b) M. Beller, A. Zapf in *Handbook of Organopalladium Chemistry for Organic Synthesis*, Vol. 1 (Ed.: E.-i. Negishi), Wiley, Hoboken, **2002**, p. 1209.

[33] P. Baumeister, W. Meyer, K. Oertle, G. Seifert, H. Seifert, H. Steiner, *Chimia* **1997**, *51*, 144.

[34] J. McChesney, *Spec. Chem.* **1999**, *6*, 98.

[35] I. Shinkai, A. O. King, R. D. Larsen, *Pure Appl. Chem.* **1994**, *66*, 1551.

[36] G. Zhang, H. Zhou, J. Hu, M. Liu, Y. Kuang, *Green Chem.* **2009**, *11*, 1428.

[37] N. Toshima in *"Fine Particles Sciences and Technology. From Micro- to New Particles"* (Ed.: E. Pellizzetti), Kluwer, Dordrecht, **1996**, p. 371.

[38] R. P. Andres, J.-D. Bielefeld, J.-I. Henderson, D.-B. Janes, V.-R. Kolagunta, C.-P. Kubink, W. Mahoney, R.-G. Osifchin, R. Reifenberger, *Science* **1996**, *273*, 1690.

[39] (a) R. Narayanan, M. A. El-Sayed, *J. Am. Chem. Soc.* **2003**, *125*, 8340.

(b) Y. Li, E. Boone, M. A. El-Sayed, *Langmuir* **2002**, *18*, 4921.

[40] (a) J. H. Sinfelt, *Acc. Chem. Res.* **1977**, *10*, 15.

(b) J. H. Sinfelt, *"Bimetallic Catalyst: Discoveries, Concepts and Applications"*, Wiley, New York, **1983**.

(c) J. H. Sinfelt, *Int. Rev. Phys. Chem.* **1988**, *7*, 281.

[41] (a) J.-H. He, I. Ichinose, T. Kunitake, A. Nakao, Y. Shiraishi, N. Toshima, *J. Am. Chem. Soc.* **2003**, *125*, 11034.

(b) Y. Shiraishi, D. Ikenaga, N. Toshima, *Aust. J. Chem.* **2003**, *56*, 1025.

(c) R. Sablong, U. Schlotterbeck, D. Vogt, S. Mecking, *Adv. Synth. Catal.* **2003**, *345*, 333.

[42] (a) M. Zhao, L. Sun, R. M. Crooks, *J. Am. Chem. Soc.* **1998**, *120*, 4877.

(b) M. Zhao, R. M. Crooks, *Angew. Chem.* **1999**, *111*, 375.

(c) M. Zhao, R. M. Crooks, *Angew. Chem. Int. Ed.* **1999**, *38*, 364.

(d) V. Chechik, M. Zhao, R. M. Crooks, *J. Am. Chem. Soc.* **1999**, *121*, 4910.

(e) M. Zhao, R. M. Crooks, *Adv. Mater.* **1999**, *11*, 217.

(f) V. Chechik, M. Zhao, R. M. Crooks, *J. Am. Chem. Soc.* **2000**, *122*, 1243.

(g) R. M. Crooks, M. Zhao, L. Sun, V. Chechik, L. K. Yeung, *Acc. Chem. Res.* **2001**, *34*, 181.

(h) L. K. Yeung, R. M. Crooks, *Nano Lett.* **2001**, *1*, 14.

(i) L. K. Yeung, C. T. Lee, K. P. Jonston, R. M. Crooks, *Chem. Commun.* **2001**, 2290.

(j) R. W. Scott, A. F. Datye, R. M. Crooks, *J. Am. Chem. Soc.* **2003**, *125*, 3708.

(k) Y. Niu, R. M. Crooks in *"Dendrimers and Nanosciences"* (Ed.: D. Astruc), Elsevier, Paris (*C. R. Chim.* **2003**, *6*, 1049).

(l) R.W. Scott, O. M. Wilson, S.-K. Oh, E. A. Kenik, R. M. Crooks, *J. Am. Chem. Soc.* **2004**, *126*, 15583.

(m) Y.-G. Kim, S.-K. Ho, R. M. Crooks, *Chem. Mater.* **2004**, *16*, 167.

(n) R.W. J. Scott, C. Sivadinarayana, O. M. Wilson, Z. Yan, D. W. Goodman, R. M. Crooks, *J. Am. Chem. Soc.* **2005**, *127*, 1380.

(o) J.-H. Liu, A.-Q. Wang, Y.-S. Shi, H.-P. Lin, C.-Y. Mou, *J. Phys. Chem. B* **2005**, *109*, 40.

[43] (a) L. Balogh, D. A. Tomalia, *J. Am. Chem. Soc.* **1998**, *120*, 7355.

(b) L. Balogh, D. R. Swanson, D. A. Tomalia, G. L. Hagnauer, A. T. McManus, *Nano Lett.* **2001**, *1*, 18.

(c) K. Esumi, A. Susuki, N. Aihara, K. Usui, K. Torigoe, *Langmuir* **1998**, *14*, 3157.

(d) K. Esumi, K. Satoh, A. Suzuki, K. Torigoe, *Shikizai Kyokaishi* **2000**, *73*, 434.

(e) K. Esumi, R. Isono, T. Yoshimura, *Langmuir* **2004**, *20*, 237.

[44] (a) J. D. Aiken III, R. G. Finke, *J. Am. Chem. Soc.* **1999**, *121*, 8803.

(b) S. Özkar, R. G. Finke, *J. Am. Chem. Soc.* **2002**, *124*, 5796.

(c) A. M. Fargo, J. F. Odzak, F. S. Lai, B. C. Gates, *Nature* **2002**, *415*, 623.

(d) V. Kogan, Z. Aizenshtat, R. Popovitz-Biro, R. Neumann, *Org. Lett.* **2002**, *4*, 3529.

(e) M. Ohde, H. Yukiohde, C. M. Wai, *Chem. Commun.* **2002**, 2388.

(f) Z. Deng, D. E. Irish, *J. Phys. Chem.* **1994**, *98*, 11169.

(g) S. Tzkar, R. G. Finke, *J. Am. Chem. Soc.* **2002**, *124*, 5796.

(h) J. Kiwi, M. Grätzel, *J. Am. Chem. Soc.* **1979**, *101*, 7214.

[45] (a) L. Strimbu, J. Liu, A. E. Kaifer, *Langmuir* **2003**, *19*, 483.

(b) J. Alvarez, J. Liu, E. Roman, A. E. Kaifer, *Chem. Commun.* **2000**, 1151.

(c) J. Liu, J. Alvarez, W. Ong, E. Roman, A. E. Kaifer, *Langmuir* **2001**, *17*, 6762.

[46] F. Lu, J. Ruiz, D. Astruc, *Tetrahedron Lett.* **2004**, *45*, 9443.

[47] (a) *Dendrimers and Nanosciences* (Ed.: D. Astruc), Elsevier, Paris, **2003**, *6* (special issue *C. R. Chim.*, vol. 8–10).

(b) G. R. Newkome, C. N. Moorefield, F. Vögtle, *Dendrimers and Dendrons: Concepts, Synthesis, Applications*, Wiley-VCH, Weinheim, **2001**.

(c) J. F. G. A. Jansen, E. M. M. de Brabander-van den Berg, E.W. Meijer, *Science* **1994**, *266*, 1226.

(d) D. A. Tomalia, A. M. Naylor, W. A. Goddard III, *Angew. Chem.* **1990**, *102*, 119.

(e) D. A. Tomalia, A. M. Naylor, W. A. Goddard III, *Angew. Chem. Int. Ed. Engl.* **1990**, *29*, 138.

[48] (a) J. A. Gladysz, *Pure Appl. Chem.* **2001**, *73*, 1319.

(b) J. Gladysz, *Chem. Rev.* **2002**, *102*, 3215 (introduction to a special issue on recoverable catalysts).

[49] (a) H. Ohde, C. M. Wai, H. Kim, M. Ohde, *J. Am. Chem. Soc.* **2002**, *124*, 4540.

(b) P. Meric, K. M. K. Yu, S. C. Tsang, *Catal. Lett.* **2004**, *95*, 39.

(c) P. Meric, K. M. K. Yu, S. C. Tsang, *Langmuir* **2004**, *20*, 8537.

[50] K. M. K. Yu, C. M. Y. Yeung, D. Thompsett, S. C. Tsang, *J. Phys. Chem. B* **2003**, *107*, 4515.

[51] B.-H. Yoon, H. Kim, C. M. Wai, *Chem. Commun.* **2003**, 1040.

[52] H. Ohde, C. M.Wai, H. Kim, J. Kim, M. Ohde, *J. Am. Chem. Soc.* **2002**, *124*, 4540.

[53] X. R. Ye, Y.-H. Lin, C. M. Wai, *Chem. Commun.* **2003**, 642.

[54] N. V. Plechkova, K. R. Seddon, *Chem. Soc. Rev.* **2008**, *37*, 123.

[55] P. Walden, *Bull. Acad. Impér. Sci. St. Pétersbourg* **1914**, *8*, 405.

[56] J. M. Thomas, R. Raja, D. W. Lewis, *Angew. Chem. Int. Ed.* **2005**, *44*, 6456-6482.

[57] C. T. Kresge, M. E. Leonowicz, W. J. Roth, J. C. Vartuli, J. S. Beck, *Nature* **1992**, *359*, 710.

[58] J. S. Beck, J. C. Vartuli, W. J. Roth, M. E. Leonowicz, C. T. Kresge, K. D. Schmitt, C. T.-W. Chu, D. H. Olson, E. E. Sheppard, S. B. McCullen, J. B. Higgins, J. L. Schlenker, *J. Am. Chem. Soc.* **1992**, *114*, 10834.

[59] M. Grün, K. K. Unger, A. Matsumoto, K. Tsutsumi, *Microporous and Mesoporous Materials* **1999**, *27*, 207-216.

[60] R. Schmidt, M. Stöcker, E. Hansen, D. Akporiaye, O. H. Ellestad, *Microporous Mater.* **1995**, *3*, 443.

[61] P. J. Branton, P. G. Hall, K. S. W. Sing, *J. Chem. Soc., Chem. Commun.* **1993**, 1257.

[62] A. Corma, M. T. Navarro, J. P. Pariente*, J. Chem. Soc.*, *Chem. Commun.* **1994**, 147.

[63] P. T. Tanev, M. Chibwe, T. J. Pinnavaia, *Nature* **1994**, *368*, 321.

[64] A. Corma, V. Fornes, M. T. Navarro, J. P. Pariente, *J. Catal.* **1994**, *148*, 569.

[65] A. Corma, *Chem. Rev.* **1997**, *97*, 2373.

[66] U. Ciesla, F. Schüth, *Microporous Mesoporous Mater.* **1999**, *27*, 131.

[67] G. J. de A. A. Soler-Illia, C. Sanchez, B. Lebeau, J. Patarin, *J. Chem. Rev.* **2002**, *102,* 4093.

[68] D. Y. Zhao, J. L. Feng, Q. S. Huo, N. Melosh, G. H. Fredrickson, B. F. Chmelka, G. D. Stucky, *Science* **1998**, *279*, 548.

[69] D. Y. Zhao, Q. S. Huo, J. L. Feng, B. F. Chmelka, G. D. Stucky, *J. Am. Chem. Soc.* **1998**, *120*, 6024.

[70] A. Galarneau, H. Cambon, F. Di Renzo, F. Fajula, *Langmuir* **2001**, *17*, 8328-8335.

[71] V. L. Zholobenko, A. Y. Khodakov, M. Impéror-Clerc, D. Durand, I. Grillo, *Advances in Colloid and Interface Science* **2008**, *142*, 67-74.

[72] A. Sayari, B.-H. Han, Y. Yang, *J. Am. Chem. Soc.* **2004**, *126*, 14348-14349.

[73] A. Galarneau, H. Cambon, F. Di Renzo, R. Ryoo, M. Choi, F. Fajula, *New. J. Chem.* **2003**, *27*, 73-79.

[74] P. Barbaro, C. Bianchini, V. Dal Santo, A. Meli, S. Moneti, C. Pirovano, R. Psaro, L. Sordelli, F. Vizza, *Organometallics* **2008**, *27*, 2809.

[75] P. Barbaro, C. Bianchini, V. Dal Santo, A. Meli, S. Moneti, R. Psaro, A. Scaffidi, L. Sordelli, F. Vizza, *J. Am. Chem. Soc.* **2006**, *128*, 7065-7076.

[76] (a) C. Bianchini, V. Dal Santo, A. Meli, S. Moneti, M. Moreno, W. Oberhauser, R. Psaro, L. Sordelli, F. Vizza, *J. Catal.* **2003**, *213*, 47.

(b) C. Bianchini, P. Barbaro, V. Dal Santo, R. Gobetto, A. Meli, W. Oberhauser, R. Psaro, F. Vizza, *Adv. Synth. Catal.* **2001**, *343*, 41.

(c) C. Bianchini, V. Dal Santo, A. Meli, W. Oberhauser, R. Psaro, F. Vizza, *Organometallics* **2000**, *19*, 2433.

(d) C. Bianchini, D. G. Burnaby, J. Evans, P. Frediani, A. Meli, W. Oberhauser, R. Psaro, L. Sordelli, F. Vizza, *J. Am. Chem. Soc.* **1999**, *121*, 5961.

[77] F. M. De Rege, D. K. Morita, K. C. Ott, W. Tumas, R. D. Broene, *Chem. Commun.* **2000**, 1797.

[78] (a) C. Bianchini, A. Meli, F. Vizza, in *The Handbook of Homogeneous Hydrogenation*; de Vries, J. G., Ed.; Wiley-VCH: Weinheim, Germany, **2006**.

(b) J. M. Thomas, R. Raja, D. W. Lewis, *Angew. Chem. Int. Ed.* **2005**, *44*, 6456.

[79] F. Solymosi, J. Raskó, *Journal of Catalysis* **1995**, *155*, 74-81.

[80] A. Galarneau, D. Desplantier, R. Dutartre, F. Di Renzo, *Microporous and Mesoporous Materials* **1999**, *27*, 297-308.

[81] B. Coasne, A. Galarneau, F. Di Renzo, R. J. M. Pellenq, *Langmuir* **2006**, *22*, 11097-11105.

[82] R. Abu-Reziq, D. Avnir, I. Miloslavski, H. Schumann, J. Blum, *Journal of Molecular Catalysis A: Chemical* **2002**, *185*, 179-185.

[83] J. Blum, D. Avnir, H. Schumann, *Chemtech* **1999**, *29*, 32.

[84] S. Bharathi, N. Fishelson, O. Lev, *Langmuir* **1999**, *15*, 1929.

[85] J. M. Tour, S. L. Pendalwar, J. P. Cooper, *Chem. Mater.* **1990**, *2*, 647.

[86] S. Chen, K. Huang, J. A. Stearns, *Chem. Mater.* **2000**, *12*, 540.

[87] C. Bianchini, V. Dal Santo, A. Meli, S. Moneti, M. Moreno, W. Oberhauser, R. Psaro, L. Sordelli, F. Vizza, *Angew. Chem. Int. Ed.* **2003**, *42*, 2636-2639.

[88] K. J. Stanger, Y. Tang, J. Anderegg, R. J. Angelici, *Journal of Molecular Catalysis A: Chemical* **2003**, *202*, 147-161.

[89] (a) T. Maschmeyer, F. Rey, G. Sankar, J. M. Thomas, *Nature* **1995**, *378*, 159.

(b) P. E. Sinclair, G. Sankar, C. R. A. Catlow, J. M. Thomas, T. Maschmeyer, *J. Phys. Chem. B* **1997**, *101*, 4232.

[90] I. J. Shannon, T. Maschmeyer, R. D. Oldroyd, G. Sankar, J. M. Thomas, H. Pernot, J. P. Balikdjian, M. Che, *J. Chem. Soc. Faraday Trans.* **1998**, *94*, 1495.

[91] (a) J. M. Thomas, R. Raja, *Stud. Surf. Sci. Catal.* **2004**, *148*, 163.

(b) A. Sakthivel, J. Zhao, F. E. Kühn, *Catal. Lett.* **2005**, *102*, 115.

[92] S. Abbet, A. Sanchez, U. Heiz, W. D. Schneider, A. M. Ferrari, G. Pacchioni, N. Rösch, *J. Am. Chem. Soc.* **2000**, *122*, 3453.

[93] S. Abbet, U. Heiz, H. Hakkinen, U. Landman, *Phys. Rev. Lett.* **2001**, *86*, 5950.

[94] (a) C. Coperet, M. Chabanas, R. P. Saint-Arroman, J. M. Basset, *Angew. Chem.* **2003**, *115*, 164.

(b) C. Coperet, M. Chabanas, R. P. Saint-Arroman, J. M. Basset, *Angew. Chem. Int. Ed.* **2003**, *42*, 156.

[95] (a) J. M. Thomas, P. A. Midgley, T. J. V. Yates, J. S. Barnard, R. Raja, I. Arslan, M. Weyland, *Angew. Chem.* **2004**, *116*, 6913.

(b) J. M. Thomas, P. A. Midgley, T. J. V. Yates, J. S. Barnard, R. Raja, I. Arslan, M. Weyland, *Angew. Chem. Int. Ed.* **2004**, *43*, 6745.

[96] J. M. Thomas, B. F. G. Johnson, R. Raja, G. Sankar, P. A. Midgley, *Acc. Chem. Res.* **2003**, *36*, 20.

[97] (a) J. M. Thomas, G. N. Greaves, G. Sankar, P. A. Wright, J. S. Chen, A. J. Dent, L. Marchese, *Angew. Chem.* **1994**, *106*, 1922.

(b) J. M. Thomas, G. N. Greaves, G. Sankar, P. A. Wright, J. S. Chen, A. J. Dent, L. Marchese, *Angew. Chem. Int. Ed. Engl.* **1994**, *33*, 1871.

CHAPTER 2:

Synthesis, characterization and application of heterogeneized chiral $[Cu^{I}(PC\text{-}L^{*})]CF_3SO_3$ complexes on silica support materials

General part

1. Cu^{I} in cyclopropanation reactions

Copper is one of the most applied metals in asymmetric catalysis. Oftentimes, the active copper species has the oxidation state (I), like in the copper-catalyzed cyclopropanation reaction of olefins.[1,2] However, Cu^{I} compounds are not highly stable; due to their thermodynamic instability, they disproportionate into Cu^{0} and Cu^{II}. Regarding the Cu^{I} catalyzed asymmetric cyclopropanation, semicorrin,[3] bis(oxazoline)[4] and bipyridine[5] are often and likely used ligands (Figure 1).[6]

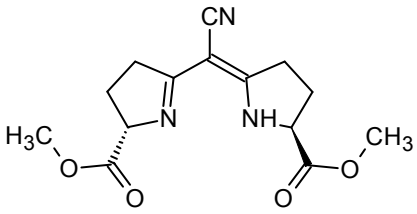

Semicorrin

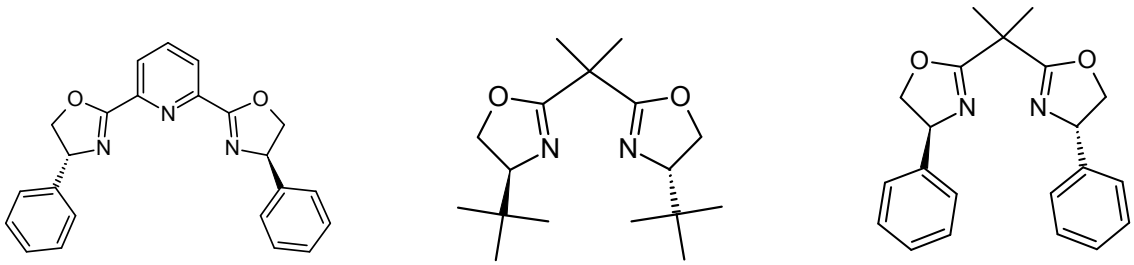

Bis(oxazoline) ligands

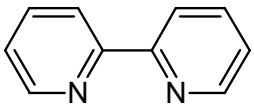

Bipyridine

Figure 1: Ligands for the Cu^{I} catalyzed asymmetric cyclopropanation.

All of these compounds show a C_2-symmetry; however, it could be shown in several recent studies that also C_1-symmetric species turned out to be efficient ligands.[7,8,9,10]

One example are the (PC-L*) ligands.[1,2] They show a chiral 12-membered structure, containing a tetraaza macrocycle. Their synthesis is performed in two steps (Figure 2), starting from tosyl aziridine and a chiral aryl amine. The second step includes the formation of the macrocycle, which is carried out under heterogeneous reaction conditions.[11] The (PC-L*) ligands **1a** and **1b** could be obtained in high yields, up to 80 %.[1]

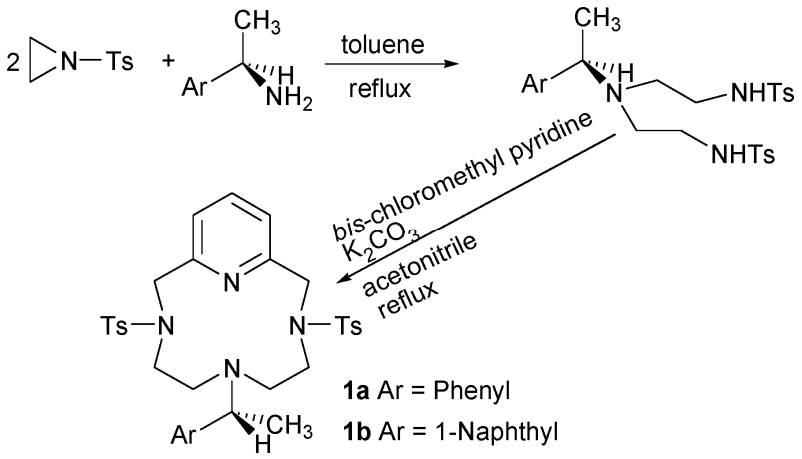

Figure 2: Synthesis of (PC-L*).[1]

The conversion of the (PC-L*) ligands **1a** and **1b** with different copper salts leads to the formation of monometallic Cu^{I} complexes (Figure 3).

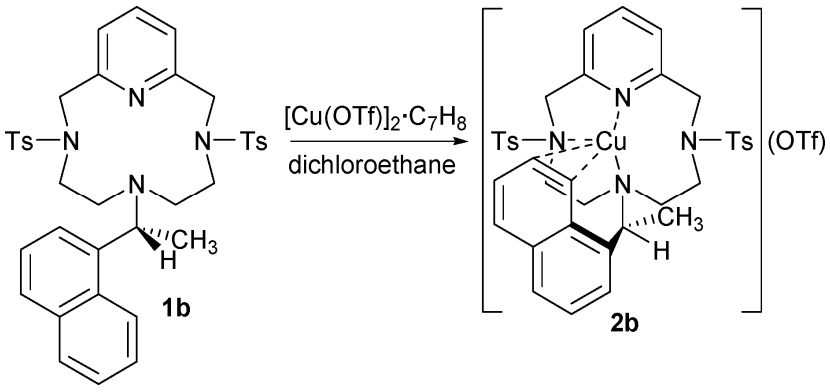

Figure 3: Synthesis of $[Cu(PC\text{-}L^*)]CF_3SO_3$.[1]

The (PC-L*) ligands **1a** and **1b** were applied in the cyclopropanation reaction of α-methyl styrene with ethyl diazoacetate (EDA) (Figure 4).[1] The macrocyclic ligands served as ligands for Cu^{I} salts.

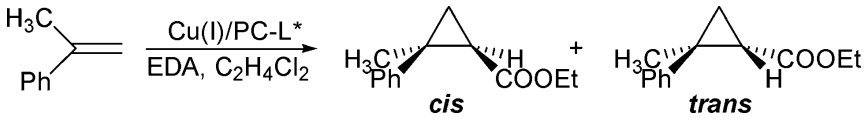

Figure 4: Cyclopropanation of α-methyl styrene with EDA.[1]

A solution of α-methyl styrene, the (PC-L*) ligand and the Cu^{I} salt in dichloroethane was prepared, with subsequent addition of EDA. It could be demonstrated that the highest yield of the cyclopropanation products was obtained when performing the reaction at 0 °C, with a slow, dropwise addition of EDA over 90 min.[1] As Cu^{I} salt, the benzene complex or rather toluene complex of $[Cu^{I}(OTf)]_2$ was applied. (PC-L*) ligand **1b** served as the ligand for the Cu^{I} salt. Under these conditions, yields up to 83 % were obtained, with a *cis:trans* ratio of 60:40.[1] It could be shown that a decrease of the temperature to -20°C did not have an impact on the selectivity; giving a lower yield of 59 %, with a *cis:trans* ratio of 64:36.[1]

Besides α-methyl styrene, also other olefins were tested in the cyclopropanation reaction. It could be shown that styrene compounds, which do not feature a substituent in α-position, have an impact on the diastereoselectivity. Using pure styrene, *p*-methyl styrene or *p*-chloro styrene, yields ranging between 45 and 68 % were obtained, giving *cis:trans* ratio of 50:50 (styrene), 53:47 (*p*-methyl styrene) or rather 47:53 (*p*-chloro styrene).

2. Cyclopropanation reactions

Cyclopropanation products are applied for instance as intermediates, in order to prepare cycloalkanes with more functionalities or acyclic compounds.[12] In particular, the enantioselective cyclopropanation is of great interest. In general, three different types of stereoselective cyclopropanation reactions exist, shown below (Figure 5a, b and c).

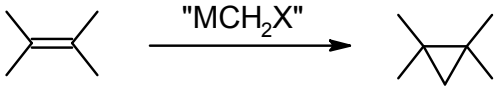

Figure 5a: "Halomethyl-metal-mediated cyclopropanation".[12]

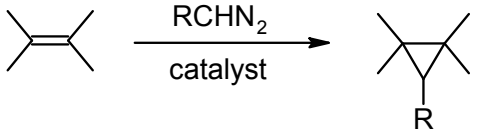

Figure 5b: "Transition metal-catalyzed decomposition of diazo compounds".[12]

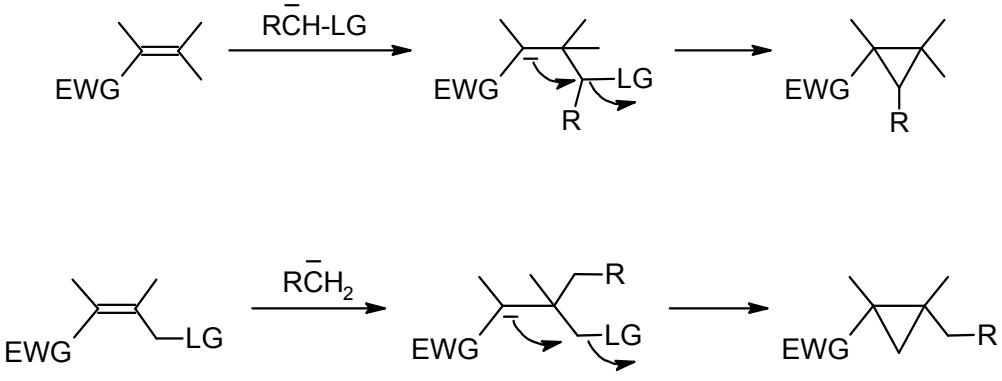

Figure 5c: "Nucleophilic addition – ring closure sequence".[12]

2.1 Halomethyl-metal-mediated cyclopropanation

The first cyclopropanation type (Figure 5a) offers a high flexibility, as a multitude of different olefins can be applied, having numerous functional groups, e.g. enamines, enol ethers, esters and ketones.[12]

2.2 Transition metal-catalyzed decomposition of diazo compounds

The second type (Figure 5b) is one of the most intensively investigated organic reactions.[12] Regarding the choice of the proper catalyst, two parameters have to be considered, i.e. the diazoalkane species and the type of the reaction, whether it proceeds inter- or intramolecular. In terms of the diazoalkanes, the following compounds are generally used (Figure 6).

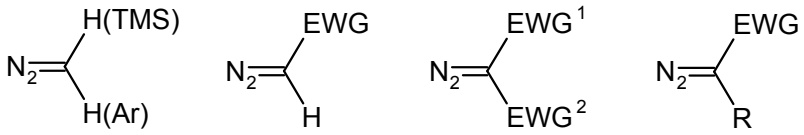

Figure 6: Diazoalkane compounds for the halomethyl-metal-mediated cyclopropanation.[12]

2.2.1 Intermolecular Cyclopropanation

2.2.1.1 Diazomethane

Diazomethane is the simplest diazoalkane, which is often used in cyclopropanation reactions, besides trimethylsilyldiazomethane and phenyldiazomethane. The latter compounds feature a higher stability compared to diazomethane. There is a multitude of metals, which can be applied in order to decompose the diazo species, amongst others also Cu. However, Pd has proved to be the most effective one.[13,14]

2.2.1.2 Diazoalkanes with one EWG

Regarding the diazoalkanes containing an electron-withdrawing group (EWG) (Figure 6), the following compounds are commonly applied (Figure 7).

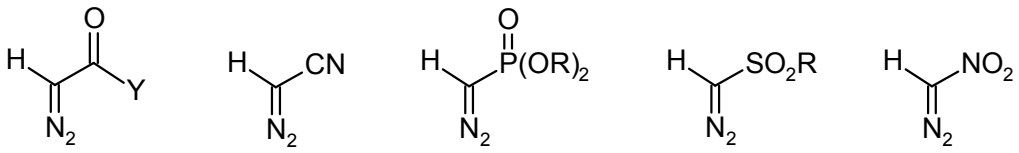

Figure 7: Diazoalkane compounds with an EWG.[12]

Various metals are able to decompose the EWG-containing diazoalkanes, for instance Cu, Rh, Ru, Co, Fe, Os, Pd, Pt and Cr.[12] Concerning the cyclopropanation catalyzed by Cu, Rh, Ru and Os, the expected mechanism is shown below (Figure 8).

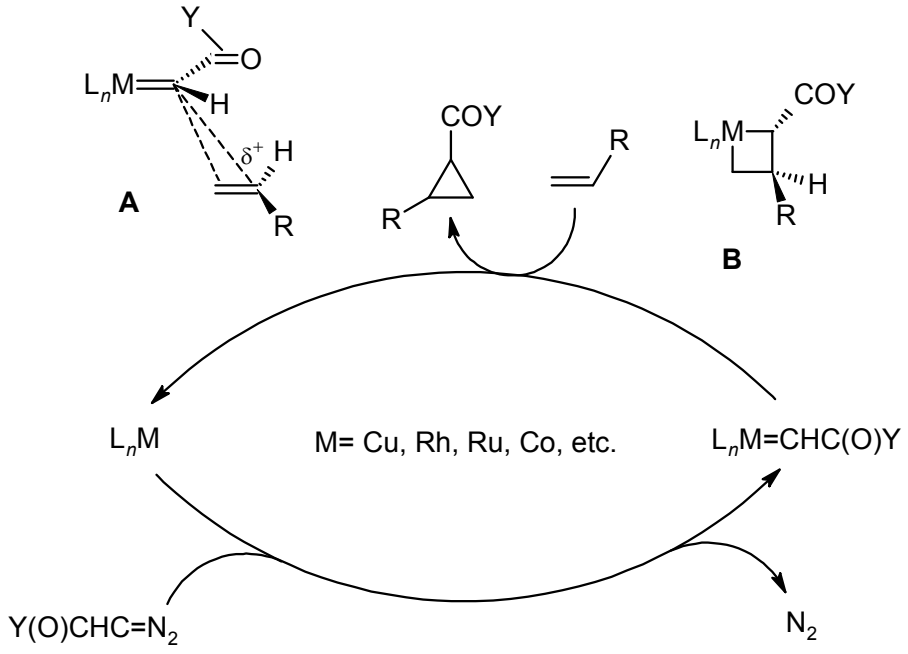

Figure 8: Mechanism of cyclopropanation using EWG-diazoalkanes.[12]

2.2.1.3 Diazoalkanes with two EWGs

Regarding the diazoalkanes with two EWGs, it is noticeable that they show a poorer reactivity compared to those ones containing only one EWG.[12] Therefore, it is necessary to increase the concentration of the catalyst, in order to get the metal carbene intermediate (Figure 8). For instance, the cyclopropanation between styrene and dimethyl diazomalonate as diazoalkane having two EWGs gives the corresponding cyclopropanes in high yields up to 97 %; however, the obtained ee is poor (50 %).[15]

2.2.2 Intramolecular Cyclopropanation

An intramolecular cyclopropanation can occur, when a compound features both the diazo functionality as well as the C=C double bond.[16,17] In this case, bicyclic products are obtained. The most familiar example is given below, showing the first intramolecular cyclopropanation (Figure 9). In 1961, *Stork* and *Ficini* showed the intramolecular conversion of an unsaturated diazocarbonyl compound, catalyzed by a heterogeneous Cu species.[18]

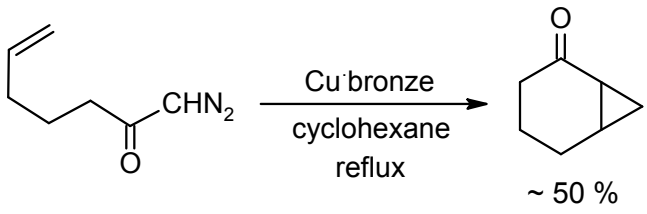

Figure 9: The first cyclopropanation, catalyzed by Cu.[18]

Cu compounds were the first catalysts for intramolecular cyclopropanation reactions.[12] They were applied in their heterogeneous form, e.g. as Cu powder, Cu bronze or cupric sulfate. Nowadays, these heterogeneous Cu catalysts are still gladly and widely used. However, one passed on to homogeneous Cu and Rh species. The above cyclization was very often used for the preparation of terpenes.[19]

2.3 Nucleophilic addition – ring closure sequence

The third type (Figure 5c and 10) of the three stereoselective cyclopropanation reactions is the nucleophilic addition, also known as "Michael-initiated ring closure (MIRC)".[12] This reaction occurs via an enolate as intermediate, which is formed by the nucleophilic addition to an electrophilic alkene. Subsequent intramolecular cyclization converts the enolate into the corresponding cyclopropane.

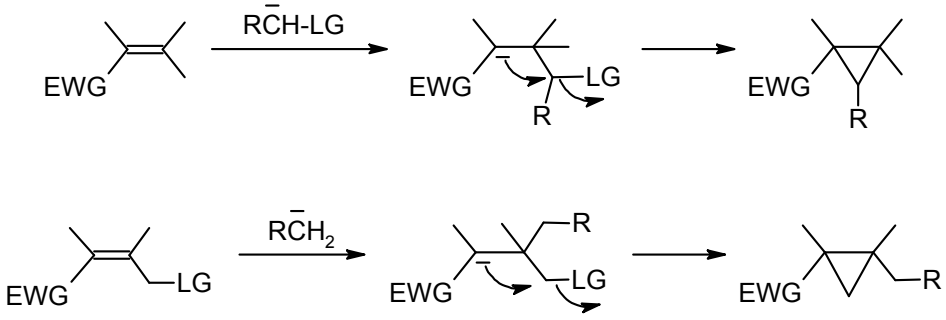

Figure 10: "Nucleophilic addition – ring closure sequence".[12]

In general, cyclopropanation reactions of the MIRC type do not occur stereospecifically, i.e. the corresponding *trans*-cyclopropanes are obtained whether (*E*)- or (*Z*)-olefins are applied as starting material.[12]

However, there is an exception, explained by the mechanism below (Figure 11). The first step **A** is the nucleophilic addition to the olefin, giving the enolate intermediate. Step **B** describes the rotation around the C-C single bond. If this step occurs slower than the cyclization step **C**, the MIRC cyclopropanation is effected stereospecifically.

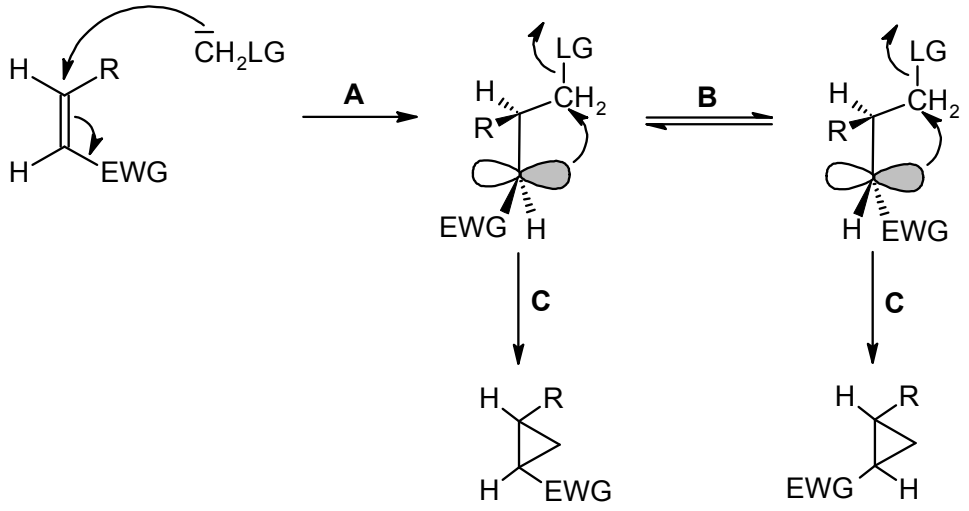

Figure 11: Mechanism of MIRC cyclopropanation.[12]

Two different types of MIRC cyclopropanation reactions exist. The first one describes the nucleophilic addition to an alkene, which contains a leaving group (Figure 12a).[12] This type includes a multitude of proper nucleophiles, for instance thiolates, cyanides, enolates, Grignard reagents, hydrides and many more.[20,21]

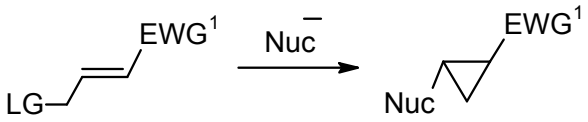

Figure 12a: First MIRC cyclopropanation type.[12]

In terms of the second MIRC cyclopropanation type, the nucleophile encloses the leaving group (Figure 12b).

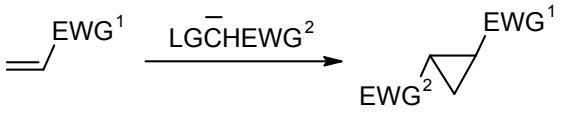

Figure 12b: Second MIRC cyclopropanation type.[12]

Results and discussion

This part of the work was carried out in collaboration with *Dr. Alessandro Caselli (Università degli Studi di Milano, Dipartimento CIMA "Lamberto Malatesta")*. Chiral Cu^{I} complexes, of the type $[Cu^{I}(PC\text{-}L^{*})]CF_3SO_3$, were immobilized on various silica support materials (MCM-41, SBA-15, Davisil B, basic silica, Aerosil) via impregnation, in order to design heterogeneized catalysts for asymmetric cyclopropanation reactions.

1. Synthesis of $[Cu^{I}(PC\text{-}L^{*})]CF_3SO_3/SiO_2$

$[Cu^{I}(PC\text{-}L^{*})]CF_3SO_3$ complexes were grafted on different powdery mesoporous ordered and non-ordered silica supports via the *"SHB"-concept ("Supported Hydrogen Bonding")*.

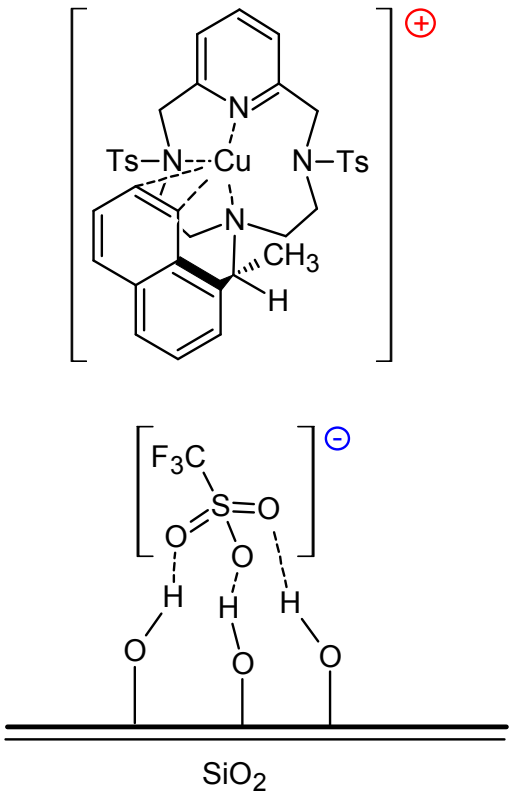

Figure 13: $[Cu^{I}(PC\text{-}L^{*})]CF_3SO_3$ supported on silica via *"SHB"-concept*.

The loadings of Cu were determined by *Inductively Coupled Plasma Optical Emission Spectrometry (ICP-OES)*; selected results are given in Table 1, showing the obtained Cu loadings, the applied silica supports and the relative form of the Cu^{I} complexes (solid and isolated or rather dissolved and non-isolated).

Table 1: Cu loadings, determined by ICP-OES, of selected $[Cu^{I}(PC\text{-}L^{*})]CF_3SO_3/SiO_2$ samples.

Entry	SiO_2 support	Form of $[Cu^{I}(PC\text{-}L^{*})]CF_3SO_3$	Cu loading [wt %]
1	MCM-41	solid, isolated	0.70
2	Davisil B	solid, isolated	0.95
3	Davisil B	solid, isolated	0.66
4	Aerosil	dissolved, non-isolated	0.45
5	basic silica	solid, isolated	0.32
6	SBA-15	dissolved, non-isolated	1.35
7	SBA-15	dissolved, non-isolated	1.79

Cu loadings between 0.32 and 1.79 wt % were obtained. In general, higher loadings could be achieved using $[Cu^{I}(PC\text{-}L^{*})]CF_3SO_3$ directly after its synthesis in the dissolved form, without isolation from the solvent (entry 6 and 7).
Regarding the silica support materials, SBA-15 proved to be the most suitable one, giving high metal loadings up to 1.79 wt % (entry 7).

2. Application of $[Cu^{I}(PC\text{-}L^{*})]CF_3SO_3/SiO_2$: Asymmetric cyclopropanation

The $[Cu^{I}(PC\text{-}L^{*})]CF_3SO_3/SiO_2$ catalysts were applied in the asymmetric cyclopropanation reaction of α-methyl styrene (and derivatives) with ethyl diazoacetate (EDA) (Figure 14).

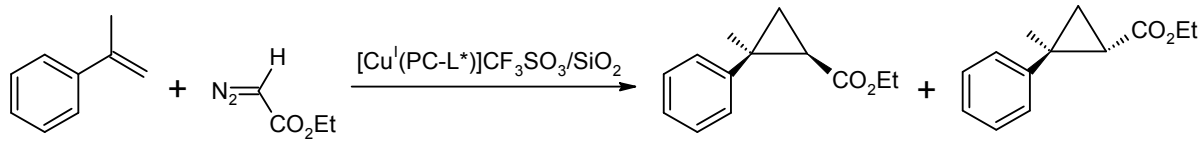

Figure 14: Asymmetric cyclopropanation of α-methyl styrene with EDA.

Selected results are shown below (Table 2). The yield was determined via GC, the *cis*/*trans*-ratio via GC-MS and the ee by HPLC.

Table 2: Asymmetric cyclopropanation – selected results.

Entry	Catalyst[a]	Yield [%]	*cis/trans*	ee *cis* [%]	ee *trans* [%]
1	$[Cu^{I}(PC\text{-}L^{*})]$ / Davisil B (0.95 wt %)	23[b]	53:47	-	-
2	$[Cu^{I}(PC\text{-}L^{*})]$ / MCM-41 (0.70 wt %)	72	72:28	35 (1S, 2R)	26 (1S, 2S)
3a*	$[Cu^{I}(PC\text{-}L^{*})]$ / Davisil B (0.66 wt %)	83	77:23	38 (1R, 2S)	27 (1R, 2R)
3b*	$[Cu^{I}(PC\text{-}L^{*})]$ / Davisil B (0.66 wt %)	80	75:25	36 (1R, 2S)	29 (1R, 2R)
3c*	$[Cu^{I}(PC\text{-}L^{*})]$ / Davisil B (0.66 wt %)	75	75:25	37 (1R, 2S)	28 (1R, 2R)

[a] Loadings of Cu in brackets.

[b] Isolated and not-optimized yield.

* Recycling test: $[Cu^{I}(PC\text{-}L^{*})]$/Davisil B has been reused for 3 runs.

High yields up to 83 % were obtained (entry 3a), giving the favoured *cis*-enantiomer in excess. In order to test the recyclability of the $[Cu^{I}(PC\text{-}L^{*})]CF_3SO_3/SiO_2$ catalysts, the same catalyst – here $[Cu^{I}(PC\text{-}L^{*})]CF_3SO_3$/Davisil B – was applied in three

successive reactions (entry 3a-c). With every run, only a slight decrease of the yield was observed, starting from 83 % (first run, entry 3a) until 75 % (third run, entry 3c). The *cis*/*trans* ratio remained constantly during all three runs. Thus, the recyclability of the $[Cu^{I}(PC\text{-}L^{*})]CF_3SO_3/SiO_2$ catalysts was proven.

3. Analytical characterization of $[Cu^{I}(PC\text{-}L^{*})]CF_3SO_3/SiO_2$

In order to verify the adsorption of the $[Cu^{I}(PC\text{-}L^{*})]CF_3SO_3$ complexes on the silica surface, DRIFT spectra of the bare silica and the impregnated silicas were compared (Figure 15). The characteristic band at 3740 cm^{-1} describes the isolated silanol groups. Its intensity decreases considerably when the $[Cu^{I}(PC\text{-}L^{*})]CF_3SO_3$ complexes are immobilized and hydrogen bonds are formed between the silanol groups and the triflate counter ion of the Cu^{I} species. Simultaneously, the broad band around
3740 cm^{-1}, signifying the hydrogen-bonded silanol groups, increases due to the immobilization of the Cu^{I} complexes. It was observed that the use of SBA-15 as support material leads to an augmented formation of hydrogen bonds between the silanol groups and the Cu^{I} species, in comparison to Davisil B. Correspondingly, a higher loading of Cu could be obtained using SBA-15 (see Table 1).

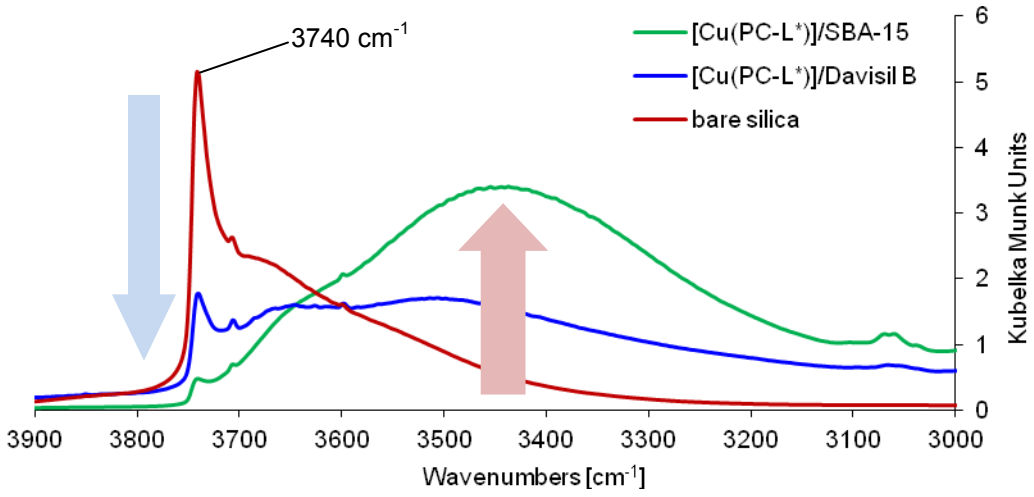

Figure 15: DRIFT spectra of the bare SiO_2 and $[Cu^{I}(PC\text{-}L^{*})]CF_3SO_3/SiO_2$, characteristic bands of isolated silanol groups at 3740 cm^{-1}.

CO-DRIFT spectra of the $[Cu^{I}(PC\text{-}L^{*})]CF_3SO_3/SiO_2$ samples were recorded in order to analyze the binding affinity of CO. The Cu^{I} complexes do not contain any functional groups, which could be identified by IR spectroscopy. Therefore, CO provides as a proper probe molecule.

It could be demonstrated that the Cu^{I} species are able to bind CO as ligand. However, this ability depends on the applied silica support, as evident from Figure 5b, showing the characteristic CO-band at 2116 cm^{-1}.

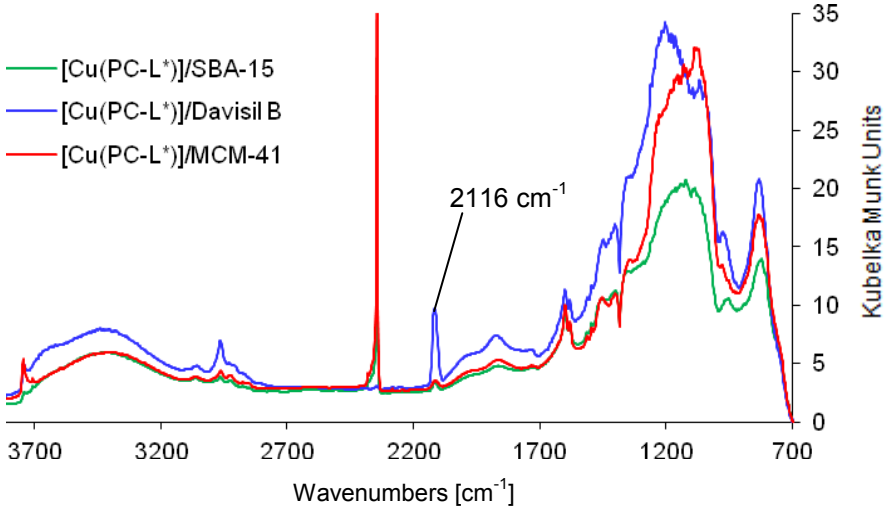

Figure 16a: CO-DRIFT spectra of $[Cu^{I}(PC\text{-}L^{*})]CF_3SO_3/SiO_2$ before catalysis.

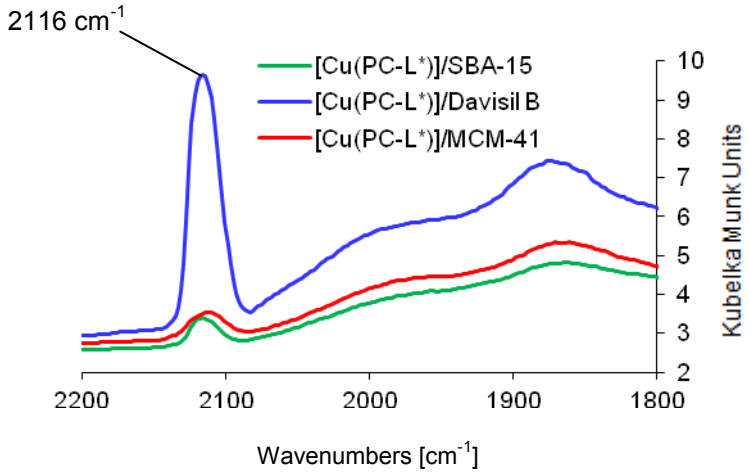

Figure 16b: The same CO-DRIFT spectra of $[Cu^{I}(PC\text{-}L^{*})]CF_3SO_3/SiO_2$ before catalysis expanded, characteristic CO-band at 2116 cm^{-1}.

CO-DRIFT spectra of the $[Cu^{I}(PC\text{-}L^{*})]CF_3SO_3/SiO_2$ samples before and after their application in catalysis were recorded and compared. In this way, it could be investigated if the use in catalysis has an influence on the catalysts' structure.

Below, a comparison between $[Cu^{I}(PC\text{-}L^{*})]CF_3SO_3$ immobilized on SBA-15 before and after its use in the cyclopropanation is given. The characteristic band at 1730 cm^{-1} indicates the cyclopropanation product (Figure 17b); a proof that the $[Cu^{I}(PC\text{-}L^{*})]CF_3SO_3$/SBA-15 is able to catalyze the reaction.

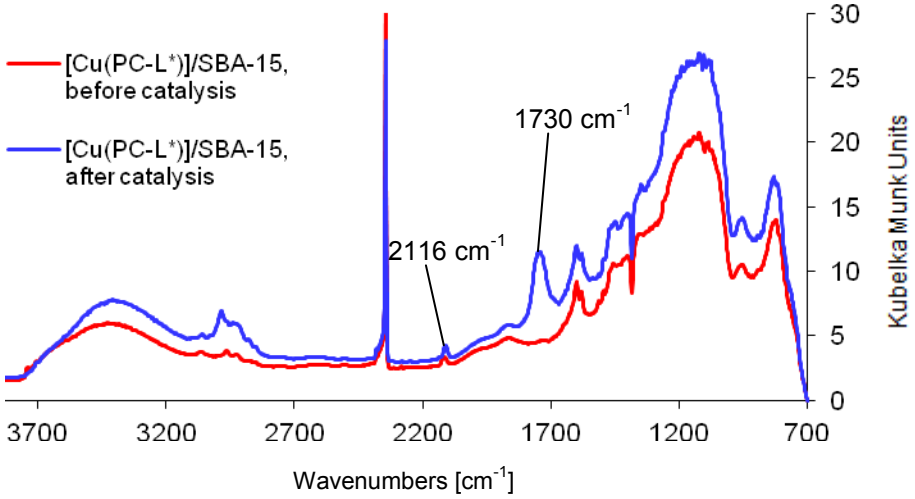

Figure 17a: CO-DRIFT spectra of $[Cu^{I}(PC\text{-}L^{*})]CF_3SO_3$/SBA-15 (SBA-15 MFDC065), before and after catalysis.

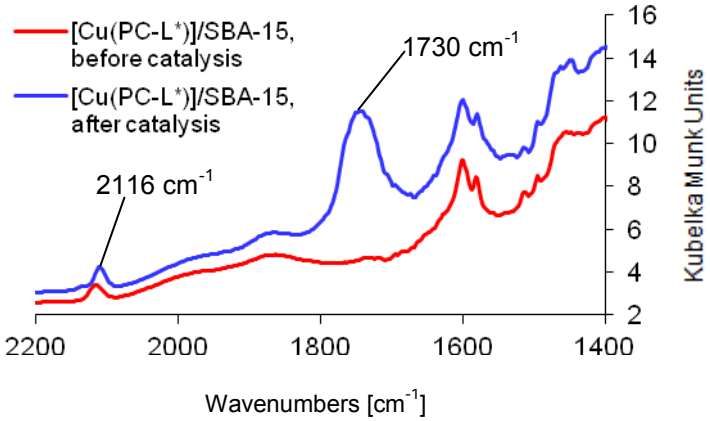

Figure 17b: The same CO-DRIFT spectra of $[Cu^{I}(PC\text{-}L^{*})]CF_3SO_3$/SBA-15 (SBA-15 MFDC065) expanded, before and after catalysis, characteristic CO-band at 2116 cm^{-1}, band of cyclopropanation product at 1730 cm^{-1}.

The same comparison of the CO-DRIFT spectra before and after catalysis was carried out with [Cu^{I}(PC-L*)]CF_3SO_3/MCM-41 (Figure 18a and 18b) and [Cu^{I}(PC-L*)]CF_3SO_3/Davisil B (Figure 19a and 19b). As apparent, the same results were obtained, giving the characteristic band of the cyclopropanation product at 1730 cm^{-1}.

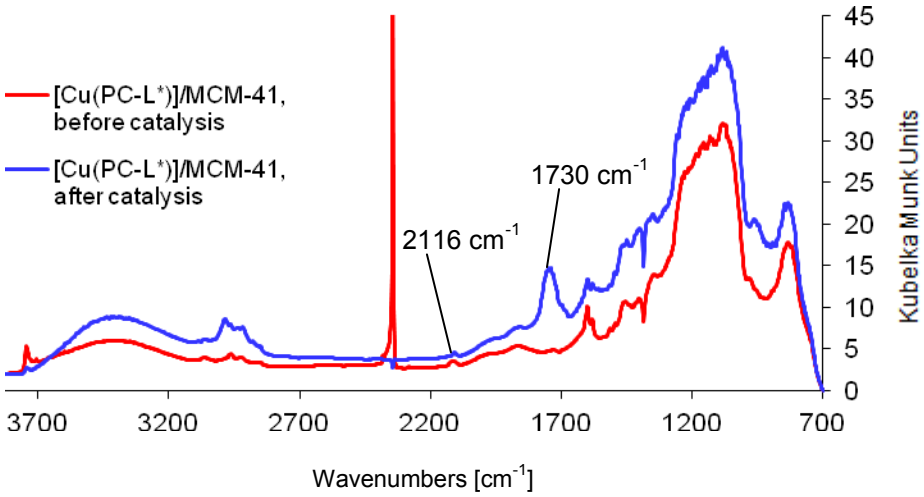

Figure 18a: CO-DRIFT spectra of [Cu^{I}(PC-L*)]CF_3SO_3/MCM-41 (MCM-41 6124), before and after catalysis.

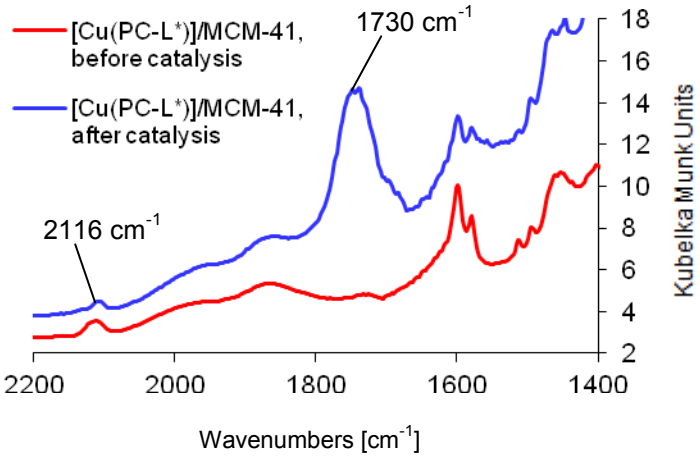

Figure 18b: The same CO-DRIFT spectra of [Cu^{I}(PC-L*)]CF_3SO_3/MCM-41 (MCM-41 6124) expanded, before and after catalysis, characteristic CO-band at 2116 cm^{-1}, band of cyclopropanation product at 1730 cm^{-1}.

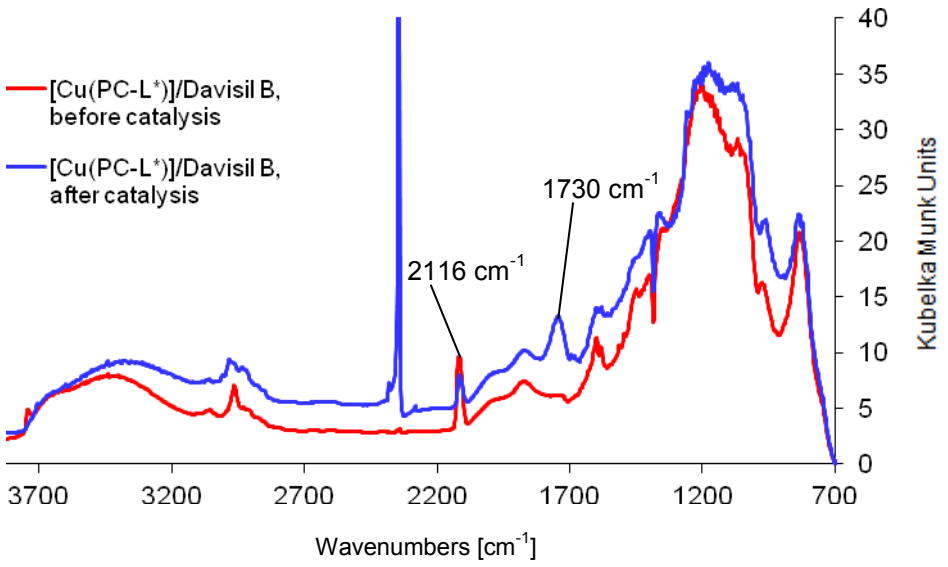

Figure 19a: CO-DRIFT spectra of $[Cu^{I}(PC\text{-}L^{*})]CF_3SO_3$/Davisil B, before and after catalysis.

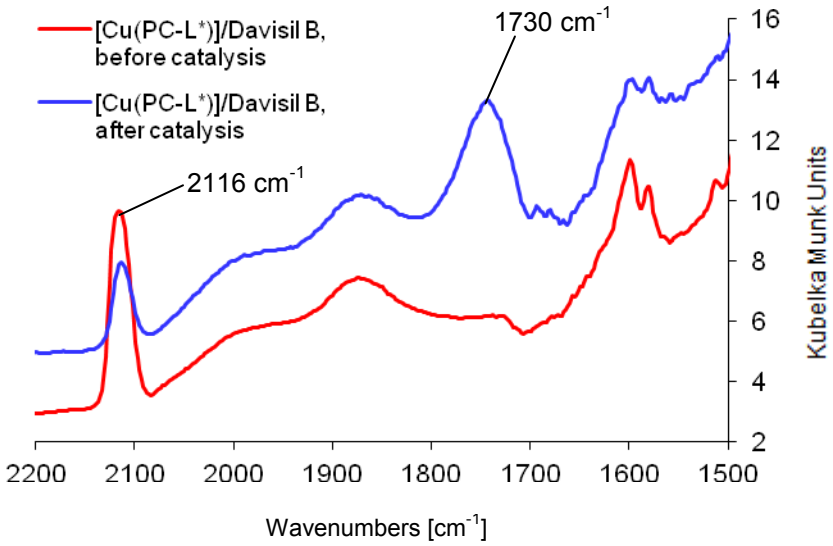

Figure 19b: The same CO-DRIFT spectra of $[Cu^{I}(PC\text{-}L^{*})]CF_3SO_3$/Davisil B expanded, before and after catalysis, characteristic CO-band at 2116 cm^{-1}, band of cyclopropanation product at 1730 cm^{-1}.

Moreover, different cyclopropanation reactions with various substrates were compared. For this purpose, DRIFT spectra of $[Cu^{I}(PC\text{-}L^{*})]CF_3SO_3$/Davisil B samples after their application in catalysis were recorded. Pattern **1** describes the $[Cu^{I}(PC\text{-}L^{*})]CF_3SO_3$/Davisil B sample before catalysis. Pattern **2** characterizes the use of $[Cu^{I}(PC\text{-}L^{*})]CF_3SO_3$/Davisil B in the cyclopropanation of *p*-chloro styrene and EDA, pattern **3** the cyclopropanation of *p*-methyl styrene and EDA and pattern **4** the cyclopropanation of α-methyl styrene and EDA. Pattern **5** specifies the cyclopropanation of α-methyl styrene and EDA after three recycles of the catalyst.

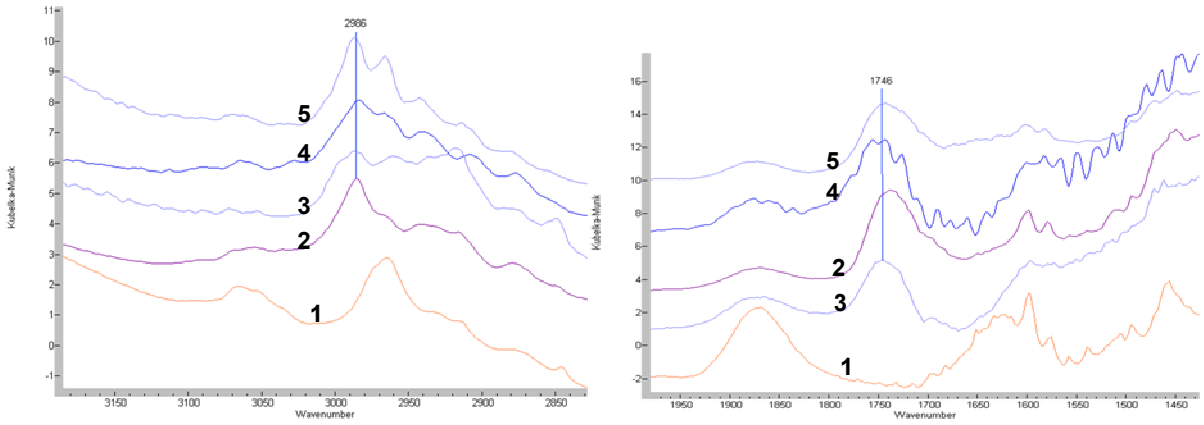

Figure 20: DRIFT spectra of $[Cu^{I}(PC\text{-}L^{*})]CF_3SO_3/SiO_2$, after catalysis, **1**: $[Cu^{I}(PC\text{-}L^{*})]CF_3SO_3$/Davisil B, **2**: *p*-chloro styrene + EDA, **3**: *p*-methyl styrene + EDA, **4**: α-methyl styrene + EDA, **5**: α-methyl styrene + EDA (after 3 recycles + washing); characteristic bands of cyclopropanation products (pure cyclopropanes) at 2980 and 1730 cm^{-1}.

As obvious from the spectra, all patterns show the characteristic bands of the corresponding cyclopropanation products at 2980 and 1730 cm^{-1}, proving that $[Cu^{I}(PC\text{-}L^{*})]CF_3SO_3$/Davisil B is able to catalyze the cyclopropanation reaction with different substrates. Moreover, $[Cu^{I}(PC\text{-}L^{*})]CF_3SO_3$/Davisil B turned out to be recyclable; even after three runs (pattern **5**) the cyclopropanation products were obtained.

Concluding remarks

Copper is an important metal in asymmetric catalysis. In particular, Cu^{I} complexes are often applied, e.g. in cyclopropanation reactions.

Within the scope of this work, $[Cu^{I}(PC\text{-}L^{*})]CF_3SO_3$ complexes could be successfully grafted on various mesoporous ordered and non-ordered silica supports (MCM-41, SBA-15, Davisil B, Aerosil, basic silica) via the *"Supported Hydrogen Bonding"*-concept. In terms of the silica, SBA-15 has proved to be the most proper support material, giving a high Cu loading up to 1.79 wt %. The immobilized $[Cu^{I}(PC\text{-}L^{*})]CF_3SO_3$ complexes were applied in the asymmetric cyclopropanation of α-methyl styrene and its derivatives with EDA. In this context it could be shown that the $[Cu^{I}(PC\text{-}L^{*})]CF_3SO_3/SiO_2$ catalysts are recyclable.

References

[1] A. Caselli, F. Cesana, E. Gallo, N. Casati, P. Macchi, M. Sisti, G. Celentano, S. Cenini, *Dalton Trans.* **2008**, 4202-4205.

[2] B. Castano, S. Guidone, E. Gallo, F. Ragaini, N. Casati, P. Macchi, M. Sisti, A. Caselli, *Dalton Trans.* **2012**, accepted (DOI: 10.1039/c2dt32347h).

[3] A. Pfaltz, *Acc. Chem. Res.* **1993**, *26*, 339-345.

[4] D. A. Evans, K. A. Woerpel, M. M. Hinman, M. M. Faul, *J. Am. Chem. Soc.* **1991**, *113*, 726-728.

[5] K. Ito, T. Katsuki, *Tetrahedron Lett.* **1993**, *34*, 2661-2664.

[6] H. Lebel, J.-F. Marcoux, C. Molinaro and A. B. Charette, *Chem. Rev.* **2003**, *103*, 977-1050.

[7] J. M. Fraile, J. I. García, A. Gissibl, J. A. Mayoral, E. Pires, O. Reiser, M. Roldán, I. Villalba, *Chem.-Eur. J.* **2007**, *13*, 8830-8839.

[8] G. Lesma, C. Cattenati, T. Pilati, A. Sacchetti, A. Silvani, *Tetrahedron: Asymmetry* **2007**, *18*, 659-663.

[9] P.-F. Teng, C.-S. Tsang, H.-L. Yeung, W.-L. Wong, W.-T. Wong, H.-L. Kwong, *J. Organomet. Chem.* **2006**, *691*, 5664-5672.

[10] C. Borriello, M. E. Cucciolito, A. Panunzi, F. Ruffo, *Tetrahedron: Asymmetry* **2001**, *12*, 2467-2471.

[11] S. Aime, M. Botta, S. G. Crich, G. B. Giovenzana, G. Jommi, R. Pagliarin, M. Sisti, *Inorg. Chem.* **1997**, *36*, 2992-3000.

[12] H. Lebel, J.-F. Marcoux, C. Molinaro, A. B. Charette, *Chem. Rev.* **2003,** *103,* 977-1050.

[13] R. Paulissen, A. J. Hubert, Ph. Teyssié, *Tetrahedron Lett.* **1972**, *13*, 1465.

[14] Y. V. Tomilov, V. A. Dokitchev, U. M. Dzhemilev, O. M. Nefedov, *Russ. Chem. Rev.* **1993**, *62*, 799.

[15] M. P. Doyle, S. B. Davies, W. Hu, *Org. Lett.* **2000**, *2*, 1145.

[16] S. D. Burke, P. A. Grieco, *Org. React.* **1979**, *26*, 361.

[17] A. Padwa, K. E. Krumpe, *Tetrahedron* **1992**, *48*, 5385.

[18] G. Stork, J. Ficini, *J. Am. Chem. Soc.* **1961**, *83*, 4678.

[19] T. Hudlicky, F. F. Koszyk, T. M. Kutchan, J. P. Sheth, *J. Org. Chem.* **1980**, *45*, 5020.

[20] D. Caine, *Tetrahedron* **2001**, *57*, 2643.

[21] J. Li, Y.-C. Liu, J.-G. Deng, *Tetrahedron: Asymmetry* **1999**, *10*, 4343.

CHAPTER 3:

Preparation of grafted silica monoliths and their catalytic application in the dehydration of D-fructose to 5-hydroxymethylfurfural (HMF)

General part

1. D-Fructose – a promising renewable resource

Sugars as attractive candidates for renewable raw materials

Due to the steady decrease of the conventional fossil fuels, like coal, petroleum and natural gas, it is inevitable to discover and employ new promising raw materials. In this context, sugars are attractive candidates because of their extensive availability.[1]

D-Fructose and its subsequent chemistry

Besides the sucrose and the glucose, the fructose as a ketohexose is an interesting starting material for a large variety of products.[1] It is generally synthesized by isomerization of glucose or rather by hydrolysis of the fructooligosaccharide inulin. Owing to its sweet flavour, the fructose is very often used as a sweetener in drinks. However, apart from the food chemistry, the field of application is quite small and limited, which is based on the unpredictable subsequent chemistry of fructose; contrary to the glucose, the transformations of fructose are not yet well-known and -studied.

Below, an overview about the possible transformations and reactions of fructose are given (Figure 1a and 1b).

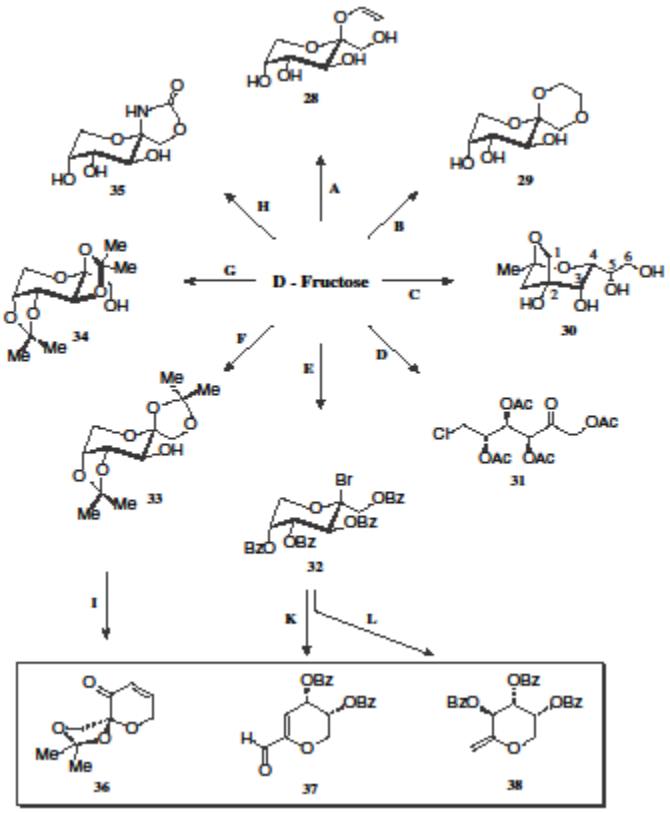

Figure 1a: Transformations of D-fructose to pyranoid derivatives.[1]

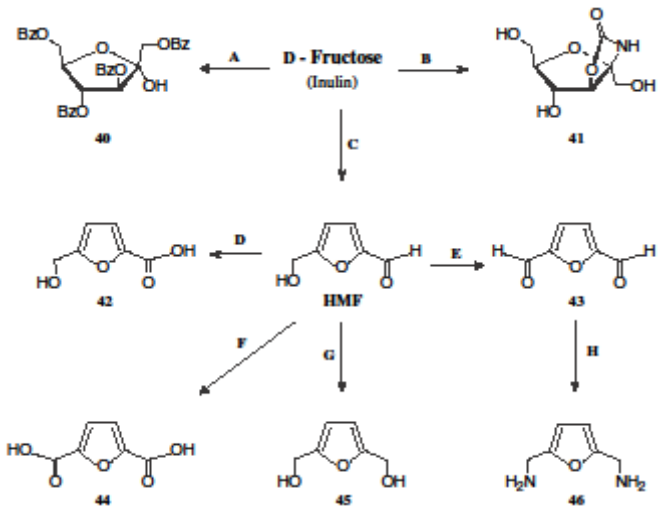

Figure 1b: Transformations of D-fructose to furanoid derivatives.[1]

The substrates **28**-**35** (Figure 1a) are pyranoid derivatives, the compounds **40**-**46** (Figure 1b) furanoid derivatives. One industrially important key product is the 5-hydroxymethylfurfural (HMF), which is characterized as “a key substance between carbohydrate chemistry and mineral oil-based industrial organic chemistry” (cit.).[2] The synthesis of HMF is quite simple; starting from either fructose or inulin, it is obtained by acid-initiated hydrolysis and elimination of 3 mol of water.[3] In this context, even an HMF-producing pilot plant has been developed.[4]

2. The dehydration of fructose to 5-hydroxymethylfurfural (HMF)

As evident from Figure 1b, HMF is a high-potential intermediate in order to generate industrially interesting products, e.g. the 5-hydroxymethyl-furoic acid (**42**) as well as the corresponding 2,5-dicarboxylic acid (**44**), the 1,6-diol (**45**) and the 1,6-diamine (**46**).[1] All of these compounds have a six-carbon-unit; therefore, they are eminent substituents for adipic acid and hexamethylenediamine (HMDA) for the large-scale production of polyamides and polyesters.

However, compared to other convenient starting materials like naphtha and ethylene, fructose or rather inulin, and thereby HMF, are too costly regarding the production of bulk chemicals. The corresponding costs prove this matter of fact: The price for one ton of naphtha or ethylene ranges between 150 and 400 Euro, whereas the ton prize for inulin or fructose is much higher and can be ranged between 500 and 1000 Euro, respectively.[1] Hence, one ton of HMF is even more costly (~ 2500 Euro per ton).[1] Due to this aspect, the large-scale production of HMF is cost-intensive and thereby, hardly to realize.

The synthesis of HMF

As already mentioned, HMF is generated by the acid-catalyzed dehydration of fructose or inulin under elimination of 3 mol of water. If the reaction is performed in an aqueous solution, the HMF continues reacting and forms the levulinic acid and the formic acid (Figure 2). However, in a non-aqueous medium, the subsequent hydrolysis is avoided. Moreover, the formation of either soluble or insoluble polymers can be observed.[3]

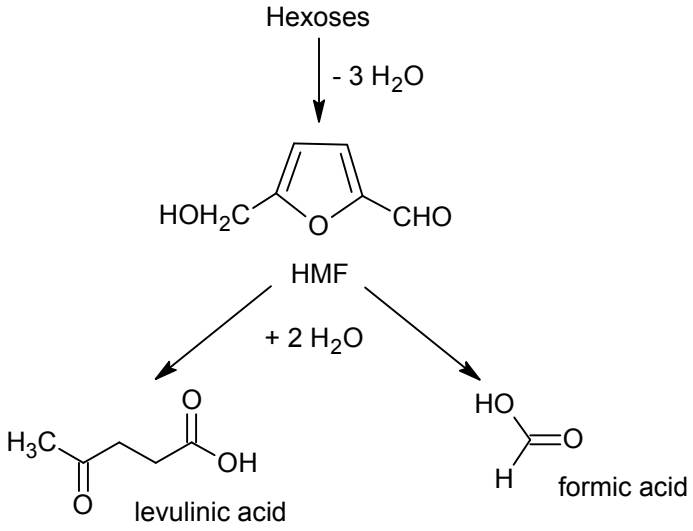

Figure 2: The generation of HMF and its subsequent products levulinic acid and formic acid.[3]

Mechanistic studies

It is difficult to make clear statements about the mechanism, due to the short life time of the intermediates.[3] Figure 3 gives an overview about the possible and proposed mechanisms. The whole route, starting from fructose and ending with the target product HMF, can be divided into several paths.

Path a describes the “acyclic route”, discussed by *Feather* and *Harris*.[5] Here, the fructose is converted into the corresponding 1,2-enediol via keto-enol tautomerism. The enediol is in equilibration with glucose and can be converted into the corresponding aldehyde. Elimination of water and subsequent cyclization yields the HMF.

The second path b is called the “cyclic route”, suggested by *Newth*,[6] and it includes the cyclization of fructose to α- or β-hexulofuranose in the first step. Elimination of water gives the corresponding enol, which can be converted either by dehydrogenation (path b) or by elimination of formaldehyde (path c). Further transformation yields the HMF in both paths.

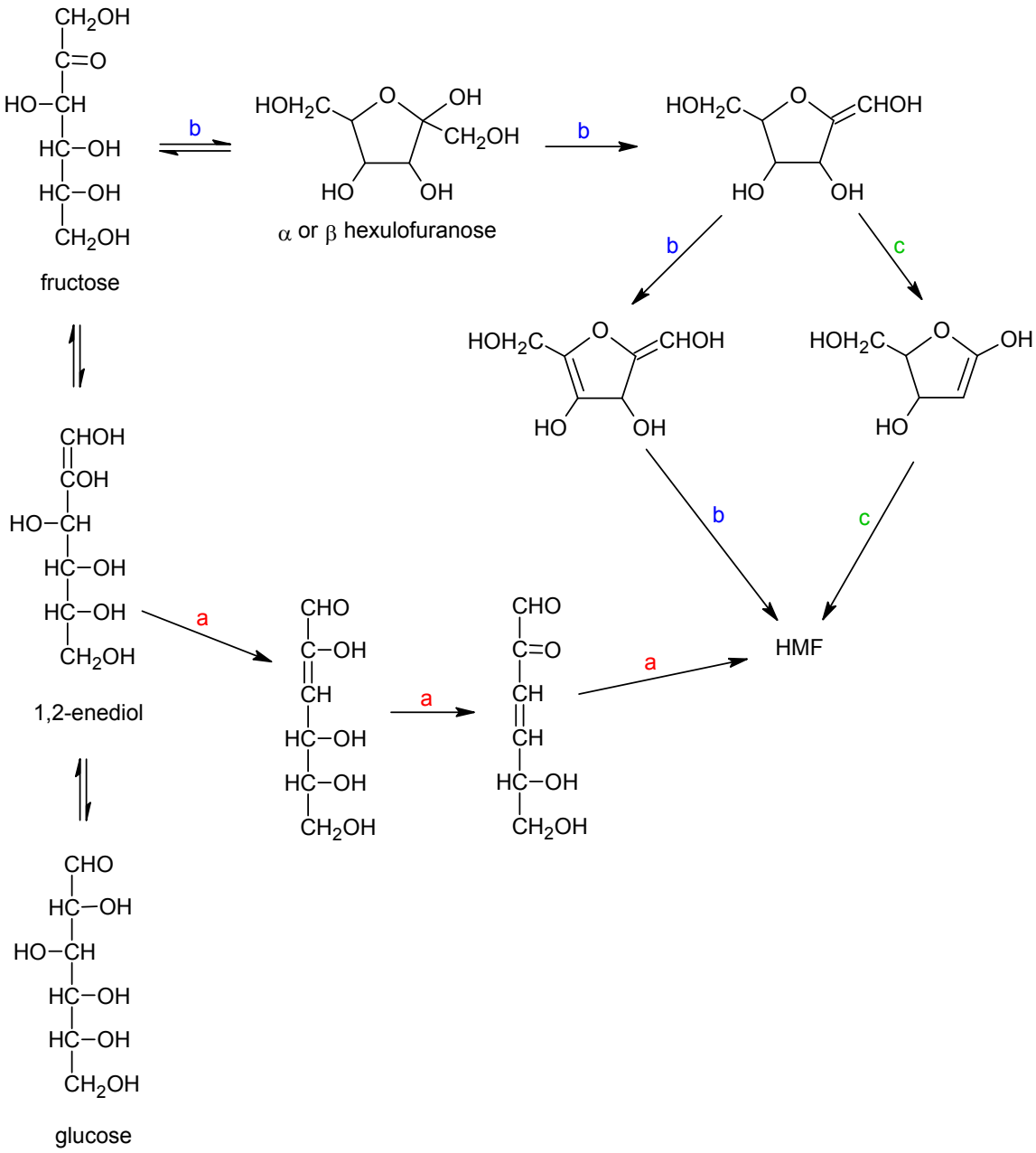

Figure 3: Suggested mechanisms for the dehydration of fructose to HMF.[3]

As demonstrated in Figure 3, HMF can be produced by various different access paths. Hence, fructose is only one of a multitude of starting compounds. In general, it is possible to obtain HMF from any hexose, e.g. glucose, as shown in Figure 3. But not only the simple monosaccharides are starting materials for the synthesis of HMF, oligo- and polysaccharides are attractive candidates as well; hydrolysis transforms them into the corresponding monosaccharides.[3] Admittedly, the synthesis of HMF is more selective when keto-hexoses are used as starting material. Fructose is the most cost-efficient starting material, it can be easily obtained either via hydrolysis of sucrose or by isomerization of glucose. Besides the fructose as convenient source, inulin is an auspicious compound for the production of HMF.

Fructose vs. glucose – which is the "better" starting material?

In comparison to glucose, fructose gives higher yields, owing to the following advantages:[3]

Firstly, glucose and fructose differ in the stability of their structure. Glucose prefers its remarkably stable ring structure; fructose, however, shows a higher stability in its open chain form. Thereby, fructose is predominantly existent in the open chain structure; accordingly, the formation of the enol occurs much faster in the case of fructose than in the case of glucose. It is supposed that the formation of the enol is the rate determining step in the formation of HMF. Thus, it is evident that higher yields of HMF can be obtained using fructose as starting material instead of glucose.

The second advantage of fructose, concerning the yields of HMF, is the better selectivity: It is observed that fructose forms di-fructose-di-anhydrides. This leads to a steric hindrance and blocking of many reactive functional groups, so that cross-polymerization can be prevented; a higher selectivity is obtained. Glucose, however, forms oligosaccharides, whose functional groups can react in order to generate cross-polymers, either with reactive intermediates or with HMF.

Because of these two reasons, fructose is preferably chosen as starting material, considering selectivity and yield of the reaction.

Proper catalysts for the synthesis of HMF

A multitude of catalysts is suitable for the dehydration reaction of fructose to HMF. In general, acids are used, protonic as well as Lewis acids.[3] Economic and thereby prevalently applied acids are e.g. H_2SO_4, H_3PO_4 and HCl. Interesting metals with a catalytic effect are amongst others Zn, Al, Cr, Ti, Th, Zr and V; they can be employed in different forms (ion, salt or complex), soluble or insoluble.

The impact of the reaction medium on reaction temperature and time

The reaction temperature and the time are greatly dependent on the choice of the reaction medium, i.e. the solvent. Common solvents are e.g. water, DMSO and polyethylene glycol.[3] In general, non-aqueous media enhance the catalyst's activity; thereby, complete conversion is obtained even after a short reaction time and a low temperature. Studies have shown that an extremely short reaction time of only 30 s was sufficient when using polyethylene glycol as solvent, working at a reaction temperature of 160 °C.[7,8]

The problem of cross-polymerization

From the economical point of view, it is desirable to work with high-concentrated reaction mixtures.[3] The higher the concentration, the more economic is the process. However, high concentrations have the disadvantage of increasing cross-polymerization reactions and thereby decreasing selectivity. One strategy in order to solve the problem of cross-polymerization is the use of non-aqueous media. It was shown that solvents like DMSO or polyethylene glycol lead to a higher selectivity; HMF can be obtained with yields around 70 %.[8,9]

The "right" solvent

As already mentioned above, the solvent has a great impact on the dehydration reaction of fructose.[3] Very often water is chosen as solvent; it has proved to be distinguished for both the fructose and the HMF. Though, it is problematical that water can take part as a reacting agent, e.g. it can hydrolyze the target product HMF. However, this problem can be solved by choosing solvent mixtures consisting of water as well as organic solvents, like DMSO, butanol or dioxane. In this manner, the hydrolysis of HMF can be prevented; higher yields of HMF are obtained.[7] However, the use of organic solvents implicates problems as well. Due to their high boiling points, their removal is not that simple. Furthermore, organic solvents involve high costs and hazards for the human health and the environment.

A very successful and promising solvent is DMSO.[3] High yields of HMF are obtained using DMSO in combination with catalysts, which act as ion-exchangers. It is even possible to perform the reaction without any catalyst, as it is reported by *Brown et al.*[10] as well as *Musau et al.*[11]. However, disadvantageously is the removal of DMSO after the reaction, due to its high boiling point.

The derivatives of HMF

HMF shows a quite poor stability during its formation.[3] Additionally, it is applied only rarely in its pure form; instead, its derivatives are more interesting concerning the subsequent chemistry.
One very important derivative of HMF is the levulinic acid (see also Figure 2).[3] Contrary to HMF, the levulinic acid is remarkably stable and therefore, it can be obtained in high yields, up to 70 %, no matter if starting from fructose or glucose. Due to its high stability, it is even possible to obtain the levulinic acid from waste material, which contains hexose. The levulinic acid can be applied for instance in the fuel industry as extender.

A further important derivative of HMF are the HMF ethers, which can appear in the form of di-HMF-ethers or 5-alkoxymethylfurfurals, the latter in the presence of alcohols.[3] Compared to HMF, the ethers are much more stable and thereby, their separation and isolation is not as difficult as in the case of HMF.
Besides the HMF ethers, also the corresponding esters are attractive compounds.[3] Their generation occurs via simple esterification of HMF. However, comparing ethers and esters, the ethers are shaped up as the more stable products.

Another interesting derivative group of HMF are the halomethylfurfurals.[3] Due to their reactive functionalities, they are very attractive for further transformations. 5-chloromethylfurfural, the chloromethyl analogue to HMF, is easily obtained via addition of hydrochloric acid, a surfactant and an aromatic or halogenated solvent to the corresponding sugar (glucose, sucrose or fructose).[12] The reaction mixture is heated and stirred for 1 h at 70-80 °C. In terms of the sugars, fructose gives the highest yields (77 %), in comparison to glucose (60 %) and sucrose (62 %).[12] Starting with fructose, the yield can be further improved up to 92 % by substitution of the hydrochloric acid and the surfactant; instead, $MgCl_2 \cdot 6H_2O$ is used.

Moreover, it is possible that HMF undergoes *in situ* hydrogenation and oxidation reactions.[3] Hydrogenation gives the bis-hydroxymethylfuran (Figure 4), a significant starting material for the large-scale production of resins. Further hydrogenation products are 5-methylfurfurylalcohol as well as 2,5-dimethylfuran (Figure 4), whereat the latter is applied as fuel extender.[13]

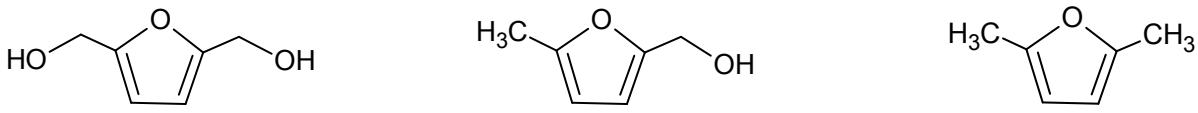

bis-hydroxymethylfuran | 5-methylfurfurylalcohol | 2,5-dimethylfuran

Figure 4: Hydrogenation products of HMF.[3]

Oxidation products of HMF are 2,5-diformylfuran, 5-hydroxymethylfuroic acid and 5-formylfuroic acid or 2,5-furan-dicarboxylic acid, respectively (Figure 5).[3]

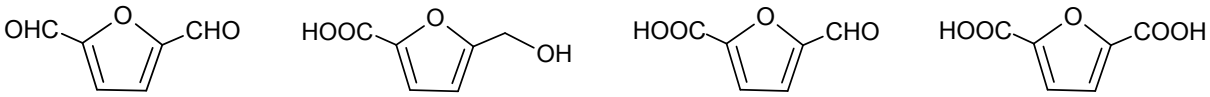

2,5-diformylfuran | 5-hydroxymethylfuroic acid | 5-formylfuroic acid | 2,5-furan-dicarboxylic acid

Figure 5: Oxidation products of HMF.[3]

The acid groups have a stabilizing effect; in addition, due to their functionality, they facilitate the separation, isolation and purification processes.

HMF – a promising and future-oriented intermediate product

Concluding, HMF is an attractive intermediate product with a broad and industrially interesting subsequent chemistry. Starting from hexoses as sufficiently available renewable raw materials, HMF can be easily obtained. Thus, HMF is a promising alternative for a large number of petrochemistry-based compounds and, hence, future-oriented.

3. Silica monoliths as microreactors for continuous flow reactions

Silica monoliths are an efficient alternative to powdery silica supports as they can be used as microreactors for continuous flow reactions.[14] Contrary to conventional batch reactors, continuous flow microreactors have many advantages, e.g. the easier handling and the associated higher safety. Moreover, they prevent the deposition of by-product and thereby, the deactivation of the active sites. Thus, reactions, carried out in continuous flow, commonly give high yields as well as excellent selectivities and productivities.

The first microreactor in the form of a monolith was composed of polymers.[15,16] Later, silica monolithic microreactors were designed.[17] In 1991, *Nakanishi et al.* developed monolithic bimodal silica gels, having a continuous macroporous or mesoporous structure.[18] The dimension of such silica monoliths ranges from 1-2 μm (macroporous diameter) to 10 nm (mesoporous diameter).
Due to their surface, which is covered with isolated silanol groups, silica monoliths can be variously functionalized.[14] For this purpose, the monoliths are grafted with organic or inorganic agents, e.g. alumina or sulphurous acid. The silica monoliths themselves are prepared as described in the *Experimental part III*.[14]

Figure 6 shows a scheme of a typical flow apparatus, as it is used for the grafting of silica monoliths as well as for the application of the grafted silica monoliths in flow catalysis.

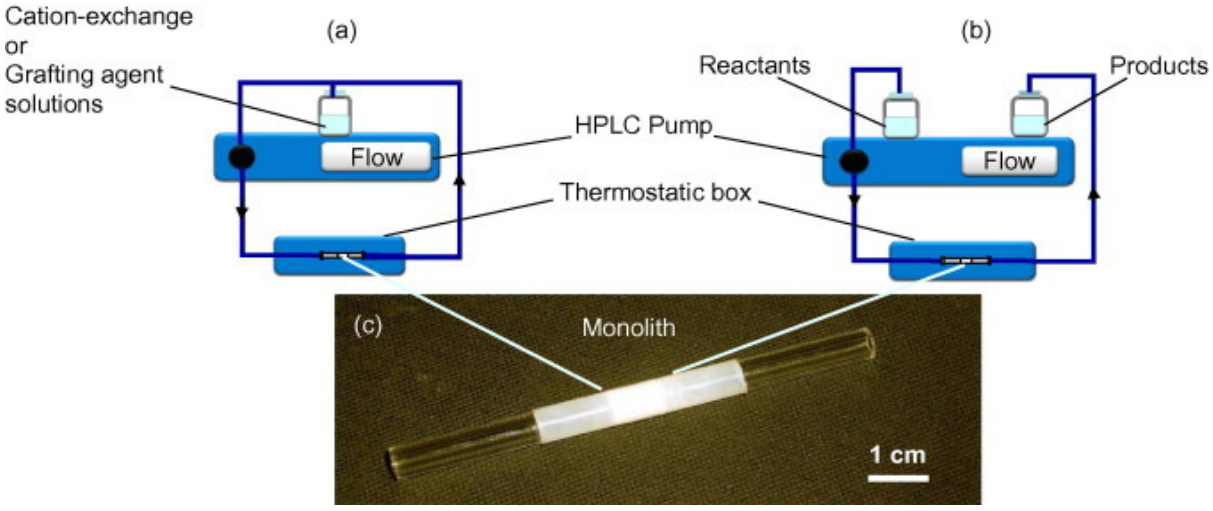

Figure 6: (a) Grafting of silica monoliths, (b) application of grafted silica monoliths in catalysis in flow, (c) cladded silica monolith.[14]

Prior to the grafting procedure, the silica monolith is cladded in the form of a microreactor as shown in Figure 6 (c) (see also *Experimental Part III*). The cladded monolith is placed into a thermostatic box, where the temperature can be individually regulated. The grafting agent solution is recycled via an HPLC micropump, which enables the adjustment of different flow rates.

Regarding the application of the grafted silica monoliths in flow catalysis, the same apparatus is used (Figure 6 (b)). However, the reactants are not recycled; instead, they pass only once through the monolithic microreactor. Here, the reaction occurs and the products are formed.

The application of silica monoliths in flow catalysis

Silica monoliths have been tested to catalyze e.g. the Diels-Alder condensation.[14] For this purpose, alumina grafted silica monoliths were applied, named as "Al-MonoSil".[14] Prior to their application in catalysis, the "Al-MonoSil" microreactors were activated at 150 °C in vacuum. The reaction mixture was prepared by adding cyclopentadiene and crotonaldehyde, dissolved in dehydrated dichloromethane. According to Figure 6 (b), the solution was transported via an HPLC micropump,

passing the “Al-MonoSil” microreactor at a reaction temperature of 37 °C with a flow rate of 0.2 and 0.5 mL·min^{-1}, respectively. In order to investigate the course of the reaction, samples were isochronously taken and analyzed by HPLC.

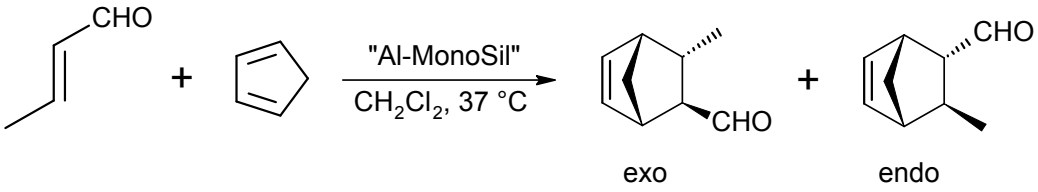

Figure 7: Diels-Alder condensation between crotonaldehyde and cyclopentadiene, catalyzed by “Al-MonoSil”.

The “Al-MonoSil” microreactor shaped up as a proper catalyst for the Diels-Alder reaction between cyclopentadiene and crotonaldehyde. This kind of reaction requires a slight acidity, what correlates perfectly with the weak acidic properties of the “Al-MonoSil” microreactor. Due to the weak acidity as well as the macropore network, the preferred endo isomer could be obtained excessively.

Regarding the slower flow rate of 0.2 mL·min^{-1}, an initial conversion of crotonaldehyde of > 99 % could be observed.[14] However, in the course of the reaction, the conversion decreased, until reaching a stable conversion of 55 % after 3 h.[14] It is supposed that the decrease of the conversion at the beginning is caused by a probable inhibition of those sites showing the strongest acidity. This inhibition is induced by an interaction between the acid sites and di-radical transition states. After 3 h, when reaching the stable conversion of 55 %, a high stereoselectivity towards the preferred endo isomer is observed (endo/exo = 9/1).

The higher flow rate of 0.5 mL·min^{-1} leads to a stable conversion of crotonaldehyde of 40 % after only 55 min.[14] The same endo/exo ratio of 9/1 was obtained.

The higher stereoselectivity towards the preferred endo isomer corresponds to the results obtained when using ionic liquids in dichloromethane.[19] In general, the endo isomer is preferably formed, when an interaction between the carbonyl- and the π-bond can be observed. Moreover, the higher stereoselectivity towards the endo

isomer can be explained by the macropore structure of the "Al-MonoSil": The macropores serve as so-called "solvent cavities", where the reactants aggregate, due to "solvophobic interactions".[20]

Moreover, besides the Diels-Alder reaction, silica monoliths have been tested e.g. in the Knoevenagel reaction of benzaldehyde and ethyl cyanoacetate as well as in the transesterification of triacetine by methanol (Figure 8 and 9).[17]

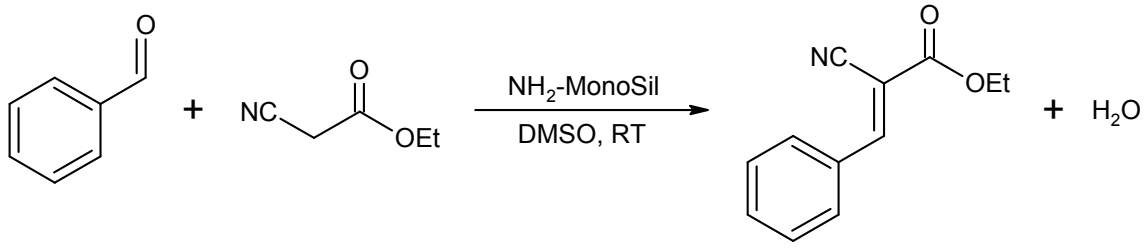

Figure 8: Knoevenagel reaction between benzaldehyde and ethyl cyanoacetate.[17]

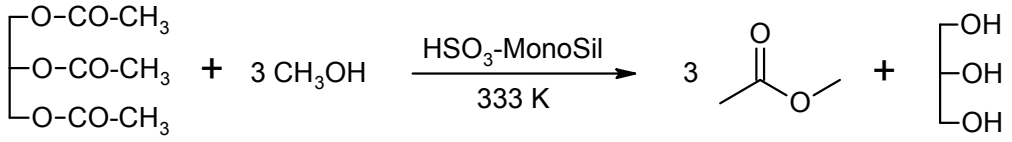

Figure 9: Transesterification of triacetine by methanol.[17]

The Knoevenagel reaction was catalyzed by basic NH_2-MonoSil, the transesterification by acidic HSO_3-MonoSil.[17] Both catalysts were prepared by using 3-Aminopropyltriethoxysilane and 2-(4-chlorosulfonylphenyl)ethyltrimethoxysilane as grafting agent, respectively.

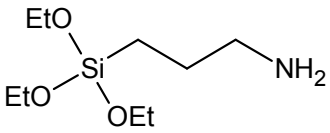

Figure 10: 3-Aminopropyltriethoxysilane.

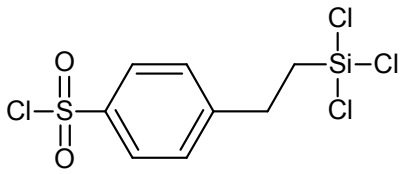

Figure 11: 2-(4-chlorosulfonylphenyl)ethyltrimethoxysilane.

It could be shown that both the basic NH_2-MonoSil and the acidic HSO_3-MonoSil enable high selectivities and activities; no deactivation of the two catalysts was observed, even after several hours.[17] In terms of the Knoevenagel reaction, a high conversion of ethyl cyanoacetate of 84 % was obtained after 28 h.[17] This performance corresponds to a remarkably high TON (turnover number) of 2280. The latter is of great interest, seeing that the Knoevenagel reaction yields water as co-product (Figure 8). Water, in general, interacts with the silica surface and thus, it is able to modify the silica structure. Therefore, the high obtained TON of this reaction is even more remarkable, as it represents an intact silica structure even after a long reaction time, despite the present water in the reaction mixture.

Generally, fine chemicals, which are prepared using heterogeneous catalysts, are synthesized in batch reactors or rather packed-bed microreactors.[17] In order to compare the outstanding activities of the basic NH_2- and the acidic HSO_3-MonoSil microreactors, both reactions, the Knoevenagel condensation as well as the transesterification, were carried out in a batch reactor and in a packed-bed microreactor. For this purpose, the basic NH_2- and the acidic HSO_3-MonoSil were crushed and applied in powdery form (batch and packed-bed). Below, the productivities of all three catalytic systems – batch reactor, packed-bed microreactor and MonoSil microreactor – are given.

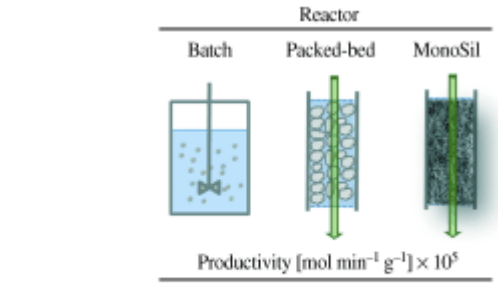

Knovenagel	24	108	178
Transesterification	2.5	28	82

Figure 12: Comparison between batch reactor, packed-bed microreactor and MonoSil microreactor.[17]

As evident, the batch reactor showed the poorest productivity of all three systems, in the Knoevenagel condensation as well as in the transesterification. Using a packed-bed microreactor, the productivity could be enhanced in both reactions. However, the by far highest productivity was obtained when using the MonoSil microreactor, i.e. the monolith reactor.

The obtained results attribute to the fact that the active sites of the monolithic MonoSil microreactor are easily accessible by the molecules of the reactants. Therefore, the molecules are able to flow much faster to and from the active sites, compared to the reactions performed in batch or in the packed-bed microreactor. Considering the structure of the MonoSil microreactor, two parameters play an important role for the fast and facile transport of the molecules to and from the actives sites of the catalyst. These parameters are explained below.

Firstly, the MonoSil microreactor features a high surface area, which enables a large contact area between the molecules of the reactants and the active sites of the catalyst.

Moreover, the diffusion path through the struts of the monolith reactor (Figure 13) is much shorter compared to that one through the grains of the crushed MonoSil. This fact facilitates both, the flow of the reactants into the porous network and the flow of the products out of the network.

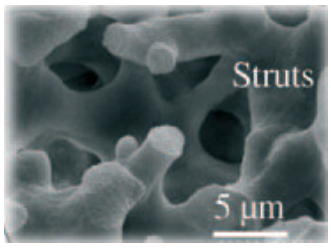

Figure 13: Struts of MonoSil microreactor.[17]

Due to these parameters, the MonoSil microreactor offers a fast flow transport of the molecules to and from the active sites of the catalyst. Therefore, the monolith reactor outperforms the batch reactor as well as the packed-bed microreactor, regarding the productivity in the considered reactions.

Summing up, the MonoSil microreactor offers a multitude of advantages compared to the conventional batch reactor or rather packed-bed microreactor. The easy accessibility of the active sites enable a fast flow of the molecules, which results in a remarkably high efficiency of the MonoSil microreactors.

Results and discussion

The present part of the work was carried out within the scope of a three-month stay at the *Institute Charles Gerhardt* in Montpellier, France under the supervision of *Dr. Anne Galarneau*. Silica monoliths were grafted and applied as catalysts in the dehydration of fructose to HMF. The reaction was tested in batch as well as in flow, varying different parameters (solvent, T, t).

Grafting of silica monoliths

Prior to the grafting, the silica monoliths were calcined in order to purify the surface and to eliminate traces of water. For this purpose, MonoSil microreactors were prepared as shown in Figure 14, covering the silica monolith by a heat-shrinkable teflon tube (see also *Experimental part III*).[14,17,21]

Figure 14: MonoSil microreactor, prior to the calcination.[21]

The MonoSil microreactors were calcined overnight at 280 °C. Owing to the heat, the teflon shrinks and covers the monolith closely.

Subsequently, the cladded monoliths were activated (reduced pressure, 150 °C, 2 h) and finally grafted, using an HPLC micropump (see also *Experimental part III*). A diluted solution of 2-(4-Chlorosulphonylphenyl)ethyltrimethoxysilane in 50 % dichloromethane was used as grafting agent (Figure 15).

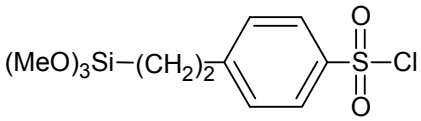

Figure 15: 2-(4-Chlorosulphonylphenyl)ethyltrimethoxysilane.

The dehydration of fructose to HMF

The grafted MonoSil microreactors were tested as catalysts in the dehydration of fructose to HMF. The reaction was analytically investigated by HPLC.
For the calibration, a sample of the pure fructose, well diluted in few mL of H_2O dest., was injected in order to obtain the retention time of the starting material. It was observed that the fructose appears at a retention time of about 11 min (Figure 16).

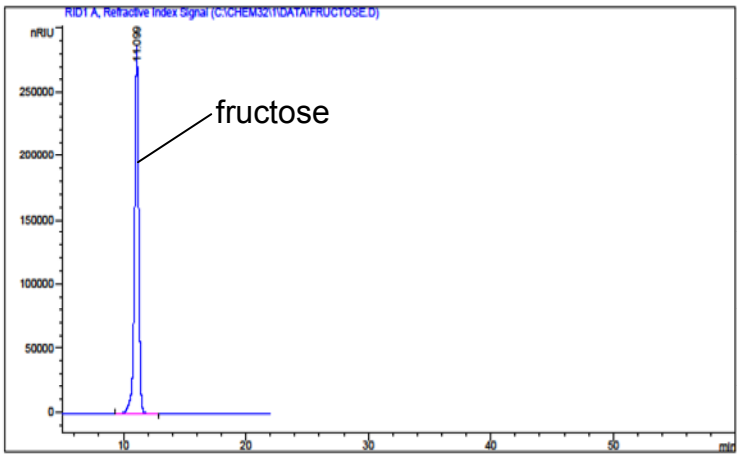

Figure 16: HPLC spectrum of the pure fructose.

The HPLC analysis of a mixture of fructose and HMF showed that the HMF appears at a retention time of about 31 min (Figure 17).

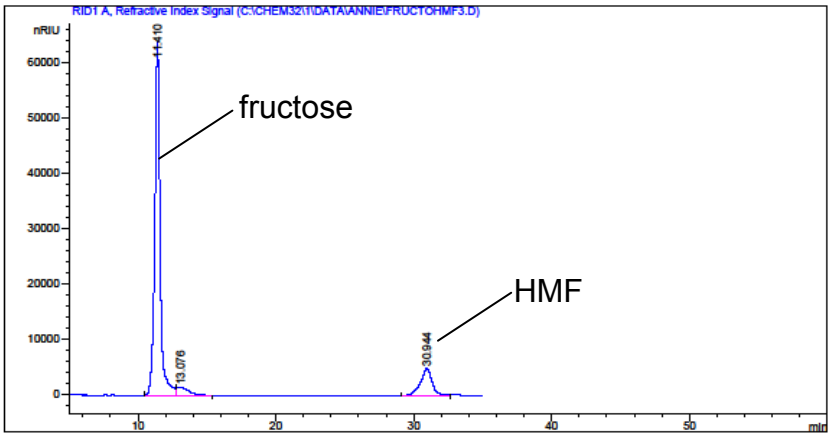

Figure 17: Comparison between fructose and HMF.

As a first test reaction, the dehydration of fructose to HMF was carried out in batch, using a grafted and crushed MonoSil as catalyst. The reaction was performed with 10 wt % catalyst loading, in H_2O dest., at 90 °C. After 1 h, the first sample was taken and analyzed by HPLC analysis. No formation of HMF was observed (Figure 18a). Therefore, the reaction was continued overnight. As it can be seen from Figure 18b, the prolonged reaction time did not have any influence on the course of the reaction.

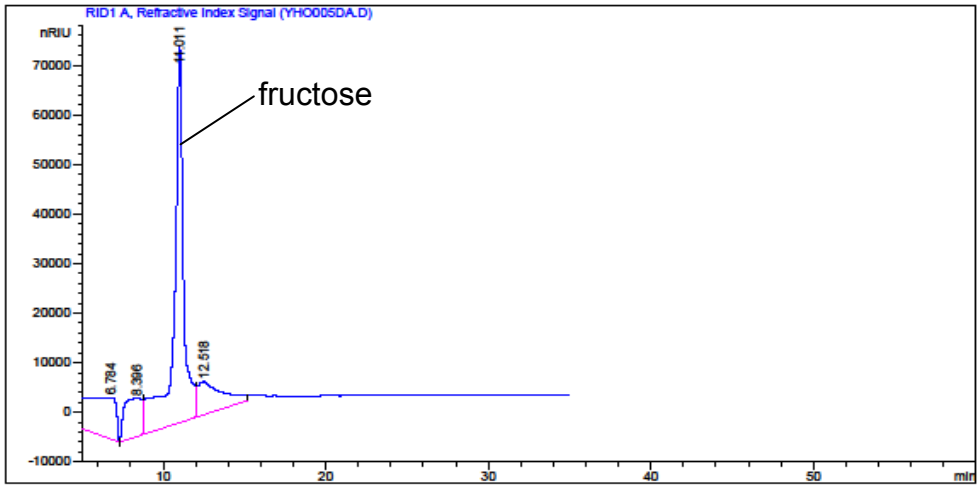

Figure 18a: Dehydration of fructose to HMF in batch, 10 wt % of grafted MonoSil (powdery), in H_2O dest., at 90 °C, after 1 h.

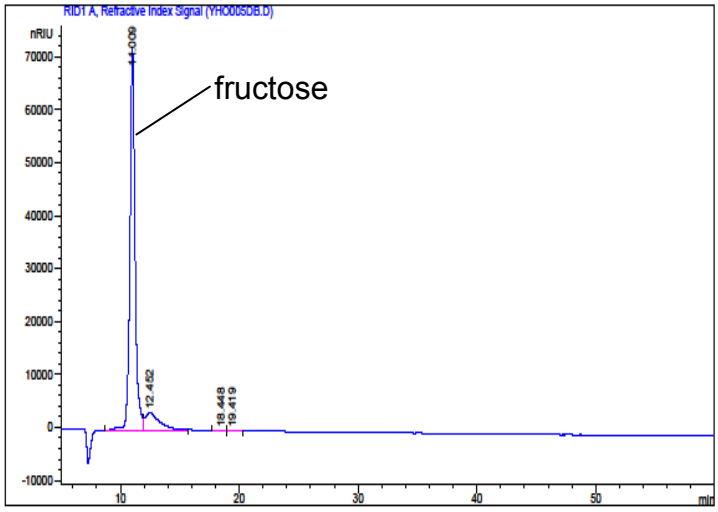

Figure 18b: Dehydration of fructose to HMF in batch, 10 wt % of grafted MonoSil (powdery), in H_2O dest., at 90 °C, overnight.

In order to investigate if the reaction works at all under these conditions (10 wt % catalyst loading, in H_2O dest., at 90 °C), the dehydration was catalyzed homogeneously, by using the unsupported grafting agent. Despite low conversion of fructose, the formation of HMF could be observed (after 22 h, Figure 19b). Accordingly, a colour change of the reaction mixture was noticed: The primarily colourless solution changed into yellow.

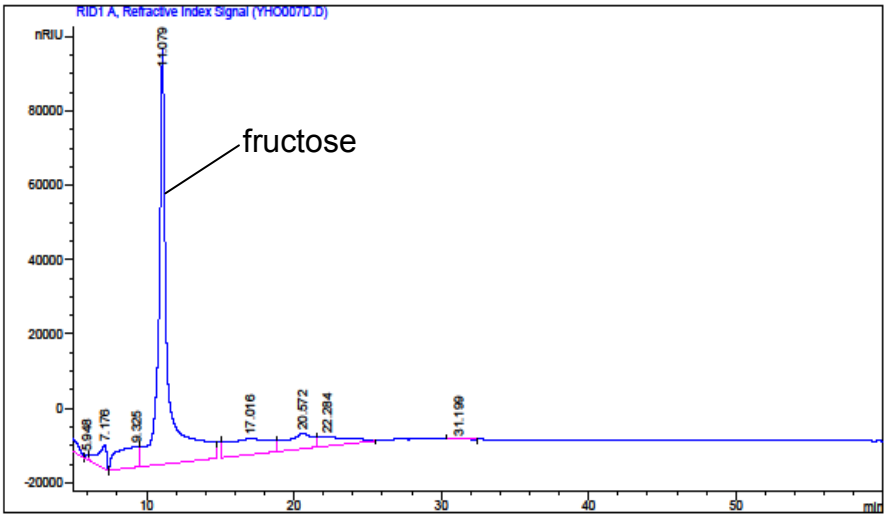

Figure 19a: Dehydration of fructose to HMF in batch, 10 wt % of grafting agent (homogeneous), in H_2O dest., at 90 °C, after 3 h.

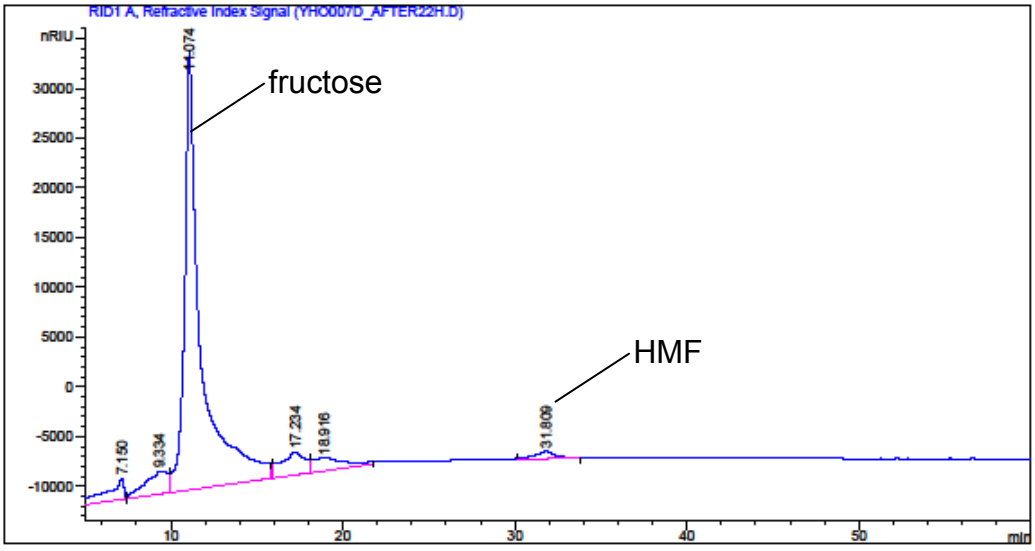

Figure 19b: Dehydration of fructose to HMF in batch, 10 wt % of grafting agent (homogeneous), in H_2O dest., at 90 °C, after 22 h.

In order to enhance the formation of HMF, different reaction parameters were verified. Due to several studies, DMSO has proven to be a suitable solvent for the dehydration of fructose to HMF.[3,10,11] Hence, the reaction was performed in DMSO, at 160 °C. Right at the beginning of the reaction, when a temperature of 140 °C was obtained, the colour of the reaction mixture turned from colourless into yellow; at around 150 °C the mixture changed into brown. After 1 h, a precipitate in the mixture could be observed. The corresponding spectrum (Figure 20a) shows that only after 1 h the conversion of fructose was completed.

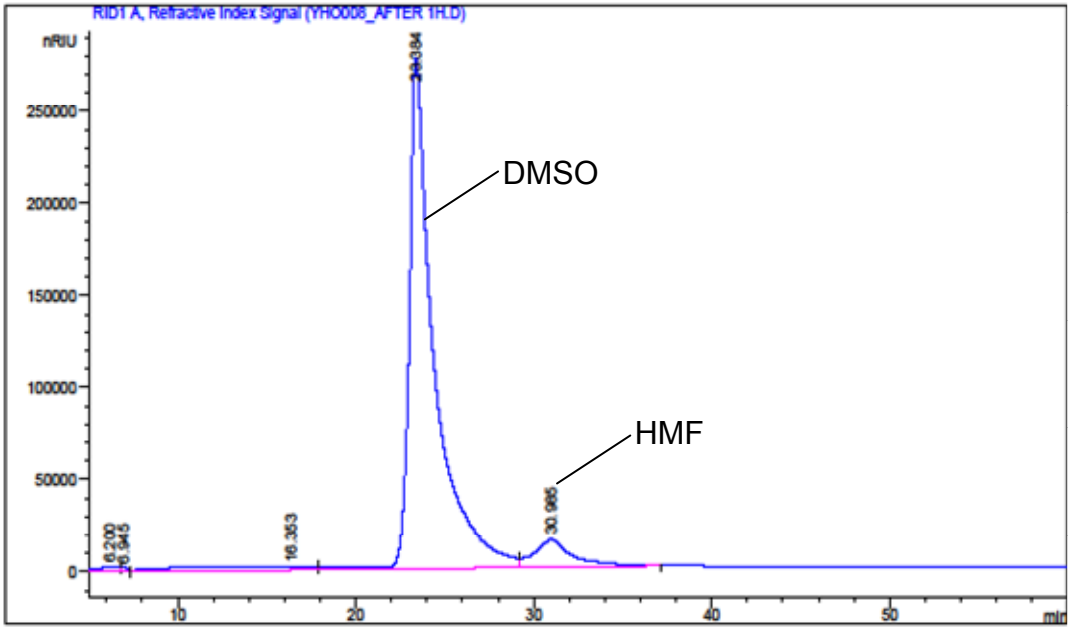

Figure 20a: Dehydration of fructose to HMF in batch, 10 wt % of grafting agent (homogeneous), in DMSO, at 160 °C, after 1 h.

However, a prolonged reaction time leads to an increased formation of byproducts (Figure 20b). Thus, a shorter reaction time of 1 h gives a higher selectivity. The noticeable peak at 20.777 min indicates a possible intermediate or secondary product, which is only formed after a longer reaction time.

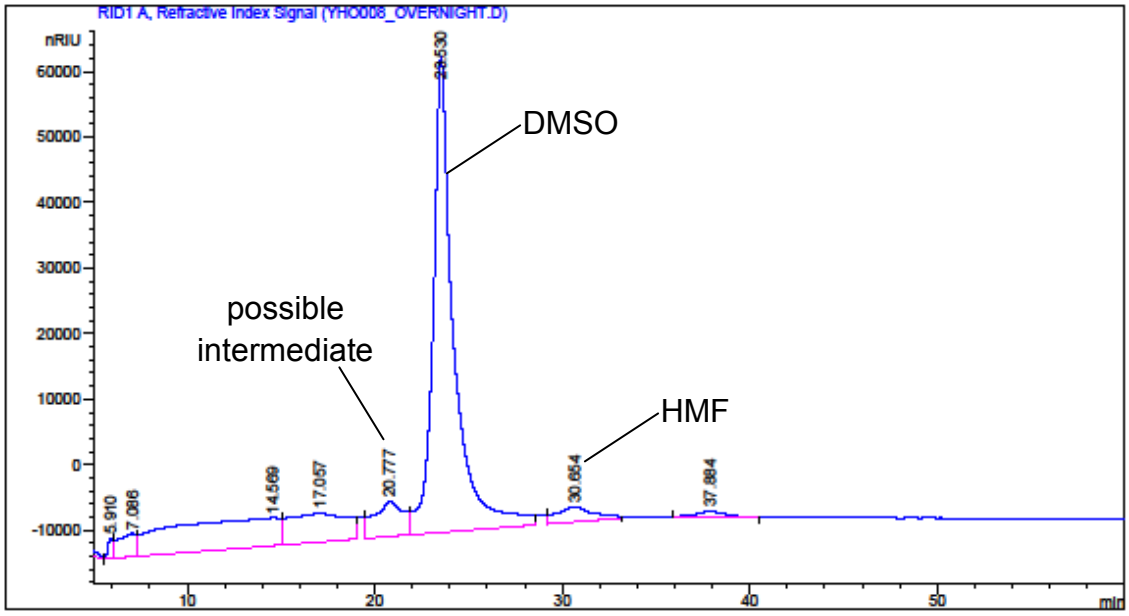

Figure 20b: Dehydration of fructose to HMF in batch, 10 wt % of grafting agent (homogeneous), in DMSO, at 160 °C, overnight.

Subsequently, the optimized reaction (conditions: in DMSO, at 160 °C, 10 wt % catalyst loading) was performed heterogeneously, catalyzed by a grafted and crushed MonoSil. The obtained result is similar to that one of the homogeneous reaction (Figure 21a). After only 1 h, the fructose was completely converted and the formation of HMF was observed.

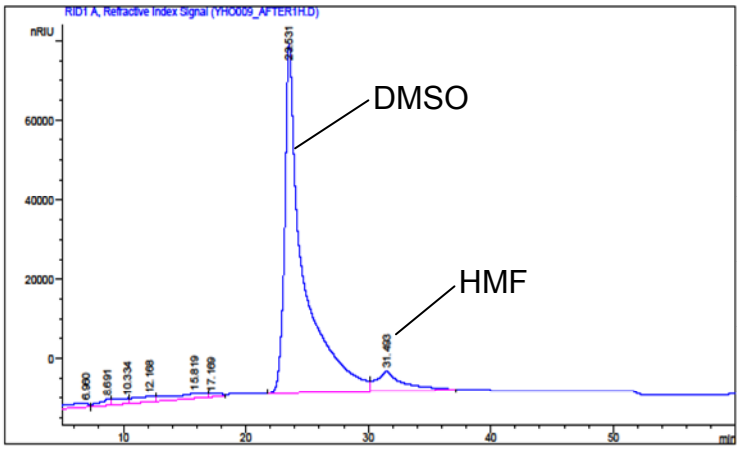

Figure 21a: Dehydration of fructose to HMF in batch, 10 wt % of grafted MonoSil (powdery), in DMSO, at 160 °C, after 1 h.

A prolonged reaction time did not show a strong influence on the products (Figure 21b). However, the formation of a possible byproduct or secondary product respectively, which appears at a retention time of about 37 min, could be observed.

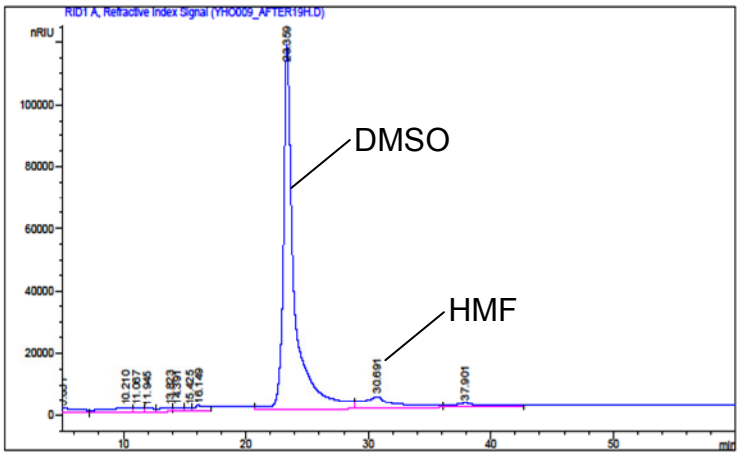

Figure 21b: Dehydration of fructose to HMF in batch, 10 wt % of grafted MonoSil (powdery), in DMSO, at 160 °C, after 19 h.

In order to work under milder reaction conditions, the temperature was lowered from 160 °C to 100 °C. The formation of HMF was observed, even when using a blank instead of a grafted silica monolith. However, a longer reaction (4 h) time was necessary to obtain the desired product (Figure 22b).

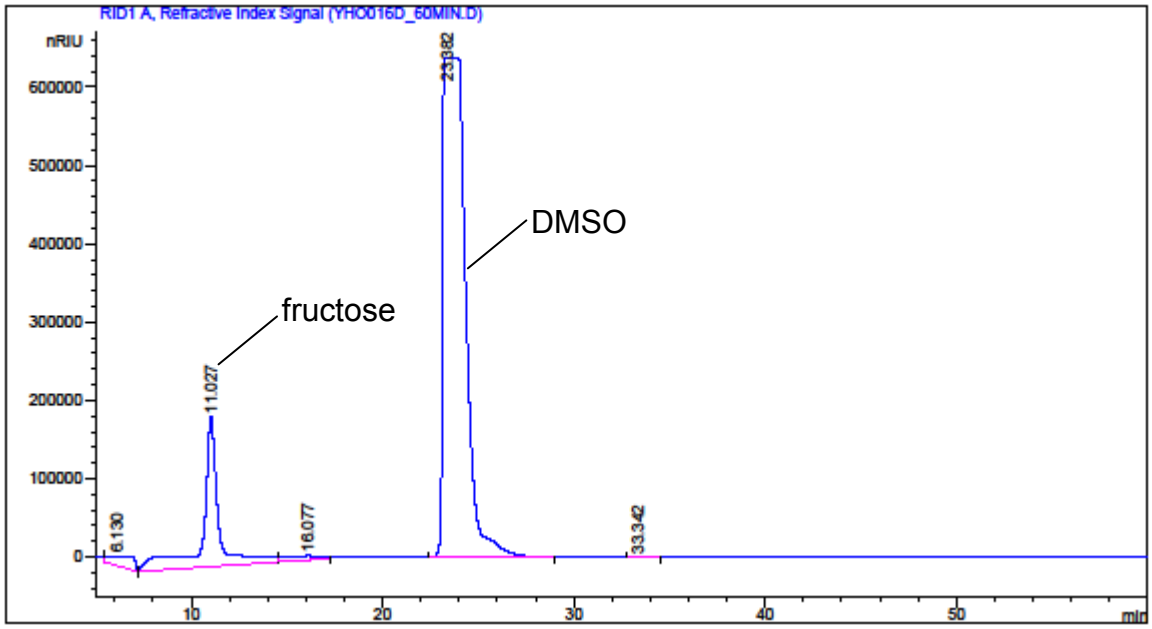

Figure 22a: Dehydration of fructose to HMF in batch, 10 wt % of blank MonoSil (powdery), in DMSO, at 100 °C, after 1 h.

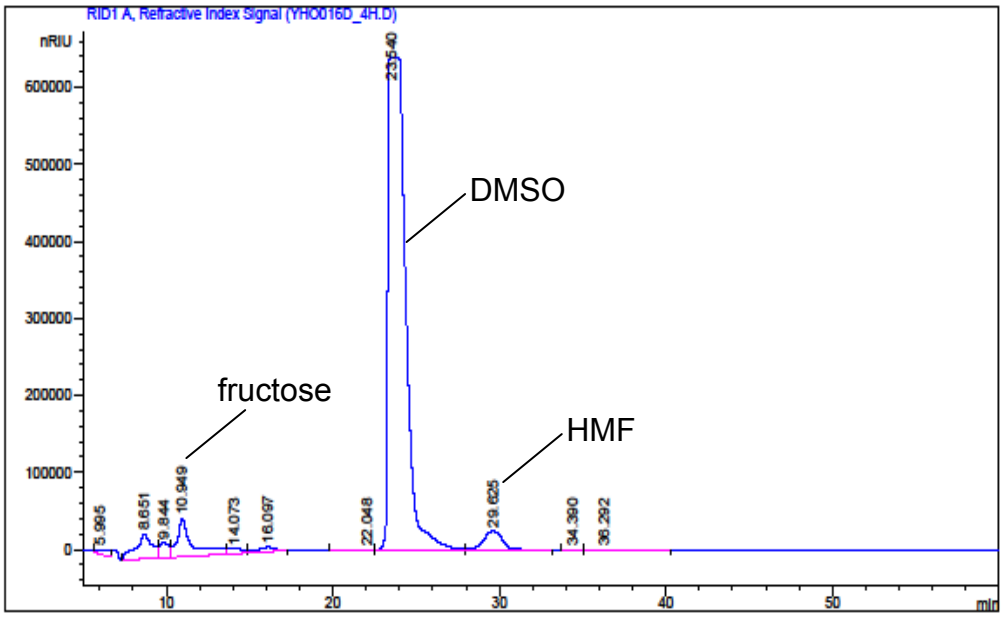

Figure 22b: Dehydration of fructose to HMF in batch, 10 wt % of blank MonoSil (powdery), in DMSO, at 100 °C, after 4 h.

In order to have complete conversion of the fructose, the reaction time was extended to 8 h (Figure 22c).

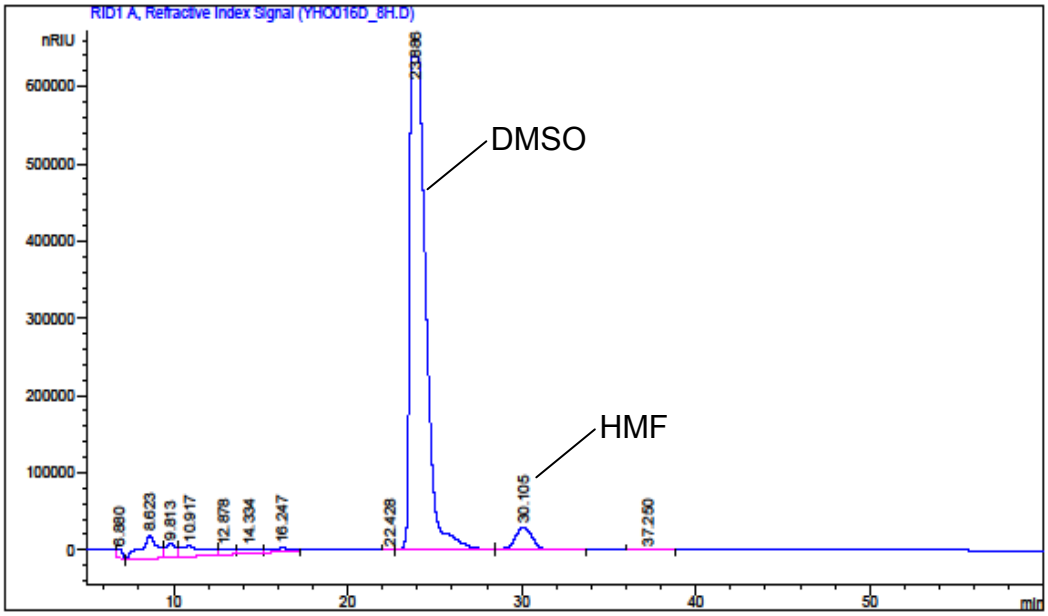

Figure 22c: Dehydration of fructose to HMF in batch, 10 wt % of blank MonoSil (powdery), in DMSO, at 100 °C, after 8 h.

According to the formation of HMF, a change in the colour of the reaction mixture was observed – from colourless (start of the reaction) to yellow (after 4 h) to brown (after 8 h).

Finally, the reaction was tested in flow, using the same HPLC-pump as for the grafting of the silica monoliths (see *Experimental part III*). The reaction was catalyzed by a blank monolith, in DMSO, at 100 °C. After 1 h, no formation of HMF was obtained (Figure 23a). However, the HPLC analysis gave a noticeable peak at 20.933 min, which probably indicates a possible intermediate.

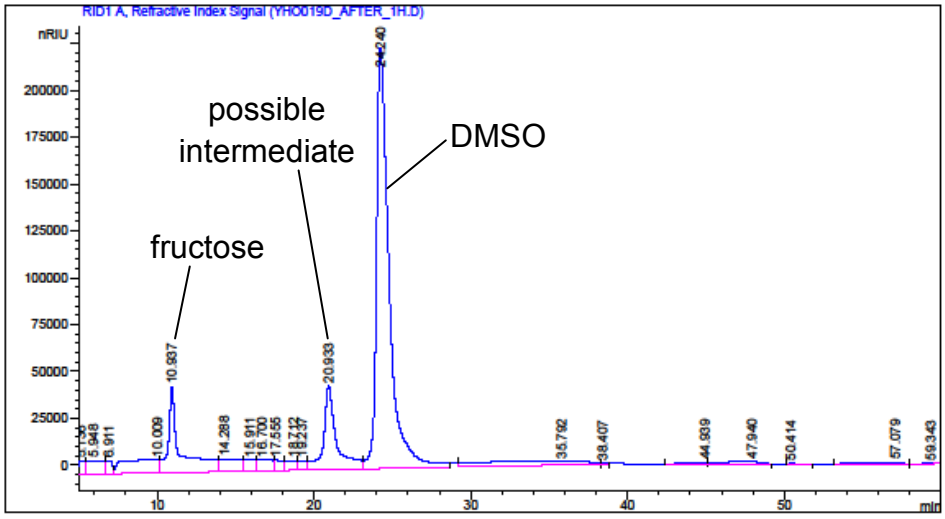

Figure 23a: Dehydration of fructose to HMF in flow, 10 wt % of blank MonoSil microreactor, in DMSO, at 100 °C, after 1 h.

A prolonged reaction time of 4 days leads to a full conversion of the fructose as well as to a probable further reaction of the intermediate to the desired HMF (Figure 23b).

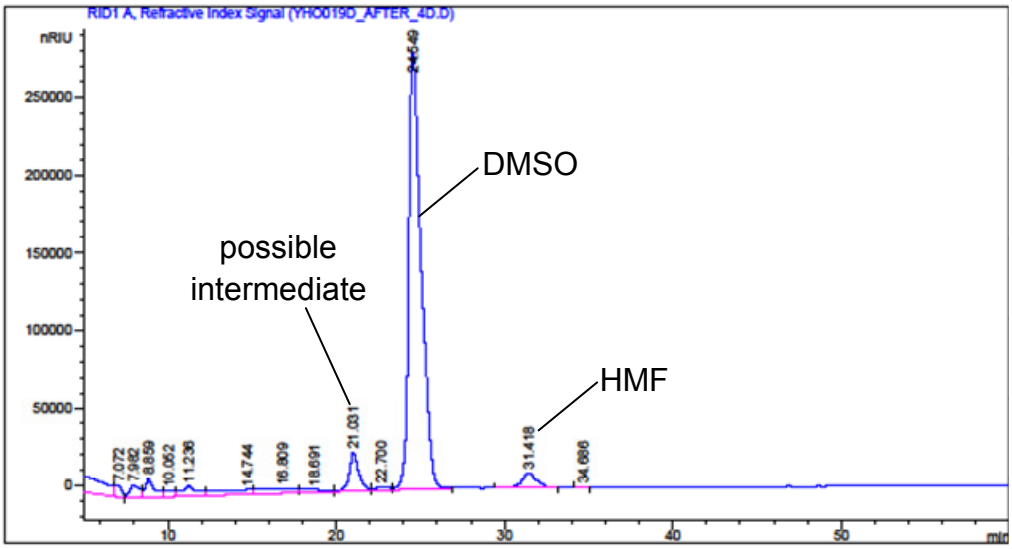

Figure 23b: Dehydration of fructose to HMF in flow, 10 wt % of blank MonoSil microreactor, in DMSO, at 100 °C, after 4 d.

In order to investigate the further course of the reaction, the reaction time was prolonged to one week (Figure 23c). In comparison to the sample analyzed after 4 days (Figure 23b), no great difference became apparent. Apart from the formation of the desired HMF, the possible intermediate, which appears at around 21 min, was still present in the reaction mixture and was not further converted.

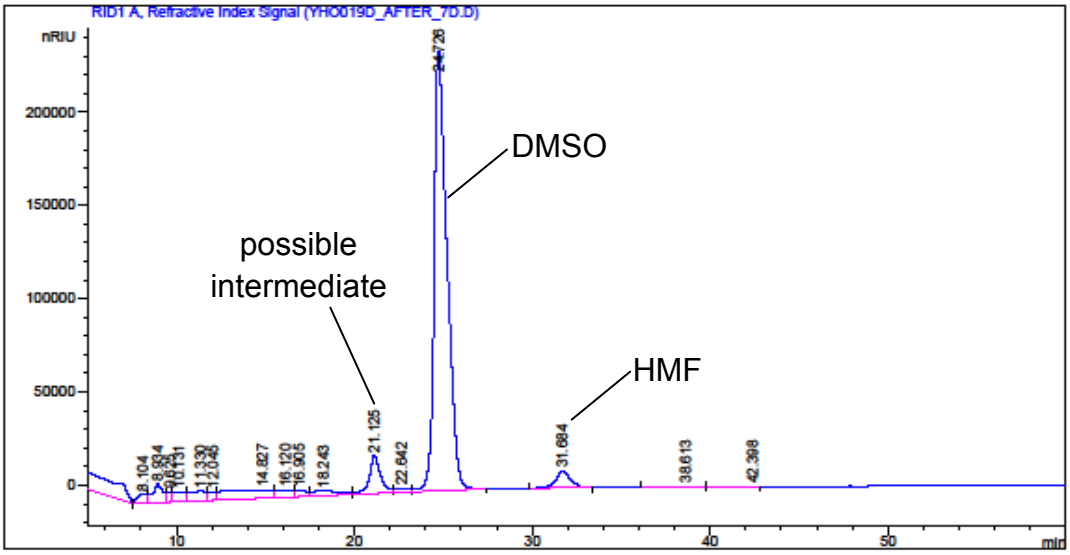

Figure 23c: Dehydration of fructose to HMF in flow, 10 wt % of blank MonoSil microreactor, in DMSO, at 100 °C, after 7 d.

In general, it could be demonstrated that complete conversion of the fructose and formation of HMF were observed using both the batch and the flow process, catalyzed by blank as well as grafted MonoSil, homogeneously (using solely the grafting agent) and heterogeneously (using the supported grafting agent).

Concluding remarks

This part of the work attended to the grafting of silica monoliths and their catalytic application in the dehydration of fructose to HMF. Prior to the grafting, the silica monoliths were cladded as MonoSil microreactors. Compared to conventional batch reactors, microreactors feature a multitude of advantages. They allow a much faster flow of the molecules to and from the active sites of the catalyst, due to their large surface area and the related broad contact area between the reactants and the catalyst. Therefore, monolithic microreactors show a much higher productivity compared to reactions carried out in a batch reactor or rather in a packed-bed microreactor.

Within the scope of this work, the MonoSil was tested both in batch (crushed powdery MonoSil) as well as in flow (monolithic MonoSil microreactor). It could be shown that the dehydration of fructose is performable under both conditions. HMF as the target product was obtained when using blank as well as grafted MonoSil. Moreover, it was possible to catalyze the reaction homogeneously, using the sole unsupported grafting agent.

The target product HMF is industrially of great interest, owing to its large subsequent chemistry. HMF is easily synthesized starting from hexoses (fructose, glucose, sucrose) as renewable raw materials. Hence, HMF is an attractive intermediate product and an alternative for many petrochemistry-based compounds.

References

[1] F. W. Lichtenthaler, S. Peters, *C. R. Chimie* **2004**, *7*, 65-90.

[2] H. Schiweck, M. Munir, K. M. Rapp, B. Schneider, M. Vogel, in: F.W. Lichtenthaler (Ed.), Carbohydrates as Organic Raw Materials, VCH Publ.,Weinheim/NewYork, **1991**, p. 80.

[3] B. F. M. Kuster, Starch/Stärke **1990**, *42*, 314-321.

[4] H. Schiweck, M. Munir, K. Rapp, M. Vogel, in: F.W. Lichtenthaler (Ed.), Carbohydrates as Organic Raw Materials, VCH Publ., Weinheim, Germany, **1991**, p. 78.

[5] M. S. Feather, J. F. Harris, *Advan. Carbohyd. Chem.* **1973**, *28*, 161-224.

[6] F. H. Newth, *Adv. Carbohydr. Chem.* **1951**, *6*, 83-106.

[7] B. F. M. Kuster, *Carbohydr. Res.* **1977**, *54*, 177-183.

[8] B. F. M. Kuster, J. Laurens, Starch/Stärke **1977**, *29*, 172-176.

[9] H. H. Szmant, D. D. Chundury, *J. Chem. Technol. Biotechnol.* **1981**, *31*, 135-145.

[10] D. W. Brown, A. J. Floyd, R. G. Kinsmann, Y. Roshan-Ali, *J. Chem. Technol. Biotechnol.* **1982**, *32*, 920-924.

[11] R. M. Musau, R. M. Munavu, *Biomass* **1987**, *13*, 67-74.

[12] K. Hamada, H. Yoshihara, G. Suzukamo, *Chem. Lett.* **1982**, *5*, 617-618.

[13] S. Morikawa, *Noguchi Kenkyusho Jiho* **1980**, *23*, 39-44.

[14] A. Sachse, A. Galarneau, F. Fajula, F. Di Renzo, P. Creux, B. Coq, *Microporous and Mesoporous Materials* **2011**, *140*, 58-68.

[15] F. Svek, J. M. J. Fréchet, *Science* **1996**, *273*, 205-211.

[16] A. Kirschning, C. Altwicker, G. Drager, J. Harders, N. Hoffmann, U. Hoffmann, H. Shonfeld, W. Sodolenko, U. Kunz, *Angew. Chem. Int. Ed.* **2001**, *40*, 3995-3998.

[17] A. El Kadib, R. Chimenton, A. Sachse, F. Fajula, A. Galarneau, B. Coq, *Angew. Chem. Int. Ed.* **2009**, *48*, 4969-4972.

[18] K. Nakanishi, N. Soga, *J. Am. Ceram. Soc.* **1991**, *74*, 2518-2530.

[19] J. Howarth, K. Hanlon, D. Fayne, P. McCormac, *Tetrahedron Lett.* **1997**, *38*, 3097.

[20] T. Fisher, A. Sethi, T. Welton, J. Woolf, *Tetrahedron Lett.* **1999**, *40*, 793.

[21] A. Sachse, A. Galarneau, F. Di Renzo, F, Fajula, B. Coq, *Chem. Mater.* **2010**, *22*, 4123-4125.

Conclusion

A comparison between homogeneous and heterogeneous catalysis highlights more advantages in favour of the homogeneous catalysis. The stoichiometry and structure of a homogeneous catalyst are well-known; in contrast, heterogeneous catalysts are often undefined in terms of stoichiometry and structure. Homogeneous catalysts are highly variable and can be easily reproduced; mostly, the mechanism is easily to explain. During the reaction, all metal atoms of the homogeneous catalyst are active, whereas the heterogeneous one possesses its active atoms only on the catalyst's surface. Activity and selectivity of the homogeneous catalyst are noticeably higher. In general, no diffusion problems occur, whereas diffusion represents a considerable problem of heterogeneous catalysts, due to their complex pore structure. Homogeneous catalysts allow significantly milder reactions conditions in contrast to the heterogeneous types; moreover, they are rarely deactivated by poisoning.
As evident, homogeneous catalysis offers a multitude of advantages. Though, one important and not negligible disadvantage is the separation and recycling of the homogeneous catalyst, which is uncomplicated using heterogeneous catalysts. Therefore, it would be desirable to combine homogeneous and heterogeneous catalysts in order to design new and effective catalysts, showing the advantages and strengths of both homogeneous and heterogeneous catalysts.

Within the scope of this work, metal NPs (Pd) and metal complexes (Rh, Cu) were immobilized and, hence, heterogeneized on silica support materials. This procedure demonstrates a simple and promising way to combine homogeneous and heterogeneous catalysis.

The first part of this work dealt with the design and characterization of Rh^{I}-Pd^{0}/SiO_2 "hybrid catalysts", consisting of silica-supported PdNPs and Rh^{I} single sites. The immobilization of the PdNPs was performed using different methods (impregnation, Ionic Exchange, CVD). In this context, CVD proved to be the most efficient procedure, giving high Pd loadings up to 1.95 wt % (exp. loading 2.00 wt %). Moreover, both powdery silica and silica monoliths were compatible with the CVD.

Regarding the grafting of Pd^0/SiO_2 with Rh^I, Rh loadings between 0.26 and 0.83 wt % were obtained, depending on different parameters (type of SiO_2, type of Rh precursor, impregnation procedure). These designed Rh^I-Pd^0/SiO_2 "hybrid catalysts" can be tested in further studies in order to show their activity and selectivity in hydrogenation reactions of prochiral substrates.

Another part of this work was the preparation, characterization and catalytic application of heterogeneized Cu^I complexes. In this context, $[Cu^I(PC\text{-}L^*)]CF_3SO_3$ complexes were grafted onto different mesoporous silica supports (MCM-41, SBA-15, Davisil B, Aerosil, basic silica), whereupon SBA-15 shaped up as the best support material, giving high Cu loadings up to 1.79 wt %. The $[Cu^I(PC\text{-}L^*)]CF_3SO_3/SiO_2$ catalysts were applied in the asymmetric cyclopropanation reaction of α-methyl styrene and its derivatives with EDA. In this context, the recyclability of $[Cu^I(PC\text{-}L^*)]CF_3SO_3/SiO_2$ could be demonstrated.

The third and last part of this work dealt with the grafting of silica monoliths and their catalytic application as MonoSil microreactors in the dehydration of fructose to HMF. The reaction was carried out both in batch (using a crushed powdery MonoSil) as well as in flow (using a monolithic MonoSil microreactor); under both conditions the formation of HMF was observed. The dehydration was performed working with both blank and grafted MonoSil. Moreover, the reaction could be catalyzed by the unsupported grafting agent as well, i.e. homogeneously.

Experimental part

Experimental part – General information

DRY BOX:

The water and air sensible compounds, i.e. Pd(allyl)Cp and all applied Rh and Cu complexes, are handled in a DRY BOX, model “MB-10-Compact”, from the MBRAUN GmbH, allowing an inert atmosphere with H_2O and O_2 concentrations < 0.1 ppm.

Inductively Coupled Plasma Optical Emission Spectrometry (ICP-OES):

Metal loadings (Pd, Rh, Cu) are determined by ICP-OES using a “Thermo X Series II” apparatus. 15 mg of each sample are mineralized by adding 3 mL of 37 % HCl, 1 mL of concentrated HNO_3, 1 mL of 98 % H_2SO_4 and 400 mg Se (0.1 % in K_2SO_4). The Se is added in order to decompose the phosphine ligands of the Rh complexes.

Diffuse Reflectance Infrared Fourier Transform Spectroscopy (DRIFTS):

IR-CO-DRIFT spectra of the [Cu(PC-L*)]CF_3SO_3/SiO_2 samples are recorded using a “FTS-60A” spectrophotometer consisting of a home-made reaction chamber. After purging the apparatus with ultra-pure He, spectra of the samples are recorded at RT in He and CO flow, before and after catalysis.

High Performance Liquid Chromatography (HPLC):

The dehydration of fructose to HMF is characterized by HPLC analysis, using a Shimadzu LC-6A pump, a refractive index RID-6A detector and a BIORAD HPX-87H column (300 mm $\times$ 7.8 mm). Before injection, the periodically taken samples are well diluted in dest. H_2O and filtered. In terms of the calibration, spectra of the pure fructose and HMF are recorded.

Experimental part I – CHAPTER 1

(1) Pretreatment and activation of the silica support materials

Davisil B (GRACE Davison, LC 150 Å, 35-70 Micron), Davisil A (GRACE Davison, LC 150 Å, 60-200 Micron) and the Silica "Aldrich 403601" are commercially available; MCM-41 and SBA-15 are prepared at the *Institut Charles Gerhardt* in Montpellier, France. The characteristics (pore diameter, pore volume, surface area) of MCM-41 and SBA-15 are listed below:

MCM-41 (6124)
Pore diameter: 3.6 nm
Pore volume: 0.61 mL / g
Surface area: 827 m^2 / g

MCM-41 (6138)
Pore diameter: 10.4 nm
Pore volume: 2.00 mL / g
Surface area: 818 m^2 / g

SBA-15 (MFDC061)
Has been prepared at 60 °C
Pore diameter: 6.7 nm
Pore volume: 0.69 mL / g
Surface area: 786 m^2 / g

SBA-15 (MFDC065)
Has been prepared at 130 °C
Pore diameter: 9.6 nm
Pore volume: 1.02 mL / g
Surface area: 525 m^2 / g

Before use, MCM-41 and SBA-15 are calcined at 550 °C for 8 h in air.

Activation of all silicas is performed in a Schlenk flask at 300 °C, for 2-3 h in air, subsequently in high vacuum (at least 10^{-5} mbar) overnight.

(2) Immobilization of PdNPs onto silica

a. Impregnation

General procedure (for 1 g of SiO_2):

3.298 mL of a $PdCl_2$ solution (2 wt % Pd; c($PdCl_2$) = 6064 mg·L^{-1}), 600 µL HCl and 10 mL H_2O mQ are stirred in a beaker at RT and subsequently poured into a 100 mL one-necked flask containing 1000 mg SiO_2. The mixture is stirred at RT for 4 h. After evaporation of the solvent, the solid is dried in vacuum overnight. Calcination (O_2, T = 500 °C, t = 1 h, v = 100 °C / 10 min), reduction (H_2, T = 300 °C, t = 1 h, v = 100 °C / 10 min) and passivation (O_2, RT, t = 30 min) give the Pd^0/SiO_2 samples.

b. Ionic Exchange

General procedure (for 1 g of SiO_2):

49.52 mg $Pd(NH_3)_4Cl_2$ (2 wt % Pd; 0.188 mmol) are dissolved in 40 mL H_2O mQ. After the control of the pH (pH ~ 9; if pH < 9: addition of one drop of NH_3 solution), the solution is poured over 1000 mg SiO_2. The mixture is stirred at RT for 24 h. The solid is filtered, washed with H_2O mQ (for 30 min) and dried overnight. Calcination (O_2, T = 550 °C, t = 6 h, v = 5 °C / min), reduction (H_2, T = 300 °C, t = 1 h, v = 50 °C / 5 min) and passivation (O_2, RT, t = 30 min) give the Pd^0/SiO_2 samples.

c. Chemical Vapour Deposition (CVD)

General procedure (for 1 g of SiO_2):

1000 mg of SiO_2 are activated in the particular glass reactor for CVD, shown below, whereat the silica is placed around the glass tube in the interior of the reactor.

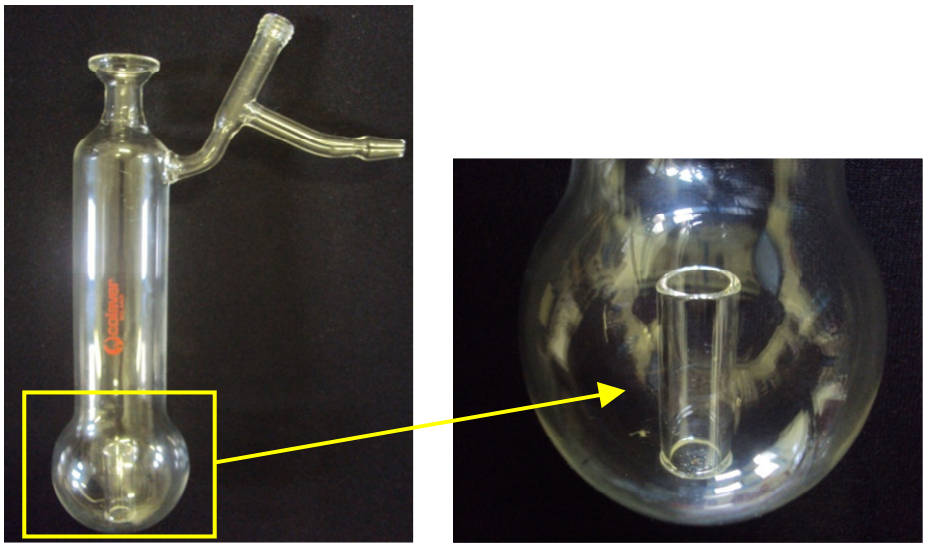

Figure 1: Glass reactor for CVD.

After cooling down to RT, the reactor is transferred into the DRY BOX. 39.92 mg of Pd(allyl)Cp (2 wt % Pd; 0.188 mmol) are weighted in a small glass tube with a height of ca. 1 cm. The glass tube is transferred into the interior glass tube of the CVD reactor. The CVD reactor is closed and taken out of the DRY BOX. A vacuum of 4 mbar is generated and the reactor is fixed at the CVD apparatus with minimal rotation, heated in an oil bath at 35 °C. Subsequent reduction (H_2, T = 200 °C, t = 1 h, v = 5 °C / 10 min) and passivation (O_2, RT, t = 30 min) give the Pd^0/SiO_2 samples.

(3) Impregnation of Pd^0/SiO_2 with Rh^I

General procedure:

In DRY BOX, 300 mg of Pd^0/SiO_2 are transferred into a 100 mL one-necked Schlenk flask. 11.24 mg (0.5 wt % Rh) of [(-)CHIRAPHOS(Rh)(NBD)]OTf are added, the flask is closed and taken out of the DRY BOX. After the addition of 5-10 mL anhydrous CH_2Cl_2 (in argon flow), the reaction mixture is stirred at RT for 4 h. Inert filtration (Ar), washing (3 x 5 mL anhydrous CH_2Cl_2) and drying in vacuum overnight give the Rh^I-Pd^0/SiO_2 samples.

Experimental part II – CHAPTER 2

(1) Synthesis of macrocyclic ligands (PC-L*)

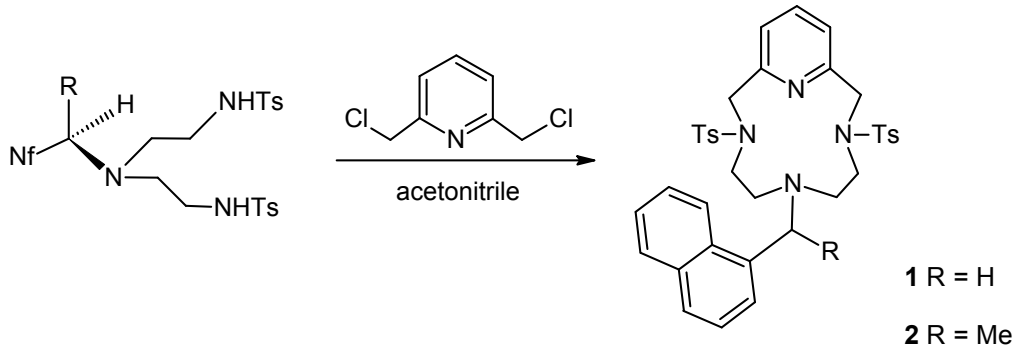

General procedure:[1]

The synthesis of the macrocyclic ligands (PC-L*) is carried out under inert conditions, using an anhydrous apparatus. A solution of naphthyl triamine, bis-chloromethyl pyridine and anhydrous potassium carbonate in distilled acetonitrile is prepared. The solution is stirred under reflux for 11 h. The reaction mixture is washed with H_2O dest. and extracted with ethyl acetate. The residue is dried under reduced pressure and purified via column chromatography (silica gel; toluene / 2-propanol /dichloromethane = 85:5:10). Recrystallization (layer of hexane on a warm solution of ethylacetate) yields the macrocyclic ligands as white solids.

Reference:

[1] Diploma thesis of Brunilde Castano, Università degli Studi di Milano, academic year 2009/2010.

(2) Synthesis of $[Cu^{I}(PC\text{-}L^{*})]CF_3SO_3$

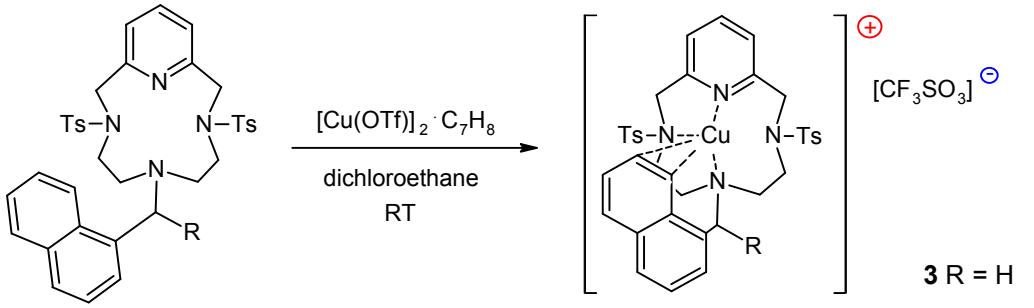

3 R = H

4 R = Me

General procedure:[1]

The synthesis of $[Cu^{I}(PC\text{-}L^{*})]CF_3SO_3$ is carried out under inert conditions. A Cu^{I} triflate toluene complex is added to a solution of the macrocyclic ligand (PC-L*) in distilled dichloroethane. The solution is stirred for 1 h. The volume is concentrated until 5 mL and 10 mL of toluene are added. After one day, the solid is filtered off in nitrogen atmosphere.

Reference:

[1] Diploma thesis of Brunilde Castano, Università degli Studi di Milano, academic year 2009/2010.

(3) Grafting of $[Cu^{I}(PC\text{-}L^{*})]CF_3SO_3$ on silica

General procedure:

$[Cu^{I}(PC\text{-}L^{*})]CF_3SO_3/SiO_2$ catalysts are prepared by two different grafting procedures:

(a) Impregnation of the activated silica (MCM-41, SBA-15, Davisil B, basic silica, Aerosil) with the solid isolated $[Cu^{I}(PC\text{-}L^{*})]CF_3SO_3$ complex, dissolved in 5-10 mL anhydrous CH_2Cl_2.

(b) Impregnation of the activated silica with a $C_2H_4Cl_2$ (distilled) solution of the non-isolated $[Cu^{I}(PC\text{-}L^{*})]CF_3SO_3$ complex.

Stirring for 4 h at RT under inert atmosphere, followed by filtration, washing (3 x 5-10 mL anhydrous CH_2Cl_2) and drying in vacuum overnight gives the immobilized $[Cu^{I}(PC\text{-}L^{*})]CF_3SO_3$ complexes.

(4) Application of $[Cu^{I}(PC\text{-}L^{*})]CF_3SO_3/SiO_2$ in catalysis

Cyclopropanation of α-methyl styrene with ethyl diazoacetate (EDA)

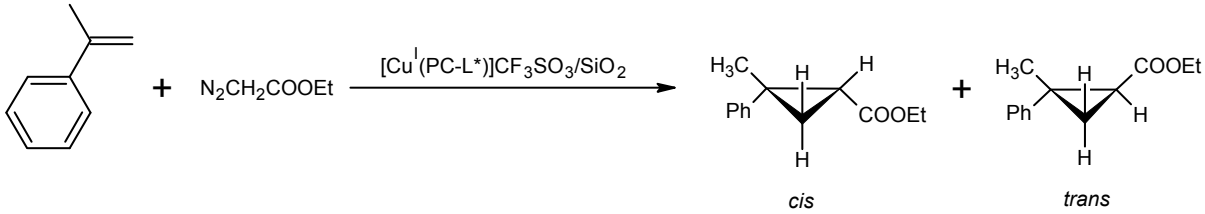

General procedure:[1]

A solution of $[Cu^{I}(PC\text{-}L^{*})]CF_3SO_3/SiO_2$ and α-methyl styrene in 5 mL distilled hexane is prepared, followed by slow addition of a solution of EDA in 1 mL distilled hexane via an infusion pump. During the addition of EDA, the reaction temperature is kept constantly at 0 °C. The catalytic ratios of the reactants are shown below:

$[Cu^{I}(PC\text{-}L^{*})]CF_3SO_3/SiO_2$	1
EDA	33
α-methyl styrene	166

The reaction process is monitored via IR spectroscopy. In this way, the diminution of the stretching band of the N=N bond of EDA at 2121 cm^{-1} can be observed. The reaction mixture is separated from the silica via filtration. The residue is analyzed by GC-MS, GC (using 2,4-dinitrotoluene as internal standard), HPLC (with chiral column in order to determine the ee; model "DAI-CEL CHIRAL CEL IB" with *n*-hexane/2-propanol 99.75/0.25 as eluent; observed wave length 230 nm) and NMR.

Reference:

[1] Diploma thesis of Brunilde Castano, Università degli Studi di Milano, academic year 2009/2010.

Experimental part III – CHAPTER 3

(1) Synthesis of MonoSil silica monoliths

General procedure:[1]

A mixture of H_2O (46.3 g) and HNO_3 (68 %; 4.6 g) is stirred at 0 °C for 15 min. 4.79 g PEO (polyethylene oxide) are added and stirring is continued for 1 h. After the addition of 37.7 g TEOS (tetraethoxysilane), the reaction mixture is stirred for 1 h and then filled into PVC tubes (10 cm length, 8 mm internal diameter), where it remains enclosed at 40 °C for 3 d. The resulting MonoSil silica monoliths are washed in H_2O and kept in an ammoniac solution (0.1 M) at 40 °C for 20 h. After drying (40 °C, 24 h), the monoliths are calcined (550 °C, 8 h).

Reference:

[1] A. Sachse, A. Galarneau, F. Fajula, F. Di Renzo, P. Creux, B. Coq, *Microporous and Mesoporous Materials* **2011**, *140*, 58-68.

(2) Pretreatment and grafting of MonoSil silica monoliths

General procedure:

a. Calcination

For the preparation of a MonoSil microreactor, a ca. 2 cm (~ 180 mg) long piece of a MonoSil silica monolith is placed between two glass tubes and covered by a heat-shrinkable teflon tube (Figure 1). The MonoSil is calcined at 280 °C in air overnight.

Figure 1: MonoSil microreactor before calcination.

b. Activation

Activation of the MonoSil microreactor is carried out in a Schlenk tube under reduced pressure for 2 h at 150 °C. After cooling down to RT, the MonoSil microreactor is functionalized via grafting.

c. Grafting

The grafting of the MonoSil microreactor is performed using an HPLC micropump (Figure 2).

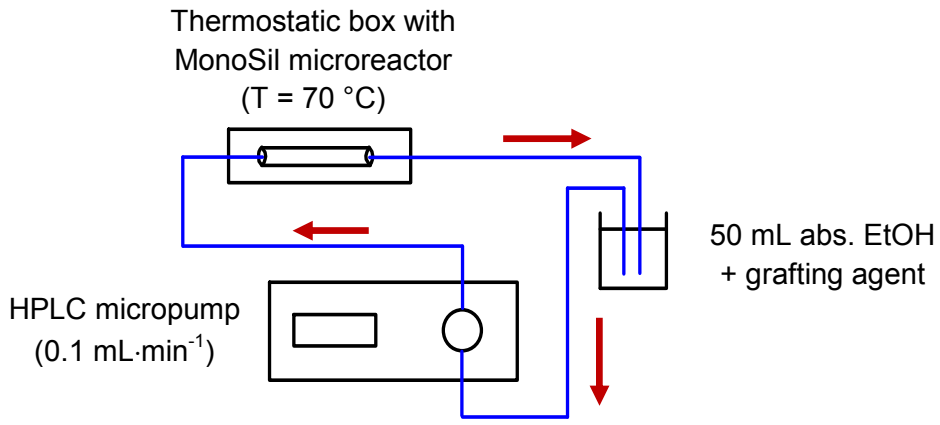

Figure 2: Apparatus for the grafting of MonoSil microreactors.

The MonoSil microreactor is placed in a thermostatic box, where the temperature is set to 70 °C. A solution of 2-(4-Chlorosulphonylphenyl)ethyltrimethoxysilane in 50 % CH_2Cl_2 is used as grafting agent. The grafting agent is diluted in 50 mL abs. EtOH and recycled with a velocity of 0.1 $mL \cdot min^{-1}$. The grafting process is run overnight. Subsequently, the MonoSil microreactor is cooled down to RT. After washing (50 mL abs. EtOH, 50 mL EtOH:H_2O (1:1), 50 mL acetone; apparatus see Figure 3), the grafted MonoSil microreactor is dried (2 h at RT, 2 h at 50 °C, 8 h at 80 °C).

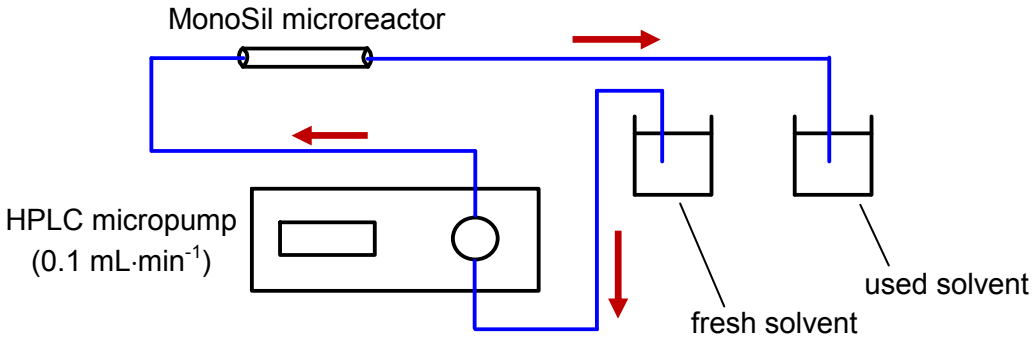

Figure 3: Apparatus for the washing of MonoSil microreactors.

(3) Dehydration of fructose to HMF

a. In batch

General procedure:

The reaction is performed in a two-necked flask for the purpose of continuous sampling via HPLC analysis. 1 g of fructose and 10 wt % (~ 100 mg) of the catalyst (homogeneous: unsupported grafting agent; heterogeneous: crushed blank or grafted MonoSil) are dissolved in 12 mL DMSO. The reaction mixture is stirred at 100 °C under reflux. Samples are continuously taken and analyzed by HPLC.

b. In flow

General procedure:

The reaction in flow is performed using the same apparatus as for the grafting. The (blank or grafted) MonoSil microreactor (183 mg of MonoSil, 10 wt %) is placed in the thermostatic box, the temperature is set to 100 °C. The fructose (1.83 g) is dissolved in 22 mL DMSO; the solution is pumped, samples are continuously taken and analyzed by HPLC.

List of figures

INTRODUCTION

Figure	Page
Figure 1: Molecular templating technique for the control of the active sites' environment.	15
Figure 2: Application of NPs in the automotive catalytic converter.	16
Figure 3: The impact of the size of AuNPs on their catalytic activity.	17
Figure 4: The preparation of precipitated catalysts by variation of different parameters.	22
Figure 5a: Wet impregnation.	23
Figure 5b: Incipient wetness impregnation.	24

CHAPTER I

Figure	Page
Figure 1: PVP.	35
Figure 2: PAMAM dendrimer.	36
Figure 3: Hydrogenation of 10-(3-propenyl) anthracene, catalyzed by PdNPs in a microemulsion system.	38
Figure 4: Imidazolium salt.	39
Figure 5: Formation of palladium carbene complex and subsequent thermal decomposition to PdNPs.	40
Figure 6: SEM of spherical MCM-41; (a) prepared with *n*-hexadecyltrimethylammonium bromide, (b) prepared with *n*-hexadecylpyridinium chloride.	43
Figure 7: X-ray diffraction patterns of MCM-41, (a) prepared with *n*-hexadecyltrimethylammonium bromide as template, (b) prepared with *n*-hexadecylpyridinium chloride as template.	44
Figure 8: Nitrogen adsorption (▲) and desorption(▼) isotherms of MCM-41, (a) prepared with *n*-hexadecyltrimethylammonium bromide as template, (b) prepared with *n*-hexadecylpyridinium chloride as template.	45
Figure 9: Three-step synthesis of SBA-15.	46
Figure 10: (a) SAXS patterns of SBA-15. 1: after 0.3 h, 2: after 1.2 h, 3: after 3.5 h, 4: after 15.6 h, 5: after 22.7 h.	47
Figure 11: (a) Low-magnification SEM image of calcined SBA-15 (prepared at 100 °C), (b) high-magnification SEM image, (c) TEM.	48
Figure 12: (A) XRD patterns of SBA-15 at (a) 60 °C and (b) 130 °C. (B) Nitrogen adsorption-desorption isotherms and pore size distributions.	49
Figure 13: Rh^{I}-Pd^{0}/SiO_2.	50
Figure 14: Rh(cod)(sulfos).	50
Figure 15: Rh(cod)(sulfos), (a) grafting of Rh(cod)(sulfos) onto silica, (b) grafting of Rh(cod)(sulfos) onto silica in combination with PdNPs.	51
Figure 16: Proposed mechanism for the Rh^{I}-Pd^{0}/SiO_2 catalyzed hydrogenation of benzene to cyclohexane.	52
Figure 17: Hydrogenation of polycyclic aromatic hydrocarbons, catalyzed by Pd-$[Rh(cod)(\mu\text{-}Cl)]_2$.	54

Figure 18: Isolated palladium atom grafted on MgO, formation of the complex $Pd(CO)_2O_2$ (blue: Mg, red: O, grey: C, black: Pd).	58
Figure 19: Immobilized organometallic complexes for metathesis reactions.	58
Figure 20: Organometallic complexes, immobilized on silica via hydrogen bonds.	59
Figure 21: Bimetallic $Ru_{10}Pt_2C_2$ cluster immobilized on mesoporous silica (NPs are marked in red).	60
Figure 22: Blocking of the exterior walls of mesoporous silica support materials by the reaction with $SiPh_2Cl_2$.	61
Figure 23: Examples for “ship-in-bottle” catalysts.	62
Figure 24: Open-structured aluminophosphate SSHC.	64
Figure 25: Procedure of Ionic Exchange.	67
Figure 26: Ionic Exchange – Calcination.	68
Figure 27: Ionic Exchange – Reduction.	68
Figure 28: Pd(allyl)Cp.	69
Figure 29: Glass reactor for CVD.	70
Figure 30: Coloration of the silica after CVD.	70
Figure 31: CVD – Reduction.	71
Figure 32: Procedure of impregnation of Pd^0/SiO_2 with Rh^I.	72
Figure 33: Chiral and achiral Rh^I complexes for grafting.	73

CHAPTER II

Figure	Page
Figure 1: Ligands for the Cu^{I} catalyzed asymmetric cyclopropanation.	89
Figure 2: Synthesis of (PC-L*).	90
Figure 3: Synthesis of $[Cu^{I}(PC\text{-}L^*)]CF_3SO_3$.	90
Figure 4: Cyclopropanation of α-methyl styrene with EDA.	91
Figure 5a: "Halomethyl-metal-mediated cyclopropanation".	92
Figure 5b: "Transition metal-catalyzed decomposition of diazo compounds".	92
Figure 5c: "Nucleophilic addition – ring closure sequence".	92
Figure 6: Diazoalkane compounds for the halomethyl-metal-mediated cyclopropanation.	93
Figure 7: Diazoalkane compounds with an EWG.	94
Figure 8: Mechanism of cyclopropanation using EWG-diazoalkanes.	94
Figure 9: The first cyclopropanation, catalyzed by Cu.	95
Figure 10: "Nucleophilic addition – ring closure sequence".	96
Figure 11: Mechanism of MIRC cyclopropanation.	97
Figure 12a: First MIRC cyclopropanation type.	97
Figure 12b: Second MIRC cyclopropanation type.	97
Figure 13: $[Cu^{I}(PC\text{-}L^*)]CF_3SO_3$ supported on silica via *"SHB"-concept*.	99
Figure 14: Asymmetric cyclopropanation of α-methyl styrene with EDA.	101
Figure 15: DRIFT spectra of the bare SiO_2 and $[Cu(PC\text{-}L^*)]CF_3SO_3/SiO_2$, characteristic bands of isolated silanol groups at 3740 cm^{-1}.	102
Figure 16a: CO-DRIFT spectra of $[Cu(PC\text{-}L^*)]CF_3SO_3/SiO_2$ before catalysis.	103
Figure 16b: The same CO-DRIFT spectra of $[Cu^{I}(PC\text{-}L^*)]CF_3SO_3/SiO_2$ before catalysis expanded, characteristic CO-band at 2116 cm^{-1}.	103
Figure 17a: CO-DRIFT spectra of $[Cu^{I}(PC\text{-}L^*)]CF_3SO_3$/SBA-15 (SBA-15 MFDC065), before and after catalysis.	104
Figure 17b: The same CO-DRIFT spectra of $[Cu^{I}(PC\text{-}L^*)]CF_3SO_3$/SBA-15 (SBA-15 MFDC065) expanded, before and after catalysis, characteristic CO-band at 2116 cm^{-1}, band of cyclopropanation product at 1730 cm^{-1}.	104

Figure 18a: CO-DRIFT spectra of [Cu^{I}(PC-L*)]CF_3SO_3/MCM-41 (MCM-41 6124), before and after catalysis.	105
Figure 18b: The same CO-DRIFT spectra of [Cu^{I}(PC-L*)]CF_3SO_3/MCM-41 (MCM-41 6124) expanded, before and after catalysis, characteristic CO-band at 2116 cm^{-1}, band of cyclopropanation product at 1730 cm^{-1}.	105
Figure 19a: CO-DRIFT spectra of [Cu^{I}(PC-L*)]CF_3SO_3/Davisil B, before and after catalysis.	106
Figure 19b: The same CO-DRIFT spectra of [Cu^{I}(PC-L*)]CF_3SO_3/Davisil B expanded, before and after catalysis, characteristic CO-band at 2116 cm^{-1}, band of cyclopropanation product at 1730 cm^{-1}.	106
Figure 20: DRIFT spectra of [Cu^{I}(PC-L*)]CF_3SO_3/SiO_2, after catalysis, **1**: [Cu^{I}(PC-L*)]CF_3SO_3/Davisil B, **2**: *p*-chloro styrene + EDA, **3**: *p*-methyl styrene + EDA, **4**: α-methyl styrene + EDA, **5**: α-methyl styrene + EDA (after 3 recycles + washing); characteristic bands of cyclopropanation products (pure cyclopropanes) at 2980 and 1730 cm^{-1}.	107

CHAPTER III

Figure	Page
Figure 1a: Transformations of D-fructose to pyranoid derivatives.	116
Figure 1b: Transformations of D-fructose to furanoid derivatives.	116
Figure 2: The generation of HMF and its subsequent products levulinic acid and formic acid.	118
Figure 3: Suggested mechanisms for the dehydration of fructose to HMF.	119
Figure 4: Hydrogenation products of HMF.	123
Figure 5: Oxidation products of HMF.	124
Figure 6: (a) Grafting of silica monoliths, (b) application of grafted silica monoliths in catalysis in flow, (c) cladded silica monolith.	126
Figure 7: Diels-Alder condensation between crotonaldehyde and cyclopentadiene, catalyzed by "Al-MonoSil".	127
Figure 8: Knoevenagel reaction between benzaldehyde and ethyl cyanoacetate.	128
Figure 9: Transesterification of triacetine by methanol.	128
Figure 10: 3-Aminopropyltriethoxysilane.	128
Figure 11: 2-(4-chlorosulfonylphenyl)ethyltrimethoxysilane.	129
Figure 12: Comparison between batch reactor, packed-bed microreactor and MonoSil microreactor.	130
Figure 13: Struts of MonoSil microreactor.	131
Figure 14: MonoSil microreactor, prior to the calcination.	133
Figure 15: 2-(4-Chlorosulphonylphenyl)ethyltrimethoxysilane.	133
Figure 16: HPLC spectrum of the pure fructose.	134
Figure 17: Comparison between fructose and HMF.	134
Figure 18a: Dehydration of fructose to HMF in batch, 10 wt % of grafted MonoSil (powdery), in H_2O dest., at 90 °C, after 1 h.	135
Figure 18b: Dehydration of fructose to HMF in batch, 10 wt % of grafted MonoSil (powdery), in H_2O dest., at 90 °C, overnight.	135
Figure 19a: Dehydration of fructose to HMF in batch, 10 wt % of grafting agent (homogeneous), in H_2O dest., at 90 °C, after 3 h.	136
Figure 19b: Dehydration of fructose to HMF in batch, 10 wt % of grafting agent (homogeneous), in H_2O dest., at 90 °C, after 22 h.	136

Figure 20a: Dehydration of fructose to HMF in batch, 10 wt % of grafting agent (homogeneous), in DMSO, at 160 °C, after 1 h.	137
Figure 20b: Dehydration of fructose to HMF in batch, 10 wt % of grafting agent (homogeneous), in DMSO, at 160 °C, overnight.	138
Figure 21a: Dehydration of fructose to HMF in batch, 10 wt % of grafted MonoSil (powdery), in DMSO, at 160 °C, after 1 h.	139
Figure 21b: Dehydration of fructose to HMF in batch, 10 wt % of grafted MonoSil (powdery), in DMSO, at 160 °C, after 19 h.	139
Figure 22a: Dehydration of fructose to HMF in batch, 10 wt % of blank MonoSil (powdery), in DMSO, at 100 °C, after 1 h.	140
Figure 22b: Dehydration of fructose to HMF in batch, 10 wt % of blank MonoSil (powdery), in DMSO, at 100 °C, after 4 h.	141
Figure 22c: Dehydration of fructose to HMF in batch, 10 wt % of blank MonoSil (powdery), in DMSO, at 100 °C, after 8 h.	141
Figure 23a: Dehydration of fructose to HMF in flow, 10 wt % of blank MonoSil microreactor, in DMSO, at 100 °C, after 1 h.	142
Figure 23b: Dehydration of fructose to HMF in flow, 10 wt % of blank MonoSil microreactor, in DMSO, at 100 °C, after 4 d.	143
Figure 23c: Dehydration of fructose to HMF in flow, 10 wt % of blank MonoSil microreactor, in DMSO, at 100 °C, after 7 d.	143

List of tables

CHAPTER I

Table	Page
Table 1: Ionic Exchange – loadings of Pd.	69
Table 2: CVD – loadings of Pd.	70
Table 3: Impregnation of Pd^0/SiO_2 with Rh^I – loadings of Pd and Rh.	75

CHAPTER II

Table	Page
Table 1: Cu loadings, determined by ICP-OES, of selected $[Cu^I(PC\text{-}L^*)]CF_3SO_3/SiO_2$ samples.	100
Table 2: Asymmetric cyclopropanation – selected results.	101

Acknowledgements

The present Ph.D. studies were accomplished in the framework of the European Marie-Curie project NANO-HOST “Homogeneous Supported Catalyst Technologies: the sustainable approach to highly-selective, fine chemicals production”, Initial Training Network - The People Programme, Proposal no. 215193-2.

First of all, I would like to thank my supervisor Vladimiro Dal Santo for his support, advice and experimental planning during my Ph.D. studies.
Furthermore, I want to thank Rinaldo Psaro for the opportunity to work in his research group.
In terms of the preparation and catalytic application of the copper catalysts, I want to thank Alessandro Caselli, Brunilde Castano and Paolo Zardi (Università degli Studi di Milano, Dipartimento CIMA “Lamberto Malatesta”).
Regarding the preparation and characterization of the Rh^{I}-Pd^{0}/SiO_2 “hybrid catalysts”, I would like to thank Claudio Pirovano for his supervision and advice during the first months in the laboratory.

Thank you to Pierluigi Barbaro (ICCOM-CNR, Sesto Fiorentino (Florence, Italy)) for giving me the opportunity to carry out my Ph.D. studies within the scope of the NANO-HOST project.
I want to thank Serena Orsi (ICCOM-CNR) for all the organization concerning the financial support.
Pertaining to the synthesis of the rhodium complexes, I would like to thank Francesca Liguori (ICCOM-CNR).

Regarding my three-month stay at the *Institute Charles Gerhardt* in Montpellier (France), I would like to thank Anne Galarneau for her supervision, experimental planning and advice as well as Vasile Hulea and Annie Finiels for their supervision and their assistance in the laboratory.

Moreover, I would like to thank Alexander Sachse (*Institute Charles Gerhardt*, Montpellier, France) and Ruben Duque (University of St. Andrews, UK) for their collaboration during their secondments at the ISTM-CNR in Milan within the scope of the NANO-HOST network.

Finally, thank you to the whole research group of the ISTM-CNR for the support and collaboration during my Ph.D. studies.